D.S.S. CONTRACT OSU82-00233

"DETERMINATION OF STRESS INTENSITY FACTORS FOR WELD TOE DEFECTS"

Final Report
(April 1984)

Prepared by:
R. Bell, P.Eng.
J. Kirkhope, P.Eng.

MICROMEDIA

154 pp

FACULTY OF ENGINEERING
CARLETON UNIVERSITY

Centre for Advanced Engineering & Design

Faculty of Engineering
Carleton University
Ottawa Canada K1S 5B6
Telephone (613)

DETERMINATION OF STRESS INTENSITY FACTOR FOR WELD TOE DEFECTS

FINAL REPORT

BY

R. Bell P.Eng.

J. Kirkhope P.Eng.

Work on this project was conducted under the auspices of Physical Metallurgy Research Laboratories Canada Centre for Mineral and Energy Technology Energy, Mines and Resources Canada.

DSS FILE NUMBER	:	14SU.23440-2-9083
DSS CONTRACT SERIAL NUMBER	:	0SU82-00233
CANMET PROJECT NUMBER	:	425251
CANMET SCIENTIFIC AUTHORITY:		Dr. O. Vosikovsky

NOV 22 1984
MICROMEDIA

April 1984

This report should be cited by D.S.S.
File No. 14SU.23440-2-9083

ACKNOWLEDGEMENT

This work was performed for the Physical Metallurgy Research Laboratories, CANMET, Energy, Mines and Resources Canada under Supply and Services Canada Contract 0SU82-00233. The authors are indebted to PMRL CANMET for permission to publish this work. The authors also acknowledge the support and input received from Dr. O. Vosikovsky, PMRL in the Scientific administration of the contract.

DISCLAIMER

Any data presented, opinions, findings, conclusions, or recommendations expressed in this report are those of the authors and do not necessarily reflect the views of CANMET. Crown copyright of this report is reserved.

ABSTRACT

The report describes the use of the ASAS finite element program to determine the linear elastic stress intensity factors at weld toe defects.

Stress intensity factors (SIF) are presented for a series of straight fronted cracks with crack depth/thickness ratios, a/t, ranging from 0.005 to 0.7 for three different weld profiles. Empirical expressions are obtained from the above results for the SIF as a function of a/t.

The substructuring capabilities of ASAS are applied to study the variation of SIF for semi-circular and semi-elliptical weld toe cracks. Crack tip stress intensity factors are presented for weld toe cracks having elliptical aspect ratios, a.c, of 1.0, 0.5 and 0.25 and depth/thickness ratios, a/t, in the range 0.05 to 0.4 for weld profiles of 30^{o}, 45^{o} and 70^{o}.

RÉSUMÉ

Ce rapport décrit l'utilité du programme ASAS des éléments finis afin de déterminer les facteurs d'intensité des contraintes linéaires élastiques relatifs aux défauts du fond de la soudure.

Les facteurs d'intensité de contraintes (SIF) sont représentés graphiquement par une série de fissures à façade rectilignes, à l'aide du rapport profondeur de la fissure/épaisseur, a/t, ayant comme intervalles les valeurs de 0.005 a 0.7, pour trois différents profils de soudures. Obtenues des résultats ci-dessus, les expressions empiriques présentent les facteurs d'intensité de contraintes comme étant une fonction de a/t.

Les capacité d'infrastructure d'ASAS sont appliquées dans le but d'étudier la variation des facteurs d'intensité de contraintes selon les fissures semi-circulaires et semi-elliptiques du fond de la soudure. Les facteurs d'intensité de contraintes (SIF) de l'extrémité d'une fissure de soudure se révèlent avoir des rapports d'aspect elliptique, a/c, de 1.0, 0.5 et 0.25 et des rapports profondeur/épaisseur, a/t, s'étendant de 0.005 a 0.4 pour les profils de soudures de 30, 45 et 70 degrés.

TABLE OF CONTENTS

			Page
		ABSTRACT	
CHAPTER I		INTRODUCTION	1
CHAPTER II		LITERATURE SURVEY	6
	2.1	Stress and Fatigue Analysis of Tubular Joints	6
	2.2	Fracture Mechanics Analysis of Offshore Structures	8
	2.3	Weld Toe Crack	11
	2.3.1	F.E. Analysis of Weld Toe Cracks	11
	2.3.2	Thickness Effect	13
	2.3.3	Weld Improvement Techniques	15
	2.3.4	Influence of Environment	17
	2.4	Finite Element Analysis	18
CHAPTER III		FINITE ELEMENT ANALYSIS	28
	3.1	Finite Element Analysis of Fracture Problems	28
	3.2	Determination of Fracture Parameters	31
	3.3	Numerical Calculation of Stress Intensity Factor	35
	3.3.1	Description of ASAS F.E. Program	35
	3.3.2	Multi-level Substructuring Capability of ASAS - H	36
	3.3.3	LEFM Capability of ASAS - H	37
	3.3.4	The FRAKAS Post-Processor	38

		Page
CHAPTER IV	2-DIMENSIONAL STUDIES	48
4.1	Introduction	48
4.2	Modelling of Welded Joint	48
4.3	'T' Specimen - 2-Dimensional Results	51
4.4	Stress Analysis of Uncracked Joints	56
CHAPTER V	3-DIMENSIONAL STUDIES	84
5.1	Introduction	84
5.2	Modelling of Semi-Elliptical Cracks	85
5.3	3-D Modelling of Weld Toe Crack	89
5.4	Results of 3-D Analyses	91
CHAPTER VI	CONCLUSIONS	140
	REFERENCES	143

CHAPTER I

1. INTRODUCTION

This report describes work carried out in accordance with Appendix A of the D.S.S. contract, "Determination of Stress Intensity Factors for Weld Defects".

During the past number of years there has been an increasing and justified interest in the design and safe operation of large offshore oil exploration and production platforms. One of the most important aspects of the behaviour of these offshore units is the ability of the structure to withstand the time varying stresses caused by the cylic loading of the waves. The resistance of the structure to withstand these fluctuations of stress decreases with the number of cycles which , in turn, leads to the development and propagation of cracks.

These structures are generally of tubular frame construction where the intersections are all welded. High local stresses are induced at the intersections of the chord and brace, adjacent to the connecting welds and it is here that fatigue damage will usually occur. Current design practice utilizes the S-N design curve approach (1) - (4), and this method has provided a successful formula for designing past structures. However, there have been some criticisms levelled at this approach (5), the most important being that the S-N curve design method only deals with a sound structure and cannot be used when the structure has sustained damage.

An alternative to the S-N design curve procedure for estimating the life of a structure is the approach of crack propagation analysis using fracture mechanics. This method is unlikely to replace the S-N curve method of life prediction for a tubular structure in the near future, but it does present a method of dealing with a structure which contains flaws and demonstrates the influence of a number of variables on fatigue crack propagation.

In offshore platforms fatigue damage occurs at the joints at the intersection of the chord and brace in the weld toe region. Initial flaws or inclusions which are present at the weld toe propagate round the joint as more pronounced cracks until they reach critical size or penetrate the thickness of the structure. The investigation of crack propagation in this region of tubular joints is a complex 3-dimensional problem because the crack propagates rapidly along the weld, whereas penetration in the depth direction is relatively slow.

The growth rate of a crack at the toe of a weld can be described using a fracture mechanics approach, by a single parameter, the stress intensity K. In this approach the crack growth rate da/dN is related to the stress intensity range ΔK by the Paris Law (6)

$$da/dN = C\Delta K^m$$

where C and m are material constants. It is therefore possible to estimate the fatigue life of the structure once the solution for K as a function of crack shape is known. The value of K for complex geometries may be obtained using the finite element method (FEM).

This report describes some work which has been carried out on the calculation of stress intensity factors for defects at the toe of welds in 'T' plate joints using the finite element method. This work is to complement the CANMET experimental research project on corrosion fatigue of welded joints for offshore structures.

WORK OUTLINE

As stated previously fatigue crack growth around a tubular joint weld region is an extremely complex problem and the experimental and analytical work is both time consuming and costly. Therefore, it was decided to confine this phase of the project to plate specimens. The specimen shape chosen was the 'T' joint loaded on 3 point bending as shown in fig. 1.1.

This report describes calculations of the stress intensity factor for a crack at the weld toe in a 'T' specimen, using the finite element method.

The following cases were considered:

1. 2 dimensional case
   a) obtain the SIF for crack depths in the range a/t = 0.01 to 0.7.
   b) investigate the effect of weld shape on SIF for shallow cracks

2. 3 dimensional case

a) obtain SIF for semi-elliptical cracks with aspect ratios $\frac{a}{c}$ = 1.0, 0.5, 0.25, with $\frac{a}{t}$ in range 0.01 to 0.3

b) investigate the effect of weld shape on SIF for shallow cracks.

Several analyses were also carried out to obtain the stress concentration and the distribution of stresses at the weld toe of uncracked joints of various thicknesses and with 45^{o} and 60^{o} welds.

The work outlined above is also preparatory to a longer term project of the prediction of fatigue crack growth and crack shape in welded joints.

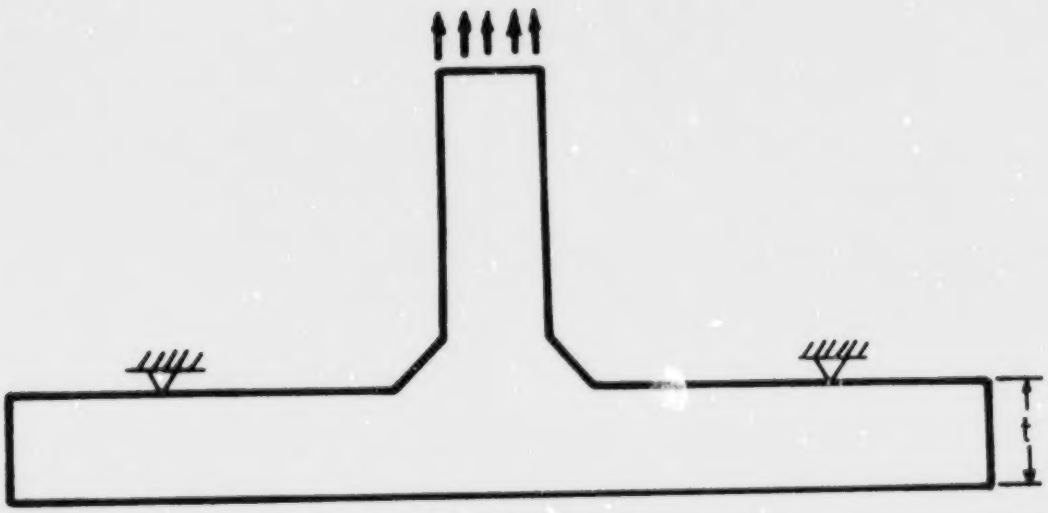

"T" SPECIMEN

FIG. 1-1

CHAPTER II LITERATURE SURVEY

2.1 Stress and Fatigue Analysis of Joints

One of the most important aspects of the enduring behaviour of offshore units is the ability of the structure to withstand the time varying stresses caused by cyclic loading. Wave loading over the anticipated operating life of 20 years will subject the structure to about 10^8 cycles of stress variation and it is this wave action which is the main cause of fatigue cracking. As a result Certifying Authorities specify requirements for fatigue analysis procedures which are published as guidelines (1), (3) and (4). The designer of offshore structures must demonstrate that these requirements are met before a certificate for that rig is issued.

In offshore structures, which are generally of tubular construction the intersection of the chord and the brace induce high local stresses adjacent to the connecting weld and it is here that fatigue damage will generally occur. Therefore, the fatigue analysis is highly dependent on the accuracy with which this high local stress at the hot spot can be calculated.

During the past decade there has been considerable development in the method used in the assessment of fatigue in offshore structures. Extensive research programs have been carried out in the United Kingdom (UKOSRP) and in Europe (ECSC) on the appropriate S-N curve to use, and on the definition of stress and life. Much of this work has been published in special conference proceedings (7), (8) and (9).

Recently the existing fatigue design rules for offshore structures published by the UK Department of Energy have been revised to take account of the substantial amount of new information produced by the UKOSRP and ECSC test programs. These revisions are described in detail with supporting documentation in ref. (2).

In the revised guidelines the fatigue design procedure is still based on the S-N approach but a new curve (the T curve) has been proposed based on experimental tests on tubular joints in the above programs. Another major change in the design procedure is that the design stress to be used in a fatigue analysis of a tubular joint has been redefined as the hot spot stress. This idealised hot spot stress is defined by linear extrapolation to the toe of the weld of the principal stresses at points A and B as shown in fig. 2.1, ref. (2).

The new guidance notes also define factors which have to be applied to the basic S-N curve, fig. 2.2, to cover the influence of other variables such as thickness effect, environment, stress concentration factors, post weld heat treatment (PWHT) and weld improvement techniques. These variables and their influence on fatigue life will be discussed later in this report.

The hot spot stress at a tubular joint weld can be determined by mathematical or experimental modelling; however, because of the many different joint configurations in a typical offshore structure, and the cost of finite element analyses and experimental tests, the designer has often to resort to stress concentration parametric formulae. The three

main collections of parametric formulae are those published by Kuang et al (10), Wordsworth and Smedley (11) and Gibstein (12). Unfortunately these formulae only exist for simple geometries and the guidance notes state that "because of the sensitivity of calculated life to the accuracy of estimates of stress (power of three) particular care must be taken that stresses are not underestimated".

Fisher (13) highlights the inadequacies of this approach by comparing actual hot spot stresses measured on T and X joints with predicted SCF's from parametric formula, fig. 2.3. It can be seen that the formula under-predicts the stresses by as much as 50 percent, which would result in an overestimate of fatigue life by a factor of 8, using the new S-N curve. Therefore, care must be exercised when using the parametric SCF formulae even for simple joints.

2.2 Fracture Mechanics Analysis of Offshore Structures

The first S-N curves used in the design of offshore structures were developed from onshore welded fabrication design curves and used a nominal member stress which enabled the fatigue life to be quickly assessed. With time, it was necessary to include in this design stress such effects as weld toe stress concentration and high local bending stresses produced by local bending of the chord and braces at the joint intersection. Thus, the basic simplicity of the S-N approach has been lost. At present, long term tests of full scale steel joints have been completed and further tests are under way to produce S-N curves for the design of tubular joints which

include the effect of thickness, environment and post-weld heat treatment. An example of this is the new DOE 'T' curve (2) and the associated penalties and allowances on life. To understand the effect of these variables on fatigue life many researchers have increasingly used fracture mechanics concepts to explain the fatigue mechanisms and crack growth behaviour of tubular joints.

The fracture mechanics design methodology is based on the presence of a crack-like defect which grows along a path perpendicular to the direction of maximum principal stresses. The cracks in a tubular joint usually occur at weld toe defects at the intersection of the brace and chord, and the rates of extension along the surface and through the thickness are dependent on the initial crack shape, the chance of multinucleation and coalescence of defects, the mean stress, the type of loading and the SCF at the weld toe.

The fatigue crack propagation can be described by the Paris Law (6)

$$da/dN = C\Delta K^{m}$$

where da/dN is the crack growth rate, C and m are material constants and ΔK is the variation of stress intensity factor given by $\Delta K = Y\Delta\sigma\sqrt{\pi a}$. The stress intensity factor (SIF), K describes the stress environment at the crack tip and for two different geometries of the same material the stress distribution will be identical if the stress intensities are equal. It follows that the fatigue crack propagation in the two bodies will be identical if the variation in SIF, ΔK is the same.

The life of a structure can be predicted by integration of the above equation as

$$\int_{o}^{N} dN = \frac{1}{w^{m/2} C\Delta\sigma^{m}} \int_{a_i}^{a_j} \frac{da}{Y^{m} a^{m/2}}$$

where a_i and a_j are the initial and final crack lengths respectively.

To date the fracture mechanics approach in the design of tubular joints has only been used in a minor role and it will not replace the S-N approach in the foreseeable future. However, the FM approach does give designers an insight into the fatigue crack growth mechanisms at joints so that the importance of variables such as geometry, loading, environment and fabrication procedures can be assessed. Also it provides a means of assessing the significance of defects found during inspections and permits the development of integrity monitoring systems and inspection periods and procedures.

Many of the areas of application of FM methodology in the design, maintenance and repair of offshore structures are described in some detail in (5) and (14), but there is still much analytical and experimental development work needed before the FM design procedures for tubular joints reaches its full potential.

2.3 Fatigue Crack Growth at Weld Toe Cracks

The study of fatigue crack growth around a tubular joint weld region is an extremely complex problem and the experimental and analytical investigations of this problem is both costly and time consuming. It is for this reason that much of the work in the UKOSRP and the ECSC programs was concerned with testing and analysis of welded plate specimens. The initial phase of the EMR Offshore Steels Research Program is confined to welded plate specimens and thus this report will concentrate on the application of fracture mechanics techniques to the analysis of the welded 'T' plate specimen, fig. 1.1. This section will review the literature concerning the analysis of crack growth in welded plate specimens and the fracture mechanics methodology used.

2.3.1 Initial Crack Size

The weld toe area in welded joints is subjected to a complex stress system and it is in this region that fatigue cracks initiate. The factors which influence the fatigue strength of the joint are the stress concentration due to the weld shape, weld defects which constitute a severe stress concentration and residual welding stresses. These extremely high local stresses cause crack initiation at the weld toe.

To date, little research has been carried out on crack initiation at welds in offshore structures, because it has been assumed that with the

existence of weld defects the initiation period can be neglected. Also, it has been assumed that the initiation period, if it exists, occupies such a small part of the total life that its neglect is not a major error.

It is, therefore, generally accepted that in predicting the fatigue life of welded plate and tubular joints initial cracks the size of the weld toe defects exist. The actual size of these initial cracks has been a topic of debate for some time with suggested sizes ranging from $a_i = 10^{-5}$ mm to $a_i = 1.0$ mm. In modelling this initial stage of crack growth by the Paris Law, which utilizes the Linear Elastic Fracture Mechanics (LEFM) approach, the initial crack size is an important consideration because it is at this stage that a large proportion of the life exists. Irvine (15) states that crack initiation takes place at weld toe defects, which lie inside a small region of plasticity caused by high local stresses. The initial defect size is comparable with this plastic zone size so therefore the LEFM conditions will not apply until crack growth has progressed some distance. Engesvik (16) suggests that the size of this region of plasticity is of the same order as the typical grain size, i.e. ~ 0.01 mm, and that the initial crack size a_i should be >> the plastic zone size, i.e. a value of 0.1 mm. Hence a reasonable lower limit for the application of LEFM to life calculations of welded joints should be $a_i = 0.1$ mm → 0.4 mm. This assumption is backed up by metallurgical examination which has shown the average depth of these weld toe defects to be 0.15 mm.

2.3.2 Thickness Effect

The major change in the new DOE guidelines for fatigue design of welded joints is the thickness effect correction factors, which apply to all joints, and impose an increasing penalty with increasing thickness. This factor on life is of the form $(32/t)^{3/4}$ for tubular joints, where the basic T curve applies for thicknesses up to 32 mm. The effect of this thickness penalty on the S-N curve is shown in fig. 2.4. The thickness correction for non-tubular joints results in a factor on life of the form $(22/t)^{3/4}$, where the basic curve refers to thicknesses up to 22 mm.

The thickness effect has been demonstrated by many authors in the literature. Berge (17) investigated experimentally the effect on increasing plate thickness on the fatigue strength of transverse non-loading carrying fillet welds in axial tension in the thickness range 12.5 - 80 mm and found that for geometrically similar joints the fatigue strength of the joint was decreased by a factor of 0.2 when the plate thickness increased from 12.5 to 80 mm. These results are shown in fig. 2.5. Also given in this paper are other results published by Johnston (18), Booth (19), Haibach (20), Wildschut (21) and Olivier(22) which, in the main exhibit the same thickness effect on weld fatigue strength. These comparisons are reproduced in fig. 2.6.

Berge also reported on some tests on load-carrying specimens with constant thickness load-carrying plate and varying weld size and attachment plate thickness. These tests showed that these parameters had a minor effect;

the weld size had only a minor influence on fatigue strength and the attachment thickness had somewhat greater influence causing a decrease in fatigue strength as the thickness increased.

Gurney (23) demonstrated analytically the thickness effect on fatigue life for non-load carrying fillet welds NLCFW. In this work Gurney developed parametric equations for the SIF for different crack depths and weld shapes using the finite element method, and demonstrated that the fatigue life decreased with increasing thickness using crack growth calculations based on the Paris Law.

The plate thickness effect may be explained using a simple geometric model, fig. 2.7. For the butt welded plates shown, which have a geometrically similar stress distribution, it can be seen that the stress gradient in the plane of the crack is steeper in the thin plate. Thus, an initial crack in the thin plate will experience a smaller stress than the initial crack of the same length on the thick plate, which will result in a smaller initial crack growth rate in the case of the thin plate. The difference in initial crack growth rate overcompensates the difference in crack length to cause failure so the thinner joint will have a longer life. The stress gradient through the thickness enters into the calculation of stress intensity factor K so therefore this thickness effect can be predicted analytically using the Paris crack growth law as demonstrated by Gurney.

3.2.3 Weld Geometry and Weld Improvement

As has been stated previously fatigue cracks in most welded joints tend to originate at the weld toe and initiate at small defects left at the toe during welding. This region is an area of high stress concentration caused by the change of shape at the weld toe. It is apparent that a reduction in this stress concentration and the removal of the defects would produce an improvement in fatigue life.

The stress concentration can be reduced by controlling the weld shape. Gurney (23) showed that by increasing the weld leg length the fatigue strength of the joint could be increased, but that this was a relatively minor effect. Berge (17) modelled the weld shape using the parameters, θ, the weld toe angle and ρ, the notch root radius. He argues that the radius ρ (which is similar in size to the initial defects) produces a more realistic model of the stress distribution at the weld toe and therefore produces a significant effect on the fatigue strength of the joint. Mullen and Merwin (24) published results of experimental work in which they investigated the fatigue life improvement of joints by weld reinforcement. Weld reinforcement is a weld treatment in which weld metal is laid down during or after the initial welding of the joint. This procedure has the effect of improving the weld angle by increasing the leg length. The authors claim that the fatigue life of the joint is improved by a factor of 3 - 4.

The DOE guidelines consider that control of weld profile alone has only a small beneficial effect on fatigue strength. However, the guidelines acknowledge that large improvements in fatigue life can be obtained by local machining of the weld toe to remove toe defects. The reason for this is that these defects are so sharp that they are effectively small cracks and their removal introduces an initiation period; thus the total life of the joint is substantially increased. The guidelines require that in order to ensure that the defects are removed, it is essential that the grinding penetrate the surface of the plate as shown in fig. 2.8. This procedure results in a factor on life of approximately 2 for joints tested in air, but this benefit is not demonstrated for unprotected joints tested in sea water. The basis of this procedure results from tests on a variety of simple joints which are summarised by Booth (25) and Gurney (26). Mullen and Merwin (24) also published results which showed improvements in life that were obtained on 'T' specimen tests by weld toe grinding, but the improvements were much higher than those suggested above (i.e. factors on life in the range 3 - 11).

The new DOE guidelines encourage weld improvement but do not permit any benefit to be claimed for this procedure except in circumstances such as in the latter stages of design where a particular joint is found to be critical. Additional work is now underway in the various offshore test programs on the overall effect of weld profile on fatigue life.

2.3.4 Influence of the Environment

The extensive testing carried out in the UKOSRP and the ECSC indicated a detrimental effect of sea water on the fatigue life of joints and the beneficial effects of cathodic protection. Therefore, the new guidance notes of DOE require that the relevant S-N curve should be reduced by a factor of 2 on life for unprotected joints and that there should be no assumed bend in the S-N curve at 10^7 cycles when considering small stress cycles. For protected joints it is required that the S-N curve in air should be used, but care should be exercised that the joints are not over-protected.

2.4 Finite Element Analysis

The fatigue crack growth in welded plate joints can be modelled using the Paris Law provided the range of stress intensity ΔK can be obtained. The value of K for complex geometries can be obtained using the finite element method.

Several researchers have published work on the calculation of stress intensity factors at weld toe cracks. Maddox (27) considered a non-load carrying fillet weld and assumed that the SIF of a crack at the toe of a weld could be derived from the corresponding SIF factor for a crack in a flat plate using a magnification factor. This can be written as $K = M_k K'$ where K' is the SIF for the equivalent flat plate. This value of M_k was obtained by finite element analysis for weld angles of 45^o and 30^o from a solution by Hayes (28).

Gurney and Johnston (29) also carried out a series of finite element analyses for non-load carrying fillet welds to obtain values of M_k, as defined by Maddox, for welded joints with a range of weld sizes and plate thicknesses. The FE analysis was carried out using a very large number of 2-dimensional constant strain triangular elements to model the cracked joint. Three different methods were used to calculate the SIF and hence the value of M_k for each crack depth. These methods were Albrecht's method (31), Emery's method (32) which are super-position procedures and a compliance method. From the results obtained the authors developed an empirical relationship for M_k, the magnification factor

given as

$$M_k = 0.8479 \left(\frac{\ell}{B}\right)^{0.063} \left(\frac{a}{B}\right)^{-0.279}$$

where B is the plate thickness, a is the crack depth and ℓ is the weld leg length.

Smith (30) also carried out a finite element analysis of a NLCFW and modelled the joint using cubic isoparametric finite elements. Unlike Gurney and Johnston, Smith modelled the stress singularity at the crack tip using a collapsed cubic element which models the $1/\sqrt{r}$ stress singularity, so therefore the results of K and hence M_k could be obtained directly from the finite element displacements by substitution in the classical Westergaard equations

The results of Gurney and Johnston, and Smith are comparable with the value of M_k approaching 1 as a/B approaches 0.7. However, the results of Maddox indicates that M_k approaches 1 at values of a/B of 0.3. Also the maximum values of M_k at small values of a/B given by Gurney and Johnston are slightly higher than those published by Maddox.

The results of Gurney and Johnston, and Smith for the NLCFW are used for comparison with the present work in Chapter IV.

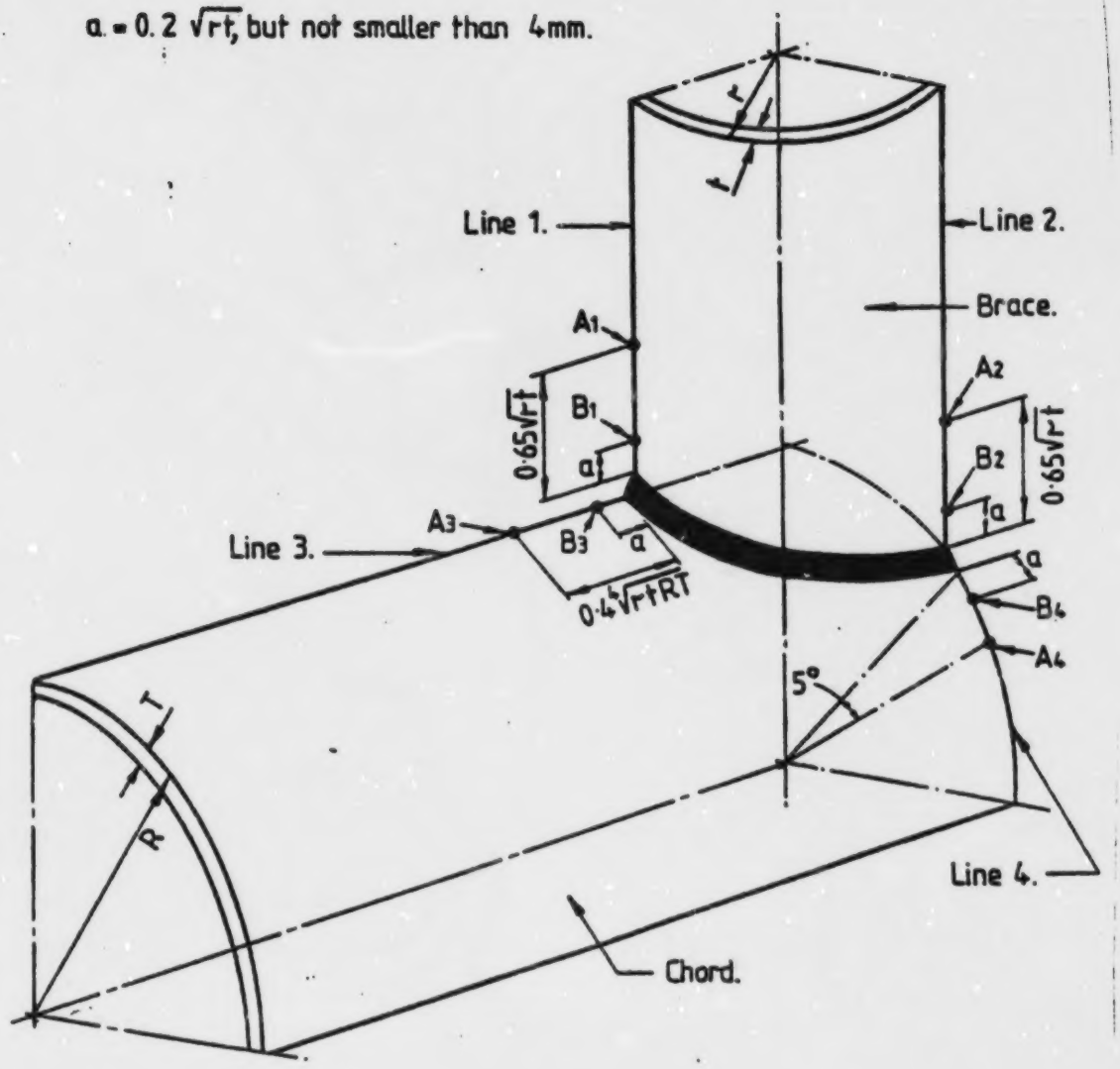

DEFINITION OF REGIONS OF STRAIN LINEARITY FOR WELDED TUBULAR T JOINT

FIG. 2.1

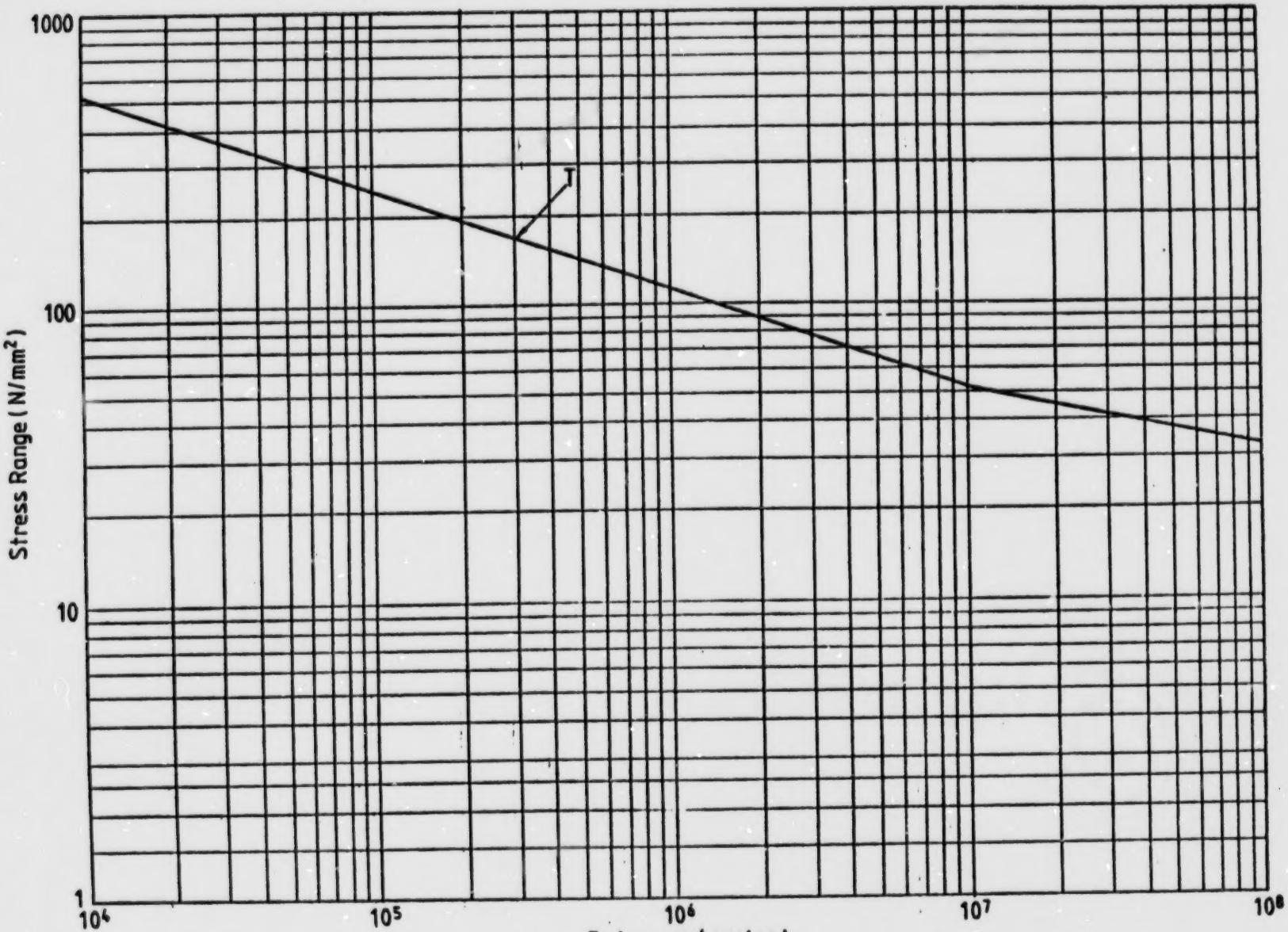

Design S-N curve for nodal joints

FIG. 2.2

COMPARISON OF PREDICTED AND EXPERIMENTAL SCFs (ref 13)

FIG. 2.3

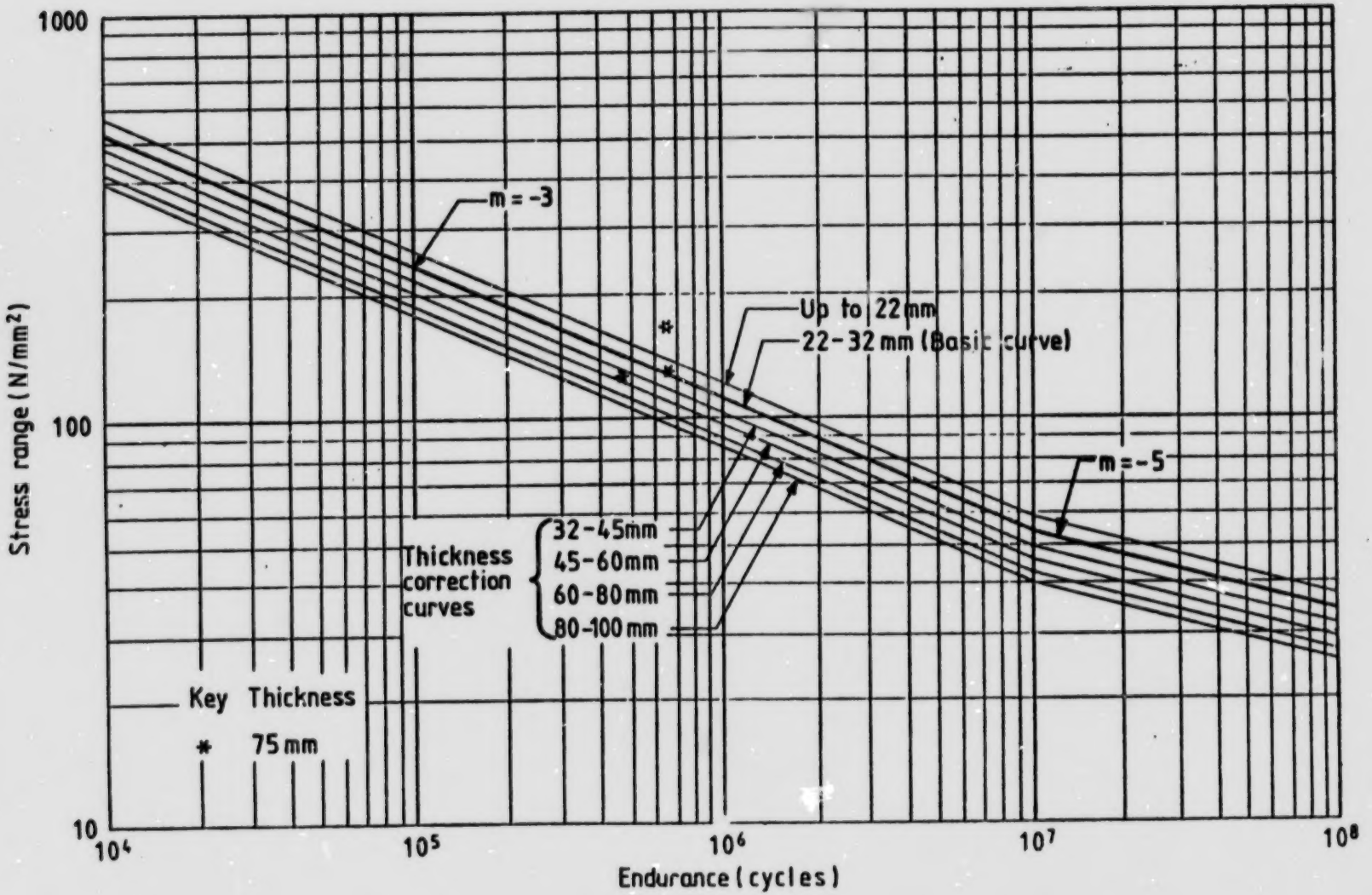

General form of S-N design curves for welded tubular joints in air

FIG. 2.4

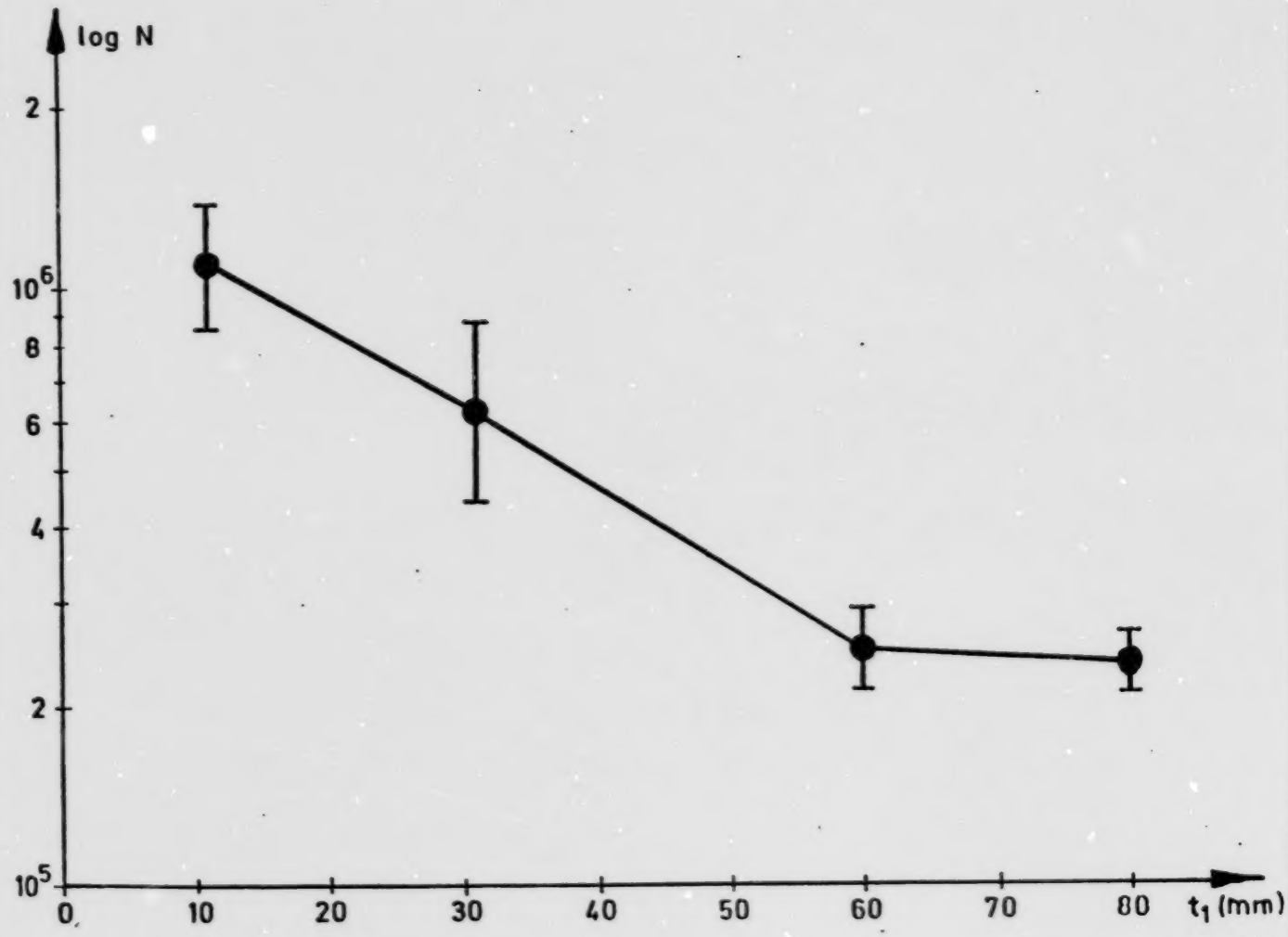

EFFECT OF THICKNESS ON LIFE (ref 17)

FIG. 2.5

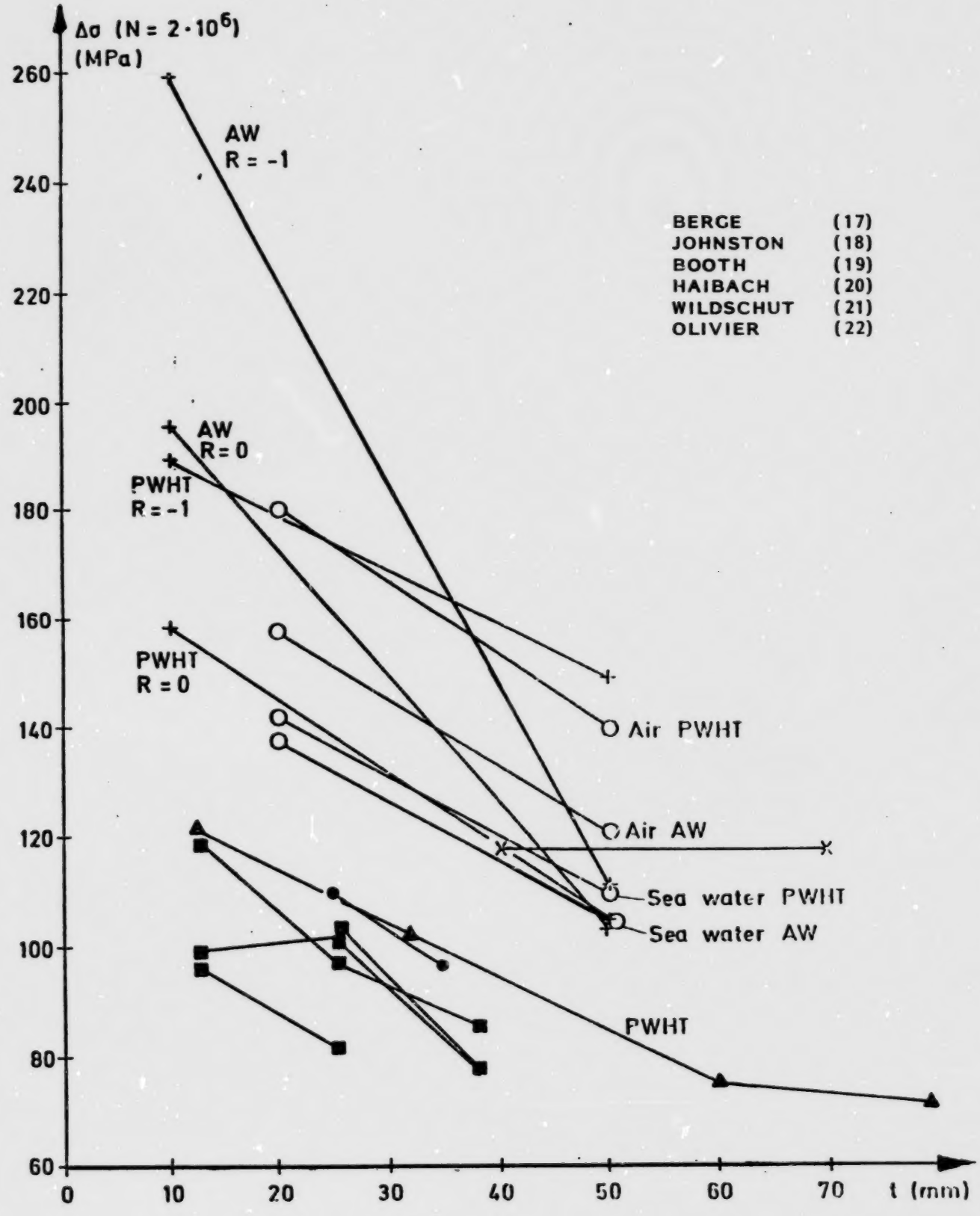
Δσ (N = 2·10^6)
(MPa)
260
240
220
200
180
160
140
120
100
80
60
0
10
20
30
40
50
60
70
t (mm)
AW
R = -1
AW
R = 0
PWHT
R = -1
PWHT
R = 0
Air PWHT
Air AW
Sea water PWHT
Sea water AW
PWHT
BERGE (17)
JOHNSTON (18)
BOOTH (19)
HAIBACH (20)
WILDSCHUT (21)
OLIVIER (22)

FIG. 2.6 (17)

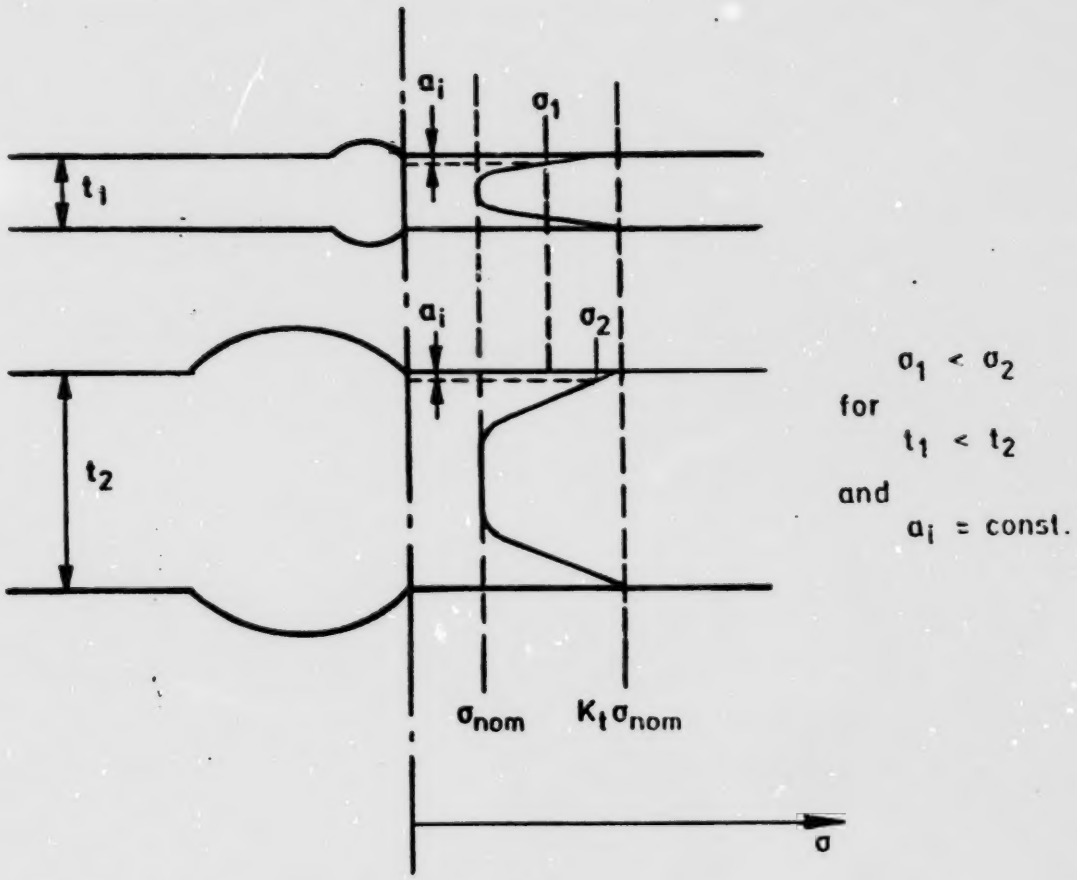

A MODEL FOR DESCRIBING THE THICKNESS EFFECT IN FATIGUE FAILURES DEVELOPING FROM THE WELD TOE

FIG. 2.7

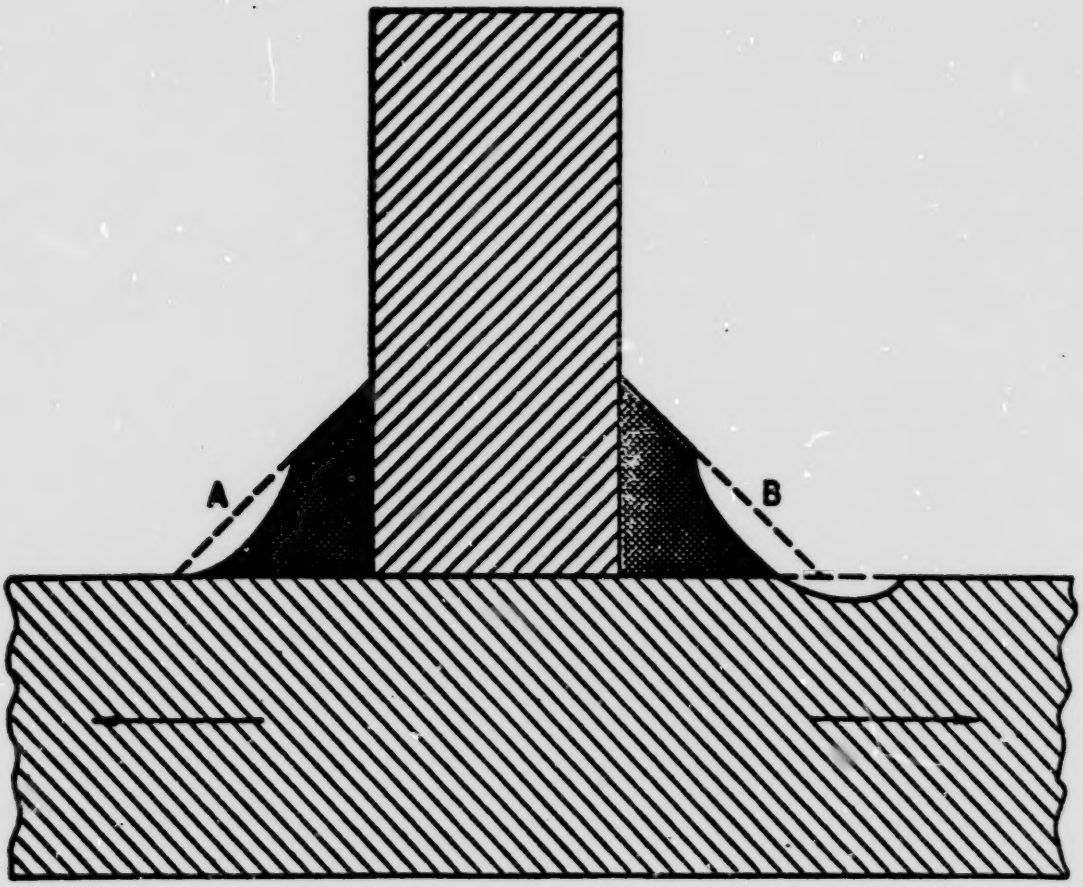

Grinding a weld toe tangentially to the plate surface, as at A, will produce little improvement in strength. Grinding must extend below the plate surface, as at B, in order to remove toe defects.

FIG. 2.8 ref (2)

CHAPTER III

3.1 FINITE ELEMENT ANALYSIS OF FRACTURE PROBLEMS

In the past fifteen years the investigation of fracture problems has been one of the most active branches of applied mechanics. In the numerical analysis of such problems, the finite element method (FEM) has been extremely useful because of the ability of this method to model geometry, material behaviour and loading in a realistic way. Several reviews of FEM techniques in fracture mechanics have been published over the past ten years and the reviews of Gallagher (33) and Mackerle and Fredrickson (44) are of particular note. Also the basic principles of finite element theory is well documented in (35) and (36), and will therefore not be covered in this report.

An important problem in the application of FEM to fracture is the modelling of the stress singularity which occurs at the crack tip. The first attempts to model cracks were simply the use of very large numbers of conventional elements, ie. elements in which no attempt was made in the element formulation to take account of the stress singularity. It has been clearly demonstrated by Chan (37) that using this approach many hundreds of elements are required to achieve even 5% accuracy. This is the approach that was used by Gurney and Johnston (29) to model a non-load carrying fillet weld (NLCFW).

Another method uses classical solution based singularity elements. In these elements the displacement functions of the element include the fundamental classical displacements present at the crack tip. Some of the element formulations used in this approach and the performance of these special elements are described in (47).

Isoparametric elements have also been used to model crack problems and they have the advantage that they are widely available in FE program and therefore no special element development needs to be carried out. These elements can model the $1/\sqrt{r}$ singularity at the crack tip if minor modifications to the basic element are made. This is the element used to model the crack tip behaviour in this work so therefore a short description follows.

Henshell and Shaw (38) were the first to recognize that by placing the mid-side nodes at the quarter point in a quadratic isoparametric quadrilateral or triangular 2D element, fig. 3.1, a singularity in strain results at the nearest adjacent corner node. The singularity was found to be of order $1/\sqrt{r}$ as required by the Westergaard solution for the stress distribution around a sharp crack. Thus a very simple modification to the geometry of a standard isoparametric element permitted the elastic crack tip singularity to be modelled.

Barsoum (39) also studied quadratic 2D and 3D isoparametric elements. They introduced the idea in the 2D case of "collapsing" nodes along one edge, and placing the adjacent edge nodes the quarter point, fig. 3.2.

These collapsed degenerate elements also exhibited the $1/\sqrt{r}$ singularity for elastic crack tip stress fields. Barsoum also demonstrated that the collapsed triangular element is more accurate than the quadrilateral element. This is a result of the quadrilateral element only having the $1/\sqrt{r}$ singularity on the boundaries whereas the collapsed formulation contains the singularity along any ray interior to the element and emanating from the crack tip node(s).

In the 3D case one face of the brick element was "collapsed" into a line and the adjacent midside nodes were moved to the quarter points. This element is shown in fig. 3.3. The two "collapsed" isoparametric elements are the elements used to model the crack tip in the 2 and 3 dimensional work described in this report.

Higher order isoparametric elements have also been used to model the crack tip. Smith (30) modified the 2D cubic quadrilateral isoparametric element, which represents a cubic variation in displacement or a parabolic variation in stress, by collapsing one side and moving the mid side nodes to the one-ninth and four-ninths positions to produce the $1/\sqrt{r}$ crack tip singularity. This element is shown in fig. 3.4. The results produced by this crack tip element for the SIF at a weld toe crack are compared with the results of the present work in a later section of this report.

3.2 DETERMINATION OF FRACTURE PARAMETERS

In Linear Elastic Fracture Mechanics (LEFM) the parameters of interest are the stress intensity factors K_I, K_{II} and K_{III} or the energy release rate, G. To these can be added the J integral in 2D problems, which is directly related to G. The relationships between these parameters of LEFM are as follows:

$$G = -\frac{dP}{da} = J$$

$$G = \frac{\lambda}{E}(K_I^2 + K_{II}^2) + \frac{(1+\nu)}{E} K_{III}^2$$

where P is the potential energy, J is a contour integral and $\lambda = 1$ for plane stress and $(1-\nu^2)$ for plane strain.

The methods of extracting these parameters can be divided into three categories:

(i) substitution of nodal stresses or displacements in the classical equations in the crack tip vicinity

(ii) calculation of energy release rate, G

(iii) contour integration techniques around the crack tip

Methods (i) and (ii) are most popular in LEFM and (iii) is used extensively in Elasto-Plastic Fracture Mechanics, (EPFM).

In LEFM the J integral is directly related to G and therefore will not be discussed further in this report.

(i) Substitution in Classical Equations

In this approach the stresses or displacements obtained in the FE numerical solution are used with the classical equations of Westergaard near the crack tip to give a direct evaluation of the stress intensity factor. These equations are of the following form,

$$u = \frac{1+\nu}{4E}\sqrt{\frac{2r}{\pi}}\, K_I \left[(2\kappa-1)\cos\frac{\theta}{2} - \cos\frac{3\theta}{2}\right] + K_{II}\left[(2\kappa+3)\sin\frac{\theta}{2} + \sin\frac{3\theta}{2}\right] \quad (4)$$

$$\sigma_x = \frac{1}{\sqrt{2\pi r}} K_I \cos\frac{\theta}{2}\left[1 - \sin\frac{\theta}{2}\sin\frac{3\theta}{2}\right] - K_{II}\sin\frac{\theta}{2}\left[2 + \cos\frac{\theta}{2}\cos\frac{3\theta}{2}\right] \quad (5)$$

with similar expressions for v, w and σ_y, σ_z, τ_{xy}, τ_{yz}, τ_{zx}; $\kappa = 3-4\nu$ for plane strain and $\frac{3-\nu}{1+\nu}$ for plane stress.

These equations can be evaluated at a series of node points along a radial line emanating from the crack tip. The results are extrapolated to give values of stress intensity factor at r = 0. It has been shown that displacement substitution generally gives better results than stress substitution. This method has been employed in many investigations for the calculation of SIF. Tracey (40) made an important contribution in this respect, by deriving closed form expressions for K_I and K_{II} in terms of the solution displacements of the collapsed node isoparametric crack

elements when applied to 2D problems. For opening mode SIF, K_I this expression is given in fig. 3.5. Recently Ingraffea et al (41) have applied the same approach to the collapsed isoparametric wedge element used in 3D problems. They derive closed form expressions for the three stress intensity factors K_I, K_{II} and K_{III} as shown in fig. 3.6.

(ii) Energy Release Method

The basis of this method is equation (2) relating the crack extension energy to the loss in potential energy rate,

$$G = - \frac{dP}{da}$$

The potential energy for a finite element mesh is of the form

$$P = \frac{1}{2} \{u\}^T [K] \{u\} - \{u\}^T \{L\} \qquad (A)$$

where $\{u\}$ is the displacement vector

$[K]$ is the stiffness matrix

$\{L\}$ is the load vector

Thus the potential energy can be found for two different portions of crack separated by Δa as

$$- \frac{dP}{da} = \frac{P_1 - P_2}{\Delta a}$$

However, this method of obtaining G requires two separate FE solutions and is uneconomic.

Parks (42) introduced a modification to this process called the stiffness derivative method, and was followed by Hellen (43) with an alternative called the virtual crack extension method. Both methods are essentially the same and require only one solution to the complete set of FE equations.

Differentiating equation (A)

$$\frac{dP}{da} = -\frac{1}{2}(u)\frac{d[K]}{da}(u) + (u)^T \frac{d(L)}{da}$$

The matrix $\frac{d[K]}{da}$ represents a change in global stiffness matrix per unit crack advance. Refering to fig.3.7 an increment of crack advance can be obtained by rigidly translating all nodes on or within the contour Γ_o about the crack tip by an infinitesimal amount δa in the x direction, all other nodes remain in their initial position. The global matrix will only change in the band of elements between contours Γ_o and Γ_1 and

$$\frac{d[K]}{da} = \sum_{i=1}^{N} \frac{d[K_i]}{da}$$

where N is the number of such elements.

The methods of Parks and Hellen differ only in the method by which $\frac{dP}{da}$ is calculated and a detailed description of the methods may be found in references (42) and (43) respectively.

3.3 NUMERICAL CALCULATION OF STRESS INTENSITY FACTOR

3.3.1 The ASAS FE Program

The finite element analysis and the calculation of K_I in this project were carried out using the finite element program ASAS. The ASAS program together with its many pre- and post-processors and graphics display system is a comprehensive general purpose finite element system. The main program incorporates facilities for linear elastic static stress analysis, natural frequency analysis and heat conduction analysis. The system has an extensive library of element types and a wide range of loading and boundary condition types. Also included are a comprehensive series of data checking procedures which check input data for errors and consistency.

The pre- and post-processors cover a wide range of capability from mesh generation and graphic display to load case combination and stress contour plotting.

Included in the H version of the program is a multi-level sub-structuring capability and an enhanced linear elastic fracture mechanics analysis capability.

3.3.2 Multi-Level Substructuring Capability of ASAS-H

This facility greatly extends the flexibility and power of the main program. This facility is described in detail in (44) but a short description is included here for convenience. The component analysis included in ASAS-H is an implementation of the technique known in other forms as substructuring or superelements. The ASAS system allows the user to create master components from finite elements or previously formed components. The model of the total structure is then formed from the component parts and solved for the displacements at the nodes, in a similar way to the assembly and solution of a single level finite element model. The displacements and stresses can then be recovered for any or all of the individual components from the ASAS backing files.

In the creation of a structural model the ASAS system provides for translation, rotation and mirroring of components so that the symmetry of the structure may be utilized to the maximum extent. An example of this procedure taken from (44) is shown diagramatically in figure 3.8. This component approach can save considerably in costs thus making possible analyses which were hitherto too expensive.

A theoretical description of the process used in this component analysis capability is given in (45).

This program capability was used extensively in this project particularly for the 3D analysis.

3.3.3 LEFM Capability of ASAS-H

ASAS-H contains three crack tip elements based on the degenerate isoparametric elements described by Barsoum (39). These elements are:

(i) a triangular membrane element with six nodes (CTM6) shown in figure 3.2

(ii) a wedge shaped brick type element with 15 nodes (CB15) shown in figure 3.3

(iii) a triangular axisymmetric ring element with six nodes (CTX6).

There is no stress output with these elements because of the stress singularity at the crack tip and the rapid variation of stress across the element. The stress intensity factors can be obtained using the global displacements as outlined in figures 3.5 and 3.6, and extrapolation to the crack tip or by the FRAKAS post-processor which will be described in a subsequent section.

3.3.4 The FRAKAS Post-Processor

As stated in the previous section the degenerate isoparametric elements in ASAS-H have no stress output and the stress intensity factor is not immediately available. For load cases producing pure mode 1 loading of the crack the stress intensity factor can be evaluated by substitution of the nodal displacements in the Westegaard equation. For more general, mixed mode problems the FRAKAS post-processor is used to calculate the energy release rate. The FRAKAS program is a post-processor which utilizes the backing files from ASAS version H to provide the energy release rate G by means of the virtual crack extension technique of Hellen (43). This post-processor can also be used in conjunction with the ASAS-H substructuring capability. In this procedure the crack area may be isolated into one small substructure and the remainder of the structure is idealized as usual, as shown in figure 3.9. These two master components can then be analysed. To investigate different crack growths the sub-structure containing the crack is rerun for slightly varied crack geometries. Therefore it is possible to analyse any number of different substructure crack geometries within the same global analysis.

In the work reported in chapter IV the stress intensity factors, in the 2D case were obtained in two ways:

(i) using the global displacements as outlined in fig. 3.5 and extrapolation to the crack tip.

(ii) using the post-processor FRAKAS. This post-processor is used in conjunction with the multilevel substructuring capability to calculate the energy release rate G. In this procedure the crack area is isolated into one small substructure and the remainder of the structure is idealized as usual, as shown in fig. 3.9. These two master components can then be analysed. To investigate different crack growths the substructure containing the crack is rerun for slightly varied crack geometries. It is thus possible to analyse any number of different substructure crack geometries within the same global analysis. Given the energy release rate and the fact that K_{II} and K_{III} are zero, equation reduces to

$$K_I = \sqrt{\frac{GE}{\lambda}}$$

In the 3D work the SIF were calculated using displacement substitution in the equations outlined in fig. 3.6.

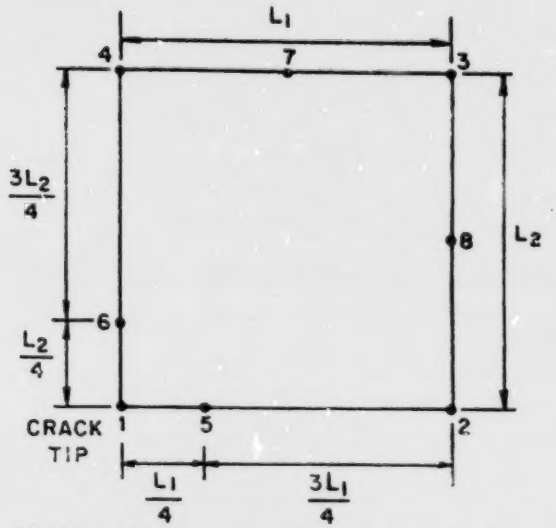

QUADRILATERAL ELEMENT WITH MID-SIZE NODES AT QUARTER POINTS

FIG. 3.1

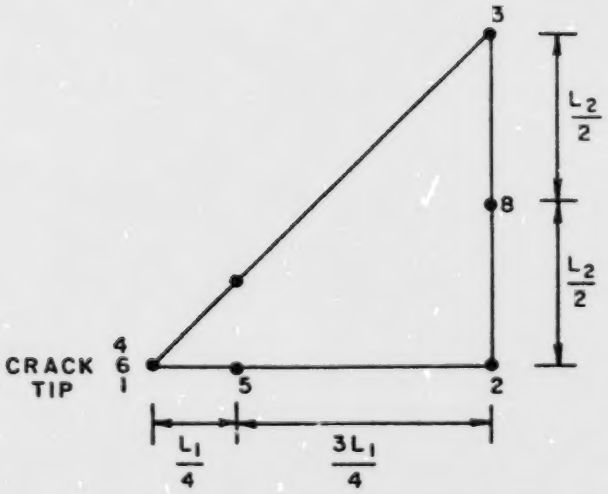

COLLAPSED ISOPARAMETRIC ELEMENT WITH MID-SIZE NODES AT QUARTER POINTS

FIG. 3.2

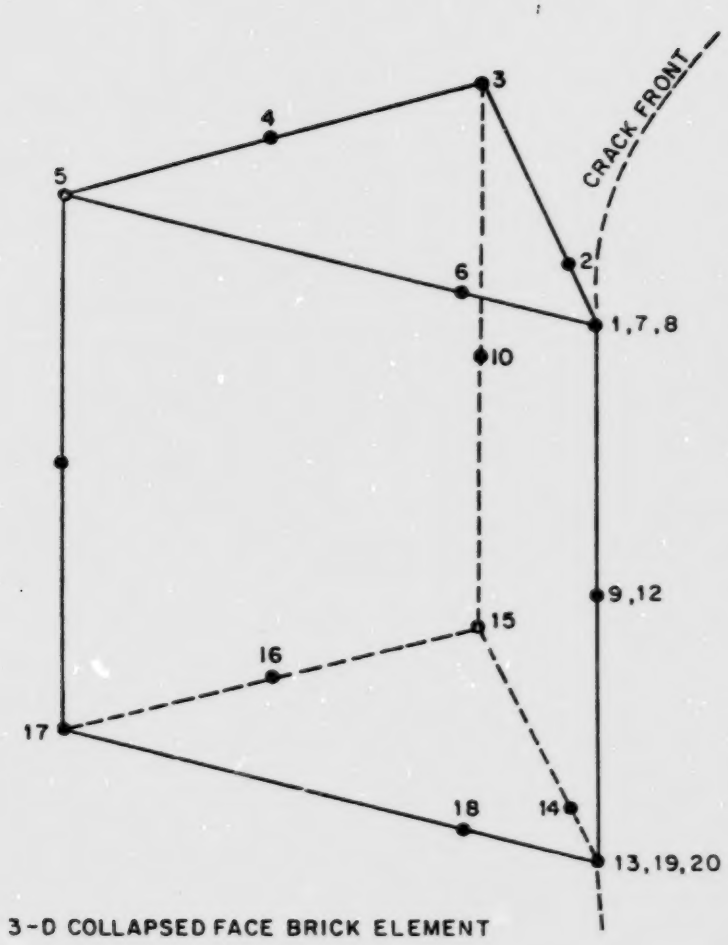

3-D COLLAPSED FACE BRICK ELEMENT

FIG. 3.3

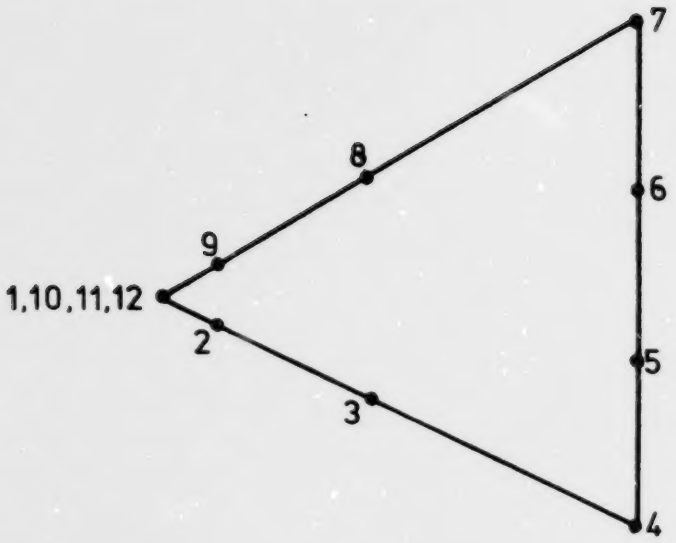

CUBIC CRACK TIP ELEMENT

FIG. 3.4

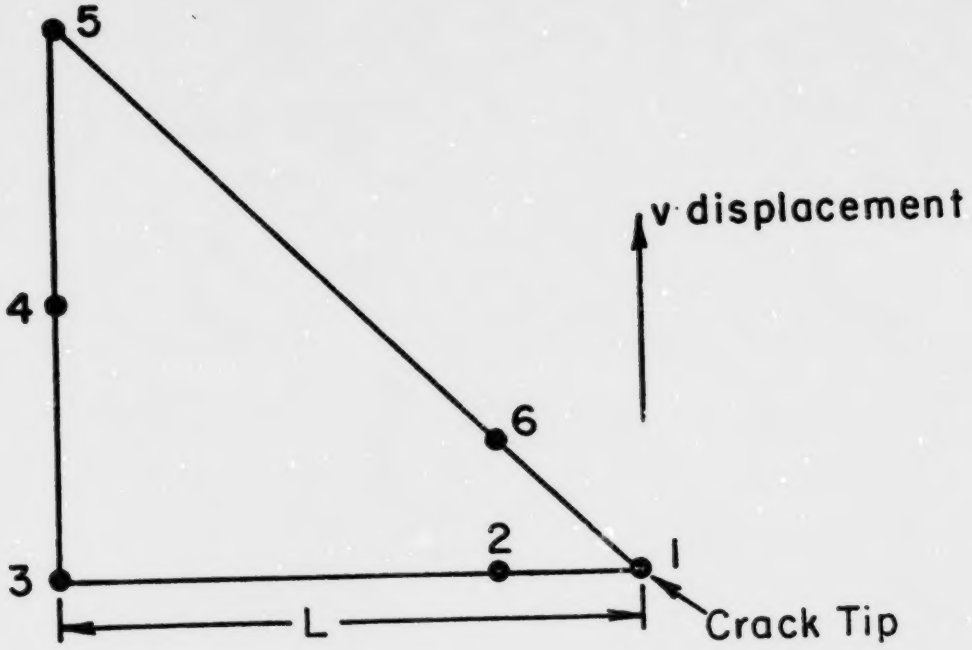

$$V_C = V_3 - V_1$$

$$V_B = V_2 - V_1$$

$$K_I = \frac{2G\sqrt{2\pi}\ (4V_B - V_C)}{(k+1)\sqrt{L}}$$

Where $k = 3 - 4\nu$ for plane strain

$k = (3-\nu)/(1+\nu)$ for plane stress

Thus K_I may be estimated using only 3 displacement values.

ALGEBRAIC CALCULATION OF K_I

FIG.3.5

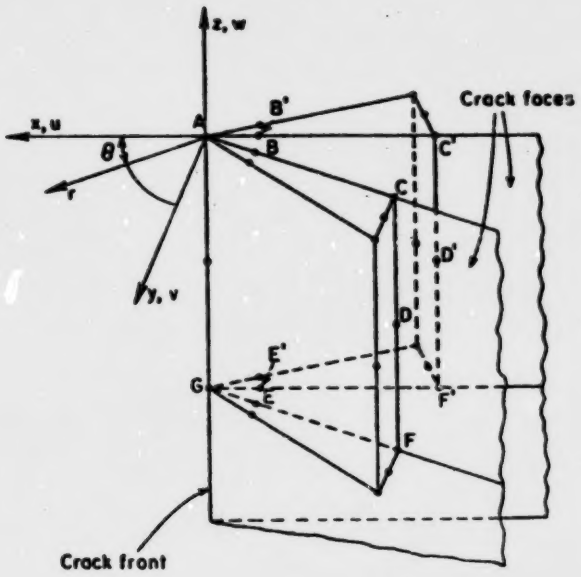

$$K_I = \frac{E}{4(1-\nu^2)}\sqrt{\left(\frac{\pi}{2L_1}\right)}[2v_B - v_C + 2v_E - v_F + v_D - 2v_{B'} + v_{C'} - 2v_{E'} + v_{F'} - v_{D'}$$
$$+\tfrac{1}{2}\eta(-4v_B + v_C + 4v_E - v_F + 4v_{B'} - v_{C'} - 4v_{E'} + v_{F'})$$
$$+\tfrac{1}{2}\eta^2(v_F + v_C - 2v_D - v_{F'} - v_{C'} + 2v_{D'})]$$

$$K_{II} = \frac{E}{4(1-\nu^2)}\sqrt{\left(\frac{\pi}{2L_1}\right)}[2u_B - u_C + 2u_E - u_F + u_D - 2u_{B'} + u_{C'} - 2u_{E'} + u_{F'} - u_{D'}$$
$$+\tfrac{1}{2}\eta(-4u_B + u_C + 4u_E - u_F + 4u_{B'} - u_{C'} - 4u_{E'} + u_{F'})$$
$$+\tfrac{1}{2}\eta^2(u_F + u_C - 2u_D - u_{F'} - u_{C'} + 2u_{D'})]$$

and

$$K_{III} = \frac{E}{4(1+\nu)}\sqrt{\left(\frac{\pi}{2L_1}\right)}[2w_B - w_C + 2w_E - w_F + w_D - 2w_{B'} + w_{C'} - 2w_{E'} + w_{F'} - w_{D'}$$
$$+\tfrac{1}{2}\eta(-4w_B + w_C + 4w_E - w_F + 4w_{B'} - w_{C'} - 4w_{E'} + w_{F'})$$
$$+\tfrac{1}{2}\eta^2(w_F + w_C - 2w_D - w_{F'} - w_{C'} + 2w_{D'})]$$

Arrangement of quarter-point wedge elements along segment of crack front with nodal lettering convention

FIG. 3.6

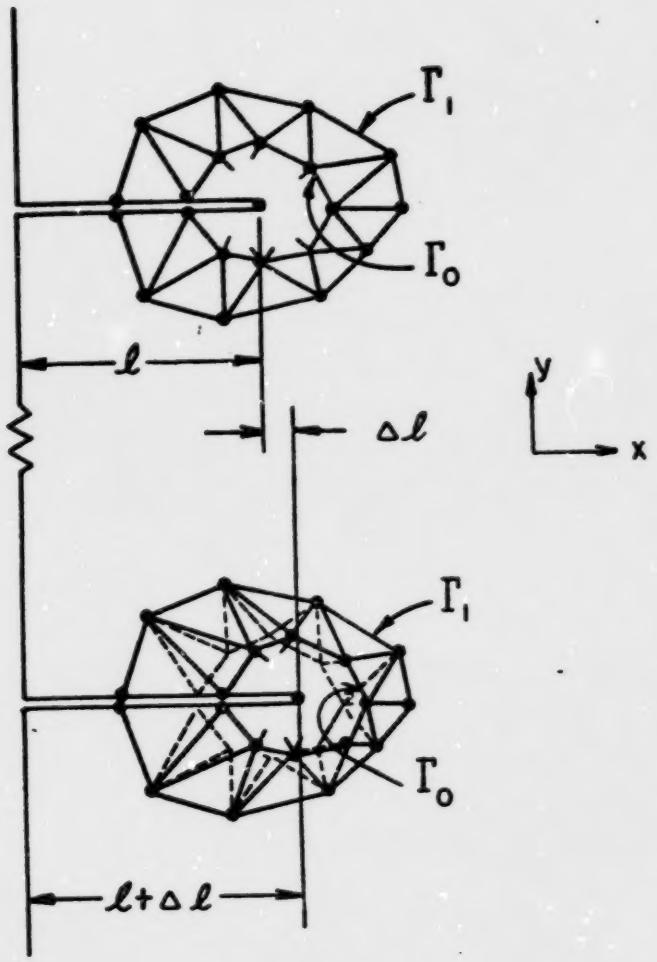

ACCOMODATION OF CRACK EXTENSION BY ADVANCING NODES

FIG. 3.7

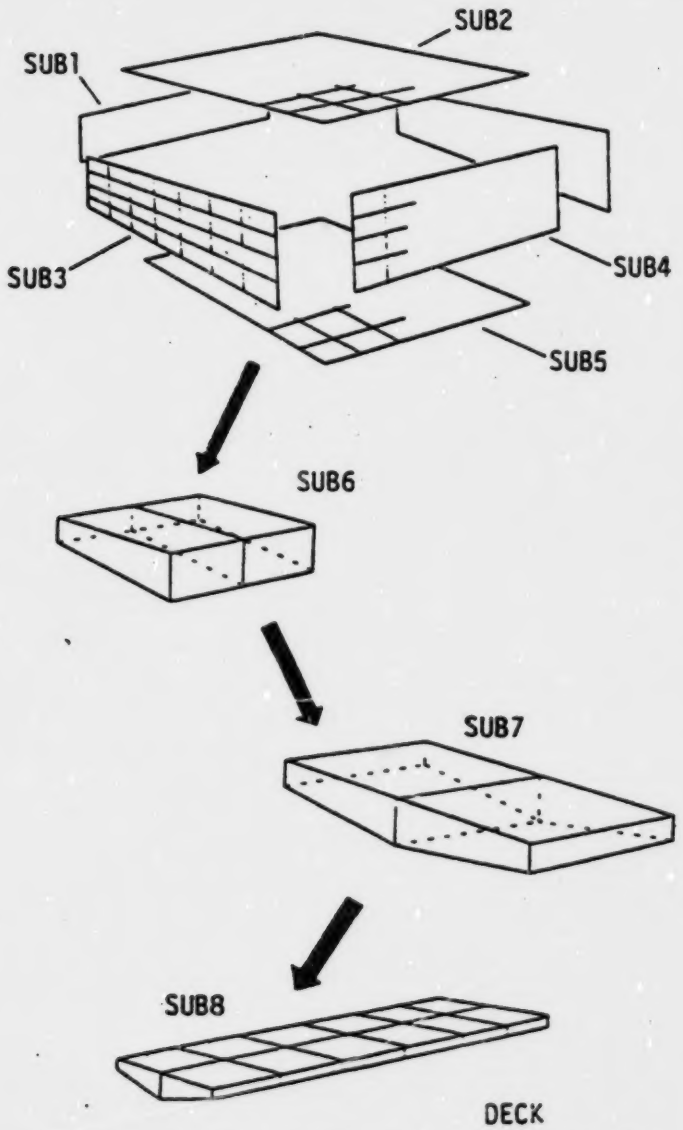

STAGES IN THE CONSTRUCTION OF A MODEL FOR A BRIDGE DECK

Multilevel Substructuring Analysis Using ASAS

FIG. 3.8

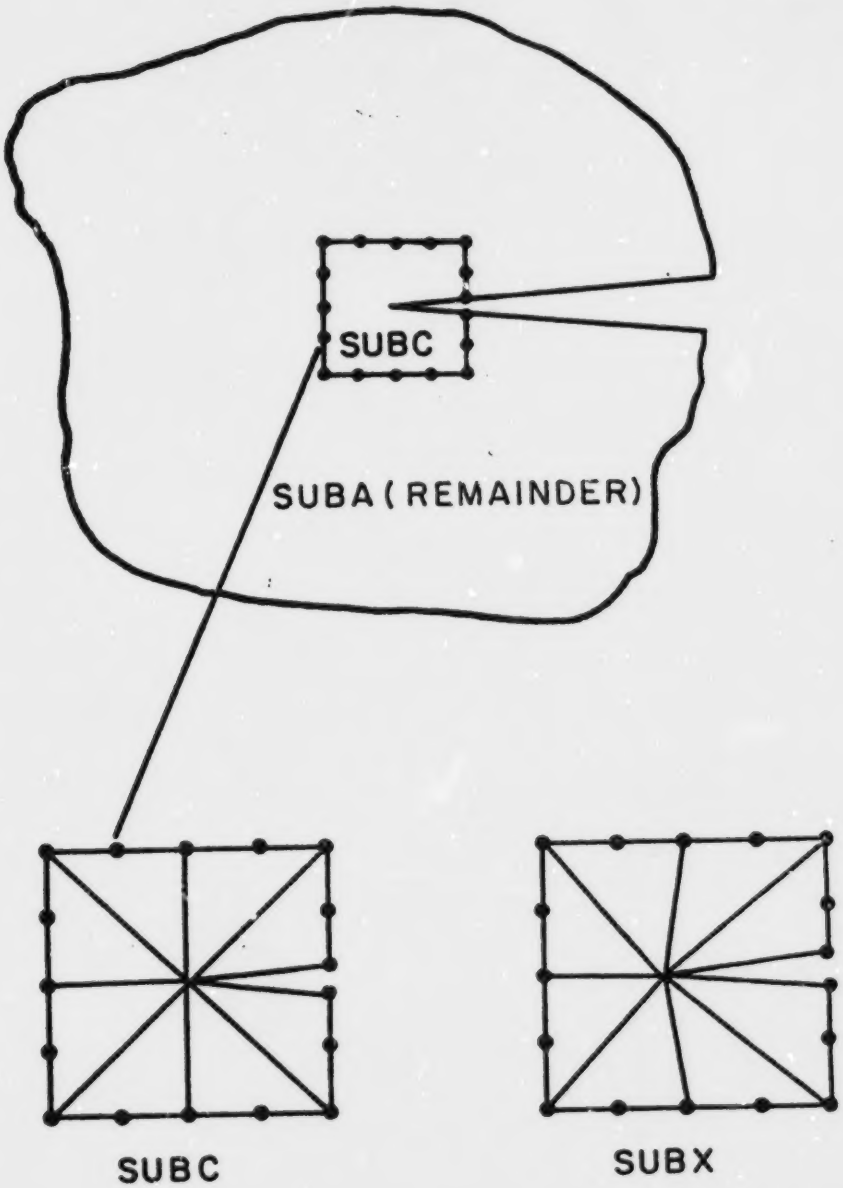

TYPICAL CRACK TIP SUBSTRUCTURES

MASTER COMPONENTS FOR A FRAKAS ANALYSIS: NOTE LINK NODES ON SUBC AND SUBX MUST CORRESPOND, ALTHOUGH INTERNALS WILL BE DIFFERENT.

FIG. 3.9

CHAPTER IV

4. 2-DIMENSIONAL STUDIES

4.1 Introduction

This chapter describes the 2-dimensional crack studies for a 'T' joint loaded in bending as required by the work statement detailed in section 1 of this report. Also included are the modelling techniques used and the accuracy checks carried out on the crack tip elements.

In the final section the stress distribution and the stress concentration factor at the weld toe of an uncracked joint is presented.

4.2 2-D Modelling of Welded Joint

In any structural FE analysis an important consideration is the modelling of the structure. This is particularly so in the case of a structure which contains a crack because of the stress singularity and the $1/\sqrt{r}$ stress variation around the crack tip. In the 2-dimensional work presented in this section the crack tip region was modelled using the ASAS CTM6 collapsed isoparametric element (as described in chapter 3) and the remainder of the structure by quadratic isoparametric QUM8 elements. The substructuring capability of the ASAS program was used extensively to reduce the costs of the weld shape investigations and to carry out the energy evaluation of K_I using the post-processor FRAKAS, as outlined in section 3.3.4.

In order to check the accuracy and performance of the FE program to analyse a weld toe crack and to assess the adequacy of the mesh some initial tests were performed using a non-load-carrying fillet weld joint (NLCFW). Some of the variables considered in these preliminary analyses were:

1) number of elements along the crack surface
2) ratio of crack tip element size to regular element size
3) use of transition elements
4) comparison of displacement prediction of K_I with the energy prediction of K_I using FRAKAS

The NLCFW joint is shown in fig. 4.1. Since there are two planes of symmetry only one quarter of the joint was analysed. A typical FE mesh is shown in fig. 4.2. This joint was also analysed by Gurney and Johnston (29) who modelled the joint using a very large number of constant strain triangular finite elements and by Smith (30) who represented the crack region of the joint by cubic isoparametric crack tip elements.

The present results are compared with those of Gurney and Johnston and Smith for a joint with a 45^{o} weld angle in table 4.1. The crack depth ratios considered were, $a/t = 0.02$, 0.1 and 0.3; where a = the crack depth and 2t = the plate thickness.

The K_I values obtained were normalised with respect to the results for a cracked plate with no weld present following the procedure first used by Maddox (27). In the case of a NLCFW joint the normalising factor is the stress intensity factor for a double edge cracked plate of width 2t. Hence, $K = M_K K'$ where K' is the K_I value of the edge cracked plate and M_K is the correction factor to account for the presence of the weld.

From the results of the preliminary analyses using the 2-D crack tip elements experience was developed regarding the mesh required, in terms of number and size of the elements along the crack face, required to give adequate accuracy in the calculation of the stress intensity factor. Also it was found that the use of transition elements, particularly in a mesh which was well designed in terms of crack tip element size, and the variation of element size along the crack face, made very little improvement in the results, so it was decided to not use transition elements in future 2-D analyses.

In addition the preliminary tests indicated, and it can be seen from table 4.1, that the displacement calculations of SIF were within a few percent of the SIF calculations using the energy approach. Therefore, it was decided that the extra effort and costs involved in carrying out the energy calculations were not justified and the displacement calculations of SIF produced acceptable accuracy.

The results of K_I for a NLCFW produced by the ASAS program were within 6% of those published by Smith (30) and this was deemed acceptable for the present work.

4.3 'T' Specimen - 2-Dimensional Results

The specimen shape chosen for these investigations is the proposed test specimen for the experimental program on corrosion fatigue at CANMET, shown in fig. 4.3. This specimen and loading configuration, 3 point bending, was chosen because it was felt that a load-carrying fillet weld joint better represented the behaviour of the weld region of a tubular joint than the non-load-carrying plate joints tested in the UKOSRP and ECSC programs.

The nominal weld leg length was restricted to 0.5t where t = the plate thickness. Three weld shapes were chosen arbitrarily for the investigation of the effect of weld shape on the SIF at the weld toe crack. These shapes are shown in fig. 4.4. The 70^{o} shape was chosen as being representative of an actual weld, the 45^{o} shape as an intermediate profile and the 30^{o} weld shape as representative of a weld after weld profiling.

A typical finite element mesh used in the calculations is shown in fig. 4.5. This model has a vertical line of symmetry and therefore the specimen modelled has a crack at each weld toe. In most cases it is expected that the 'T' joints tested in the experimental program will have only toe cracks at one of the welds. This discrepency was investigated by carrying out an analysis on a complete 'T' model with one unsymmetrical crack as shown in fig. 4.6. This analysis, reported

in (48) showed that there was no significant difference between the SIF for a 'T' specimen with a single crack and one with symmetrical toe cracks. Therefore it was decided in the FE analyses to model the joint with a vertical line of symmetry to reduce computing costs.

The FE model was also divided into substructures as shown in fig. 4.7 so that the computing costs for modelling the combinations of weld shapes and different crack depths was reduced.

The FE models were loaded in both 3-point bending (load-carrying) and also in 4-point bending (non-load-carrying). The loads between the two load cases were adjusted so that the bending moments in each case at the plane of the crack were identical.

The results for the a/t ratios detailed in section 1.2 and for the weld shapes and loading cases described above are given in tables 4.2 - 4.3 and are presented graphically in figs. 4.8 and 4.9 . Once again the results are presented in terms of a magnification factor M_K. In these cases the normalising configurations were a single edge crack in a plate subjected to 3-point and 4-point bending, and the SIF of each case was calculated using formulae presented by Rooke and Cartwright (46).

The plots shown in figs. 4.8 and 4.9 demonstrate the variation of M_k for increasing values of crack depth a/t. It can be seen that the value of M_k approaches 1.0 for a/t >0.7 which is similar to the findings

reported by Gurney and Johnston (29). For values of a/t from 0.7 to 0.1 the variation of M_k is approximately linear and at values of a/t < 0.1 there is a rapid increase because of the influence of the weld. The trends are essentially the same for both 3-point and 4-point bending loadcases. The magnitude of the difference between the results for the two loadcases is less than anticipated with a maximum difference in M_k of 8.4% for a/t = 0.01. At value of a/t > 0.3 this difference is negligible as shown in table 4.4.

It is evident from tables 4.2 and 4.3 that the weld angle has a significant effect on the stress intensity factor particularly for small crack sizes. The effect of weld profiling can be demonstrated by considering the results shown in table 4.5; for example for a crack depth ratio of a/t = 0.005 there is a 30% reduction in M_k between a simulated as welded profile (70^o) and a profiled weld (30^o). This effect disappears rapidly with increasing crack depth.

Some calculations were performed using the finite element displacements on the crack face from the 3-point bending loadcase to obtain estimates of K_{11} but the relevant displacements were very small and there was not enough significant figures in the FE displacement results to make accurate calculations.

Using the results shown in table 4.2 for the 3-point bending loadcase empirical expressions were obtained for M_k as a function of a/t. A log-log plot of M_k vs a/t confirmed the two regions which were governed

by different power relationships between M_k and a/t. These regions are $a/t < 0.1$ and $0.1 < a/t < 0.7$. Approximate empirical relationships were fitted to the finite element results in these two regions.

In the region $a/t < 0.1$ the effect of weld geometry is significant and a power relationship of the following form was obtained.

$$M_k = C(a/t)^m \qquad \text{I}$$

where C and m are both functions of θ, the weld angle. The following values of C and m were obtained for the values of weld angle considered:

θ	C	m
30^o	0.758	-0.218
45^o	0.668	-0.278
70^o	0.594	-0.329

It is of interest to note that Gurney and Johnston (29) obtained the same value of m for a 45^o weld angle on a cruciform joint loaded in tension.

C and m, can be obtained by the following approximate expressions for the weld angle considered ($30^o \leqslant \theta \leqslant 70^o$)

$$C = 0.582 \sin \theta^{-0.386} \qquad \text{II}$$

$$m = -0.3447 \sin \theta^{0.654} \qquad \text{III}$$

All results obtained using expressions I - III for $a/t < 0.1$ are in agreement with the finite element results to within $\pm$ 3%.

In the region $a/t > 0.1$ the effect of weld geometry on the values of M_k is less significant. The following expression was obtained for M_k in this region.

$$M_k = 1.031 \, (a/t)^{-0.111} \qquad \text{IV}$$

All results obtained using this expression for $a/t > 0.1$ agree with the finite element results to within $\pm$ 2%.

4.4 Stress Analysis of an Uncracked Joint

A stress analysis was carried out on a series of uncracked 'T' joints of different thicknesses and with weld angles of 45^{o} and 60^{o}, as required by the amended work statement included in appendix I. The geometries considered are shown in fig. 4.10.

The joints were modelled using ASAS QUM8 isoparametric elements and the loading was 3-point bending. For each joint thickness and weld angle the length L (fig. 4.10) was kept constant at 300 mm and the load P was adjusted so that the maximum nominal stress σ_x at the weld toe was unity. For each case the weld leg length was t/2.

The stress variation σ_x along the x direction in the vicinity of the weld toe for the required five thickness values and two weld angles are shown in figs. 4.11 to 4.15, and the numerical values of stress concentration at the weld toe are tabulated in table 4.6. Figures 4.16 to 4.20 give the variation of σ_x through the thickness in the plane of the weld toe, (section AA, fig. 4.10).

As can be seen from table 4.6, the stress concentration factor (SCF) at the weld toe increases with increasing thickness. It should be noted that if the joints of different thickness were geometrically similar, (i.e. the size and loads were scaled), then the S.C.F. for each joint thickness would be identical.

In order to check that the increase in S.C.F. with increasing thickness was not a FE mesh effect, the mesh for the 15 mm joint with weld angle 45^{o} was geometrically scaled to model the 103 mm joint. This scaling included the support distance. It was found from this analysis that the S.C.F. for the 103 mm joint was identical to the S.C.F. for the 15 mm joint, thus confirming that the change in S.C.F. with increasing thickness was not due to the FE mesh.

In the results reported in table 4.6 the only variable which was not scaled was the distance from the support to the weld toe, i.e. (300 - t/2). This distance was different for each joint thickness and the load P was modified in each case so that unit nominal stress σ_x was maintained at the weld toe. It can therefore be concluded that the distance from the support point to the weld toe is responsible for the above increase in the S.C.F.

TABLE 4.1

Variation of M_k with crack depth for NLCFW:

Weld leg length $.5t$ and Weld Angle 45^o

	M_k		
a/t	Present Study	Gurney & Johnston (29)	Smith (30)
0.02	2.169 D 2.234 E	2.432	-
0.1	1.294 D 1.303 E	1.50	1.38
0.3	1.103 D 1.122 E	1.159	1.1

D displacement calculation

E energy release calculation

TABLE 4.2

Variation of M_k with a/t for 3-Point Bending Loadcase

a/t	M_k		
	30^o Weld	45^o Weld	70^o Weld
0.005	2.443	2.978	3.514
0.01	2.064	2.390	2.680
0.015	1.882	2.121	2.309
0.02	1.754	1.938	2.090
0.03	1.630	1.765	1.854
0.04	1.489	1.604	1.676
0.05	1.454	1.522	1.570
0.07	1.367	1.416	1.449
0.08	1.336	1.378	1.404
0.1	1.331	1.332	1.353
0.3	1.160	1.161	1.160
0.5	1.122	1.122	1.122
0.7	1.074	1.074	1.080

TABLE 4.3

Variation of M_k with a/t for 4-Point Bending Loadcase

a/t	M_k		
	30^o Weld	45^o Weld	70^o Weld
0.005	2.331	2.791	3.271
0.01	1.945	2.247	2.471
0.015	1.800	2.002	2.175
0.02	1.692	1.852	1.967
0.03	1.563	1.674	1.745
0.04	1.447	1.526	1.586
0.05	1.387	1.447	1.483
0.07	1.308	1.353	1.370
0.08	1.282	1.314	1.333
0.1	1.256	1.270	1.284
0.3	1.115	1.112	1.115
0.5	1.085	1.093	1.093
0.7	1.074	1.080	1.080

TABLE 4.4

% Difference in M_k Between 3-Point Bending and 4-Point Bending Load Cases

a/t	% Difference Between 3 and 4 Point Bending		
	30^o Weld	45^o Weld	70^o Weld
0.005	4.8	6.3	7.4
0.01	6.1	6.3	8.4
0.015	4.5	5.9	6.2
0.02	3.6	4.6	6.3
0.03	4.3	5.1	5.4
0.04	2.9	5.1	5.7
0.05	4.8	5.1	5.9
0.07	4.5	4.6	5.8
0.08	4.2	4.9	5.3
0.1	5.9	4.9	5.3
0.3	4.0	4.3	4.0
0.5	3.4	1.7	1.7
0.7	-	-	-

TABLE 4.5

% Change in M_k Due to Weld Shape

for 3-Point Bending Loadcase

a/t	Weld Shape		% Reduction ($70^o \rightarrow 30^o$)
	70^o	30^o	
0.005	3.514	2.443	30.5
0.01	2.680	2.064	23.0
0.015	2.309	1.882	18.5
0.02	2.090	1.754	16.1
0.03	1.854	1.630	11.6
0.04	1.676	1.489	11.1
0.05	1.570	1.454	7.3
0.07	1.449	1.367	5.6
0.08	1.404	1.336	4.8
0.1	1.353	1.331	1.6
0.3	1.160	1.160	-
0.5	1.122	1.122	-
0.7	1.080	1.074	0.5

TABLE 4.6

S.C.F. at Weld Toe of Uncracked 'T' Joint

$t_{(mm)}$	S. C. F.	
	45^{o} Weld	60^{o} Weld
15	3.29	3.49
28	3.32	3.53
53	3.38	3.62
78	3.44	3.71
103	3.51	3.94

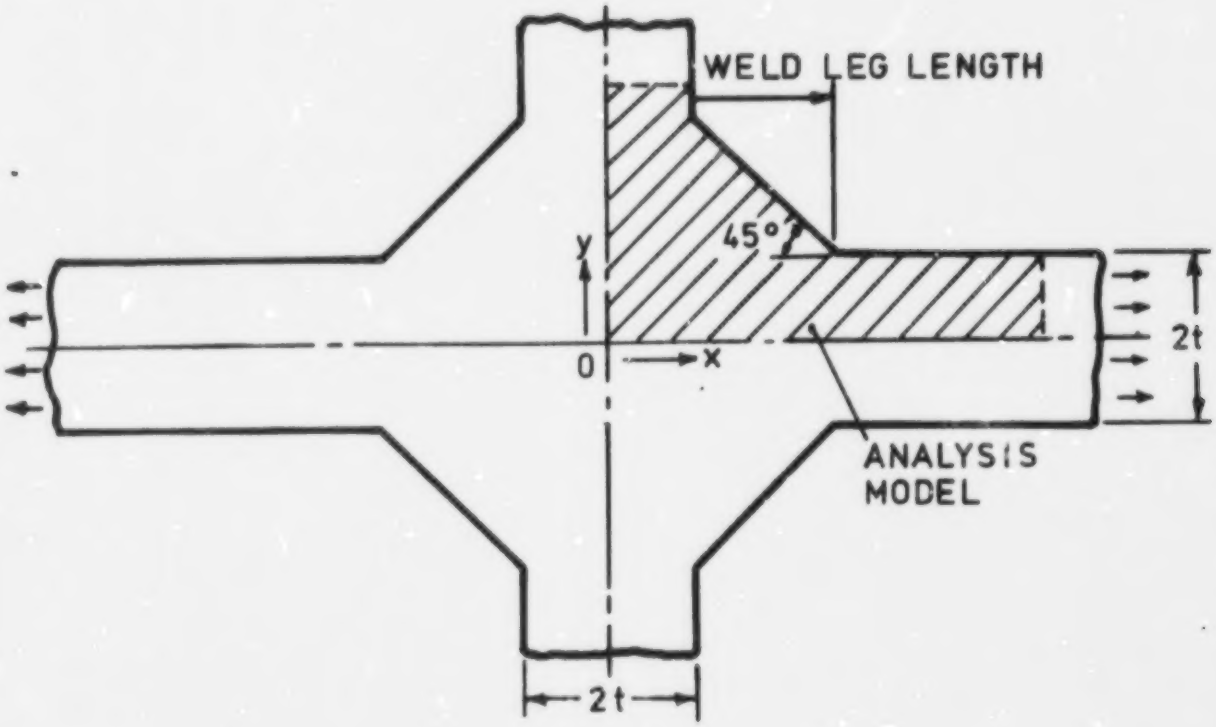

NON-LOAD-CARRYING FILLET WELD (NLCFW) JOINT

FIG. 4.1

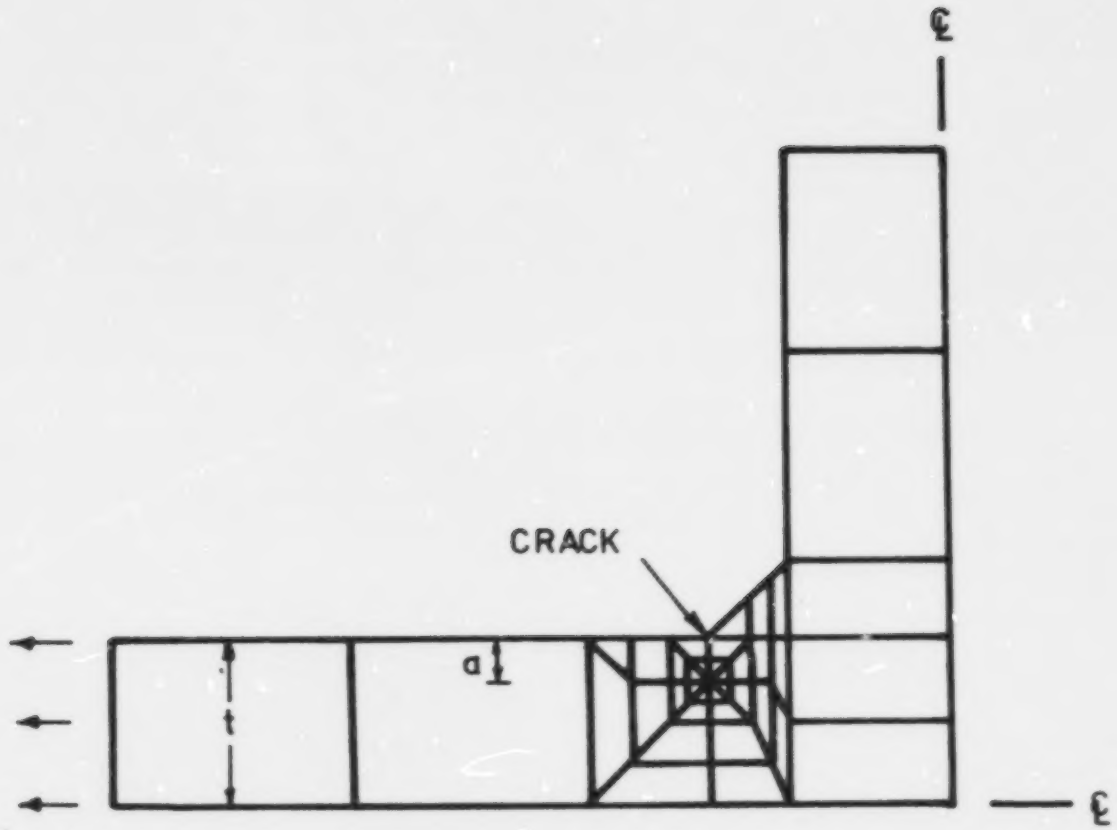

FE MODEL

FIG. 4.2

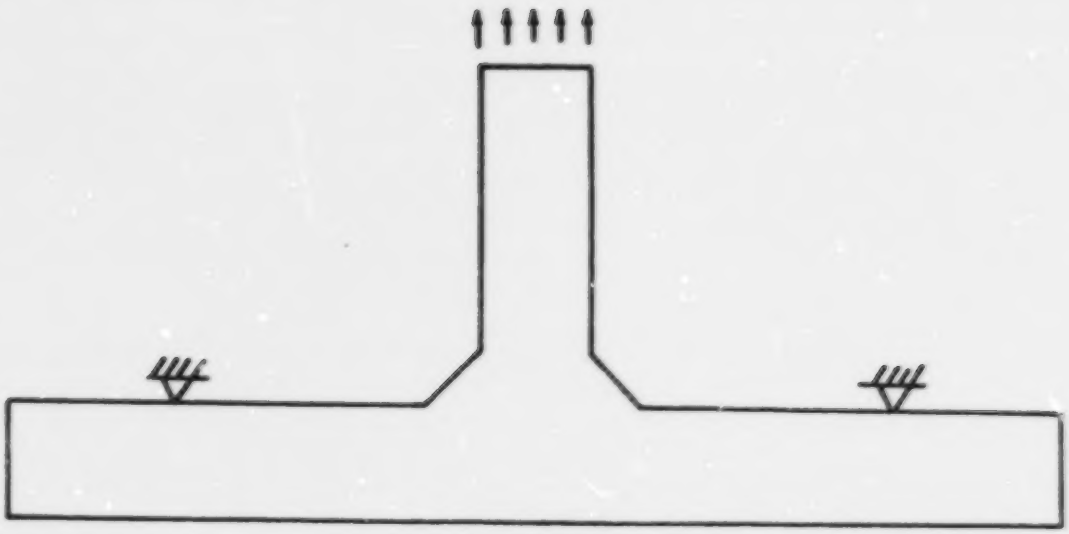

"T" SPECIMEN

FIG. 4.3

WELD SHAPES

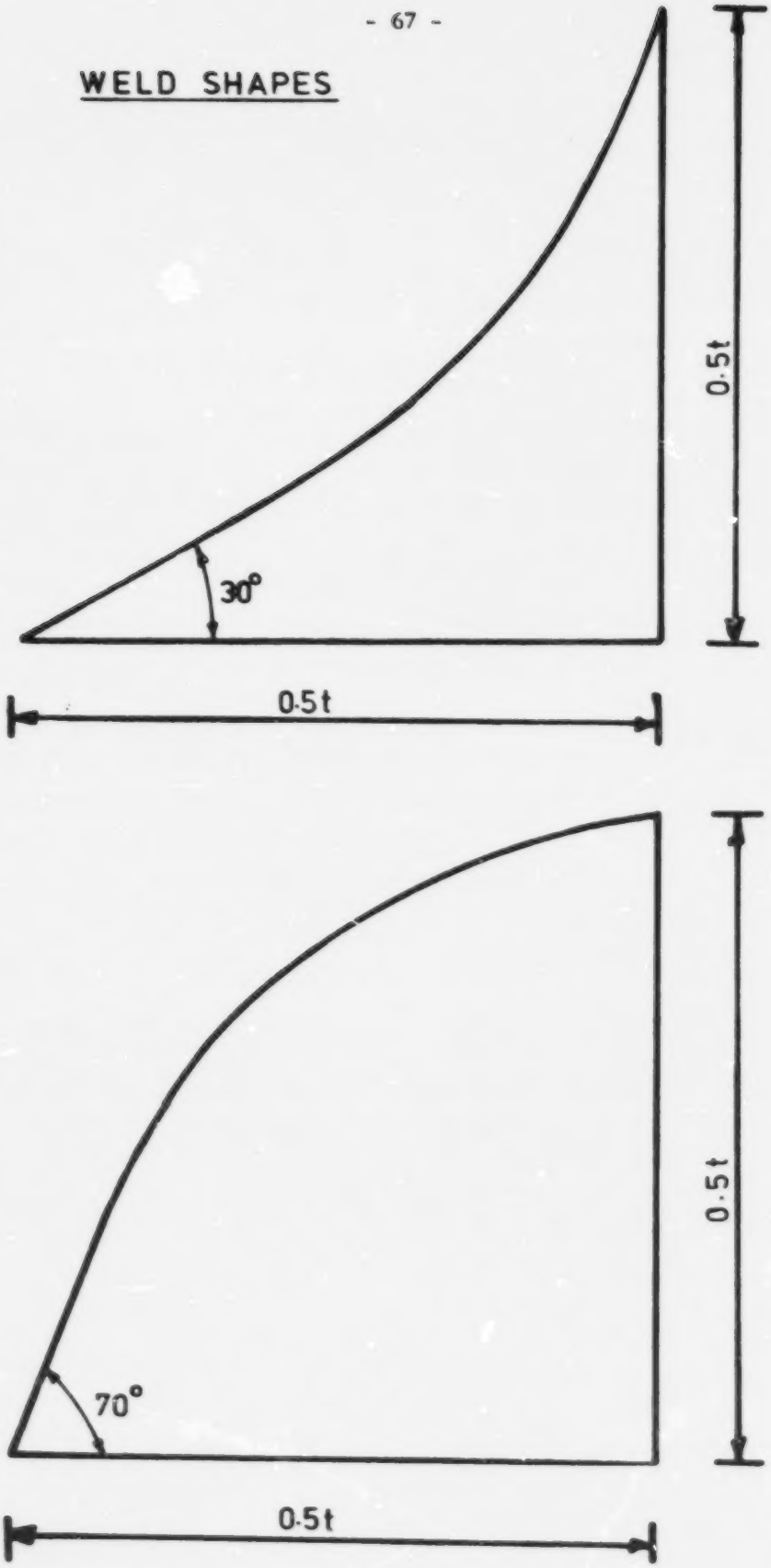

FIG. 4.4

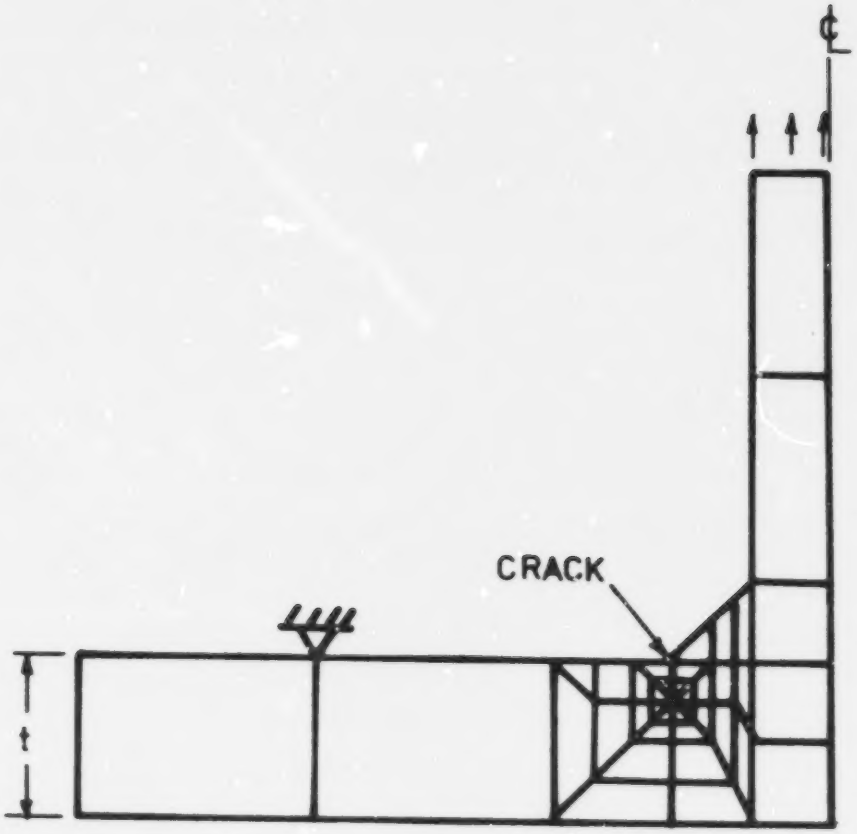

FE MODEL FOR "T" SPECIMEN

FIG. 4.5

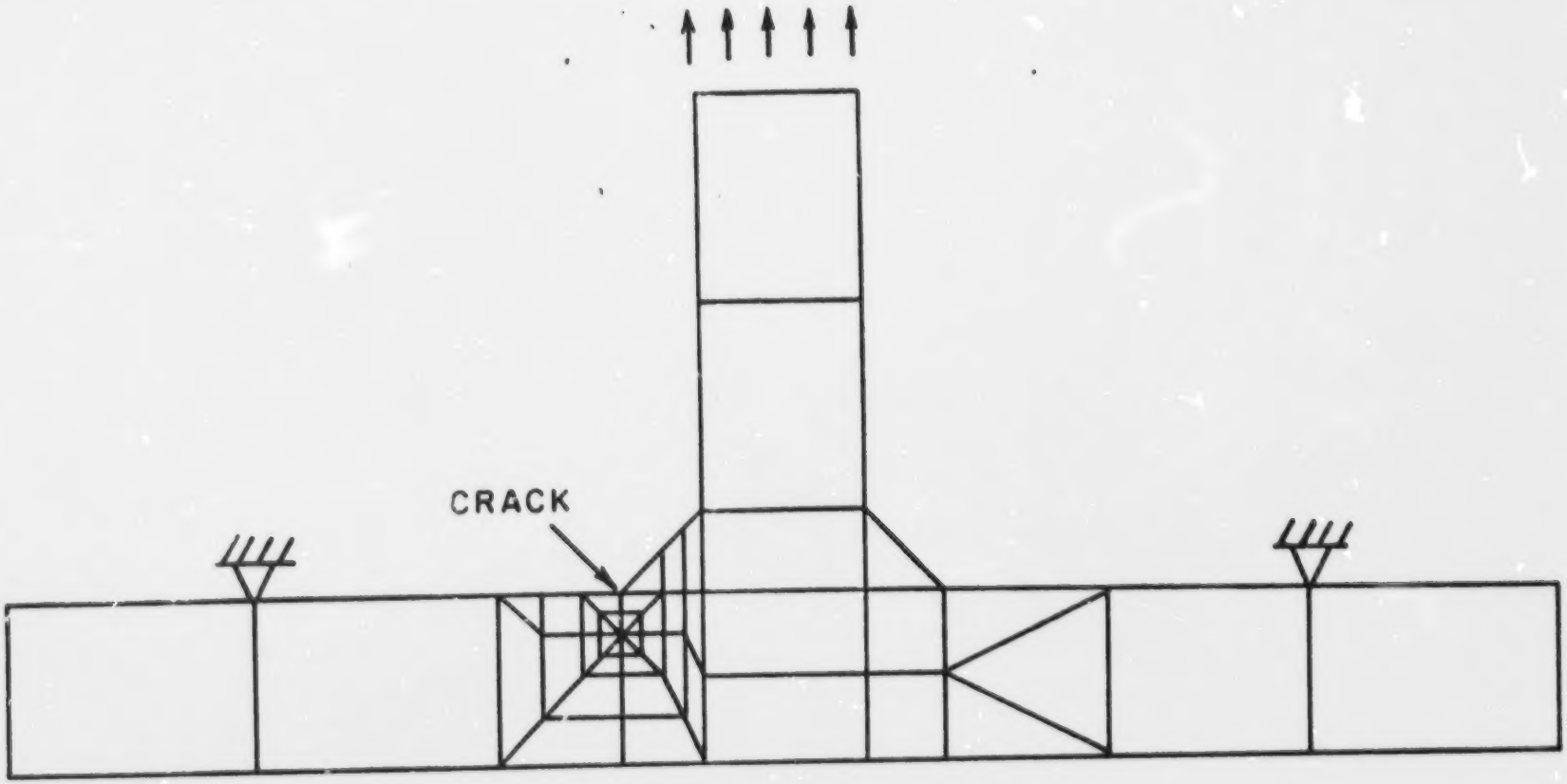

SINGLE – CRACK "T" SPECIMEN

FIG. 4.6

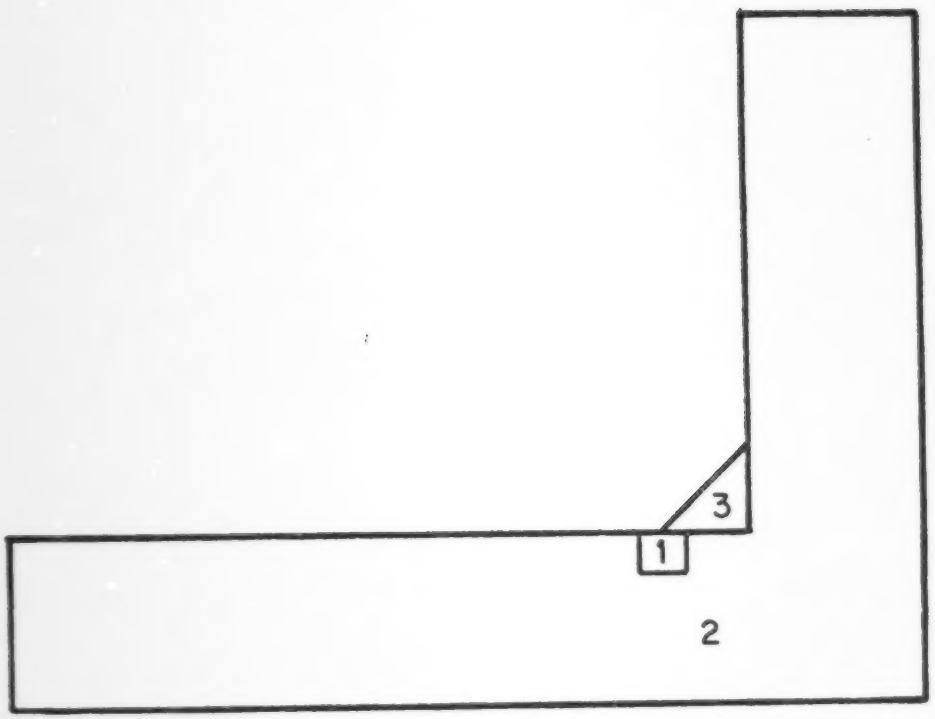

SUBSTRUCTURE REPRESENTATION

FIG. 4.7

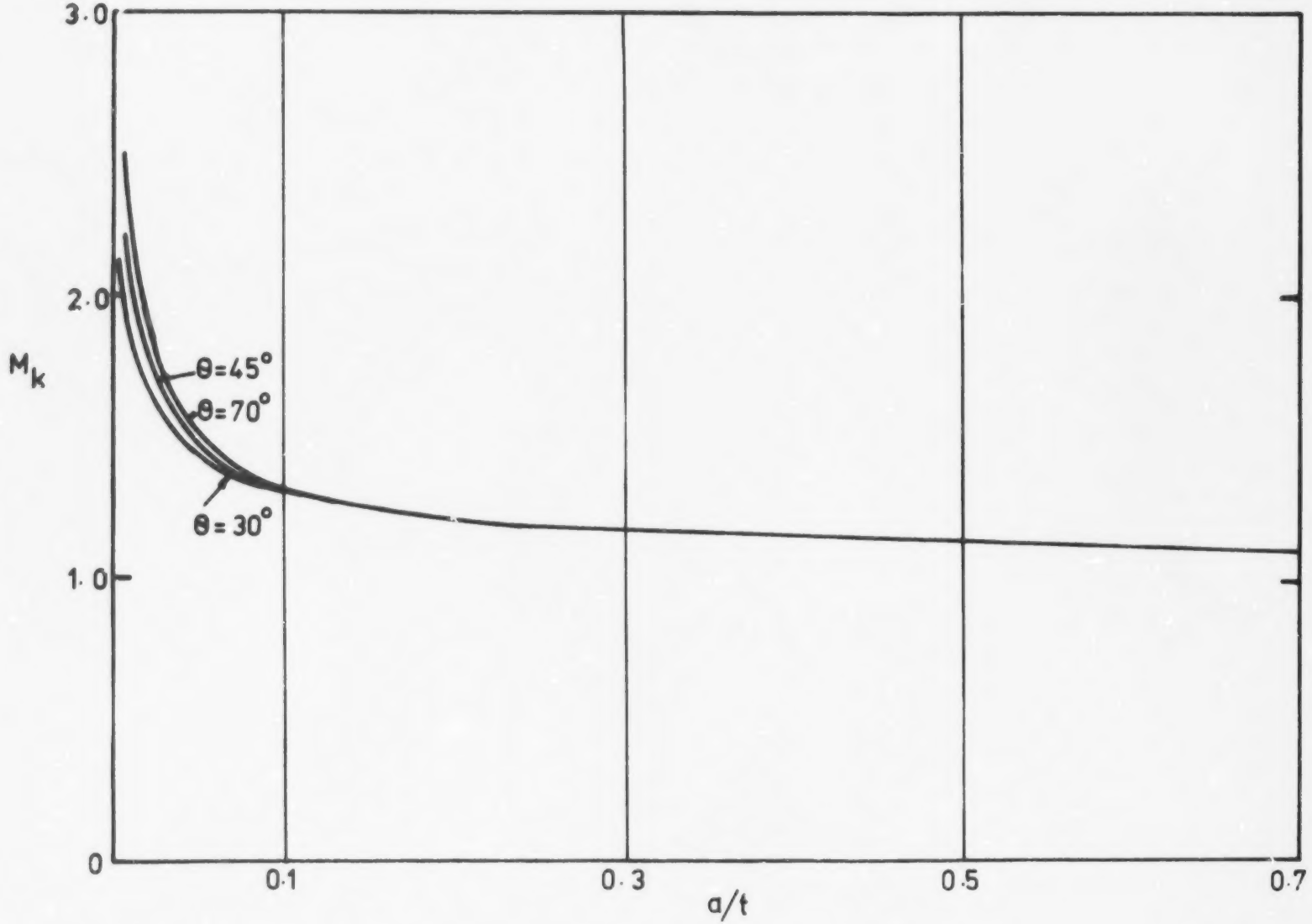

M_k vs a/b FOR 3 POINT BENDING

FIG. 4.8

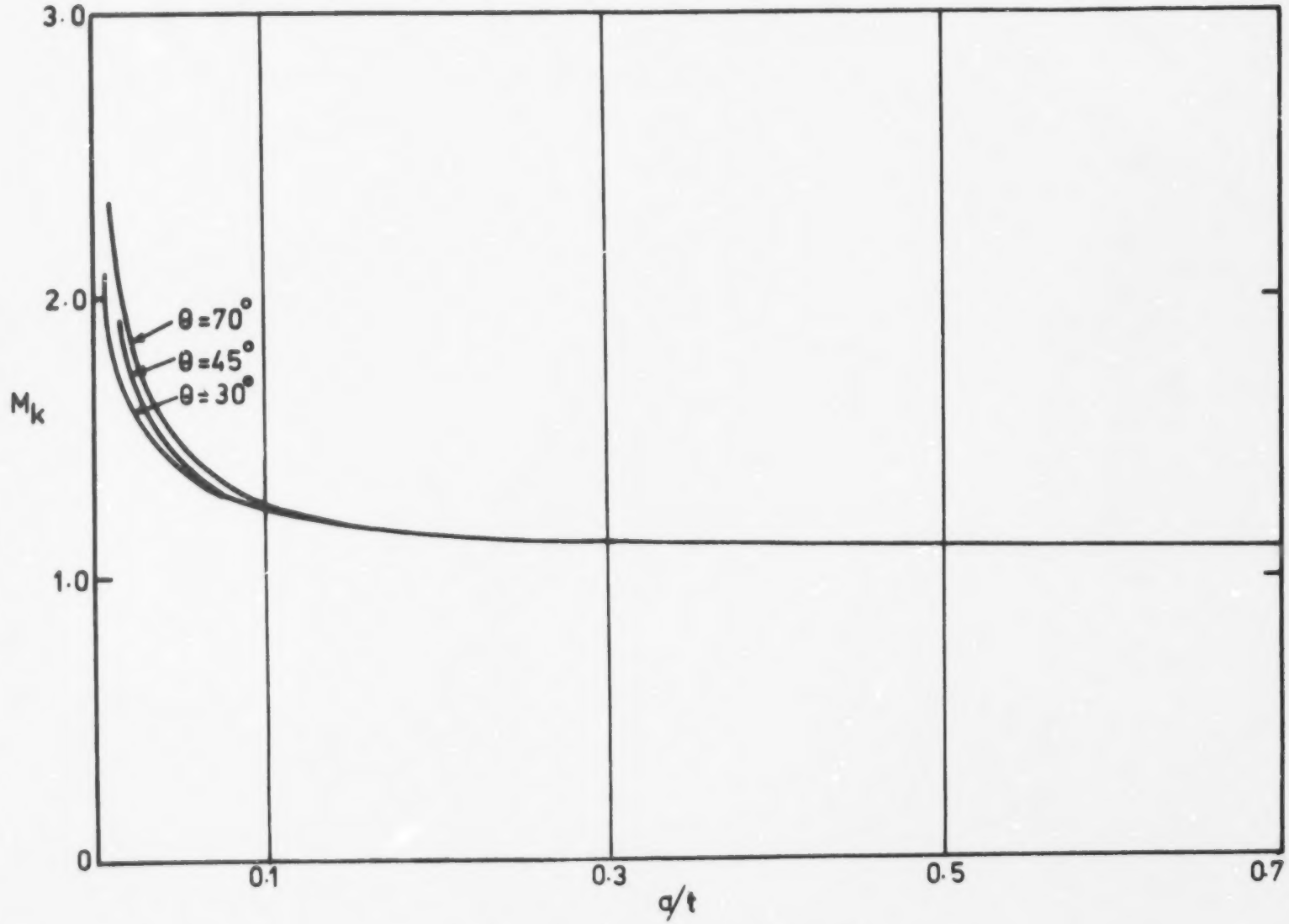

M_k vs a/b FOR PURE BENDING

FIG. 4.9

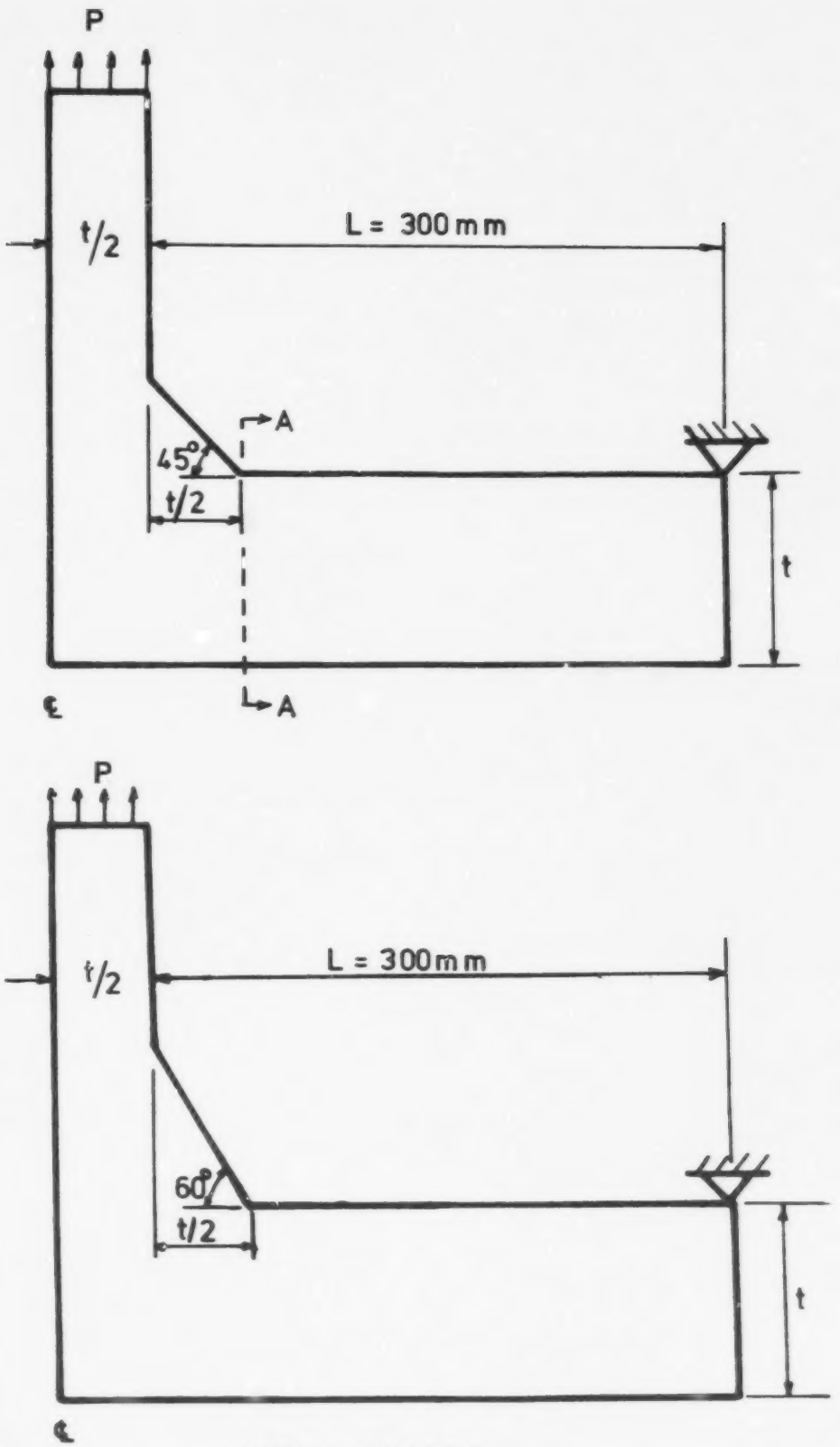

WELD SHAPES

FIG. 4.10

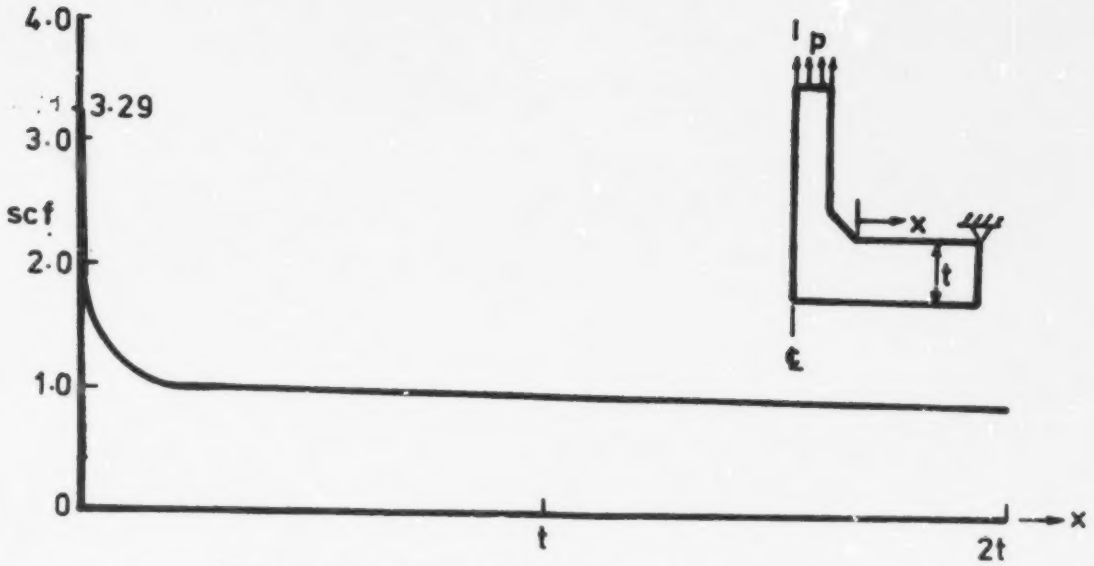

STRESS CONCENTRATION FACTOR AT WELD TOE
VARIATION OF σ_x IN x DIRECTION
WELD ANGLE 45° t = 15 mm

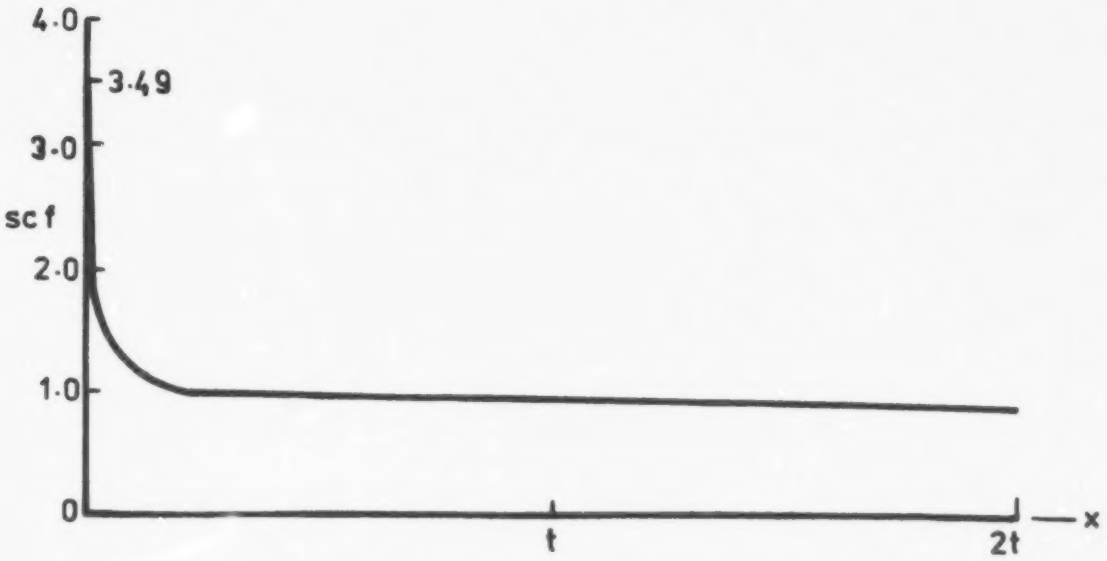

STRESS CONCENTRATION FACTOR AT WELD TOE
VARIATION OF σ_x IN x DIRECTION
WELD ANGLE 60° t = 15 mm

FIG. 4.11

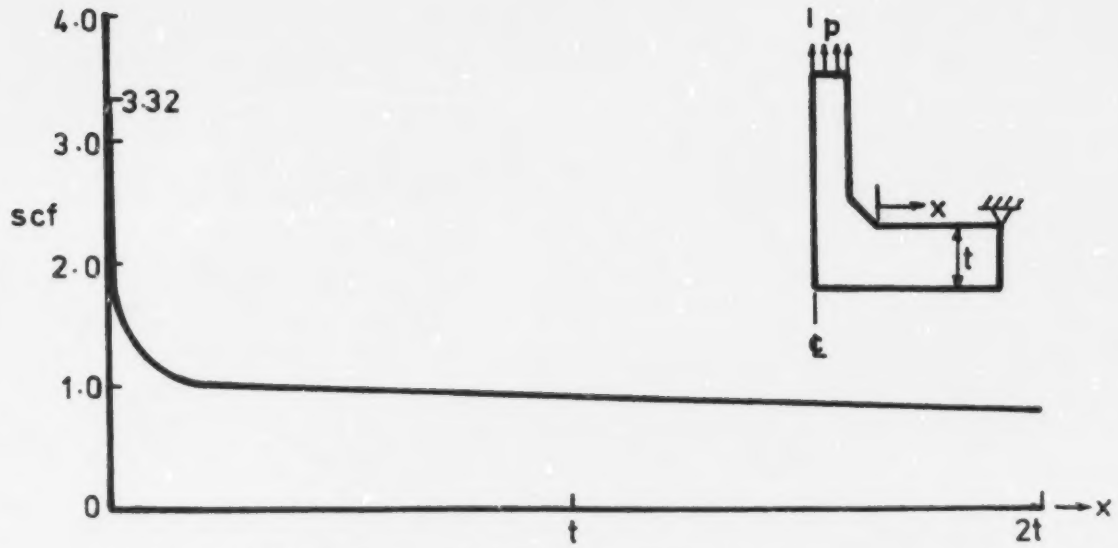

STRESS CONCENTRATION FACTOR AT WELD TOE
VARIATION OF σ_x IN x DIRECTION
WELD ANGLE 45° t = 28 mm

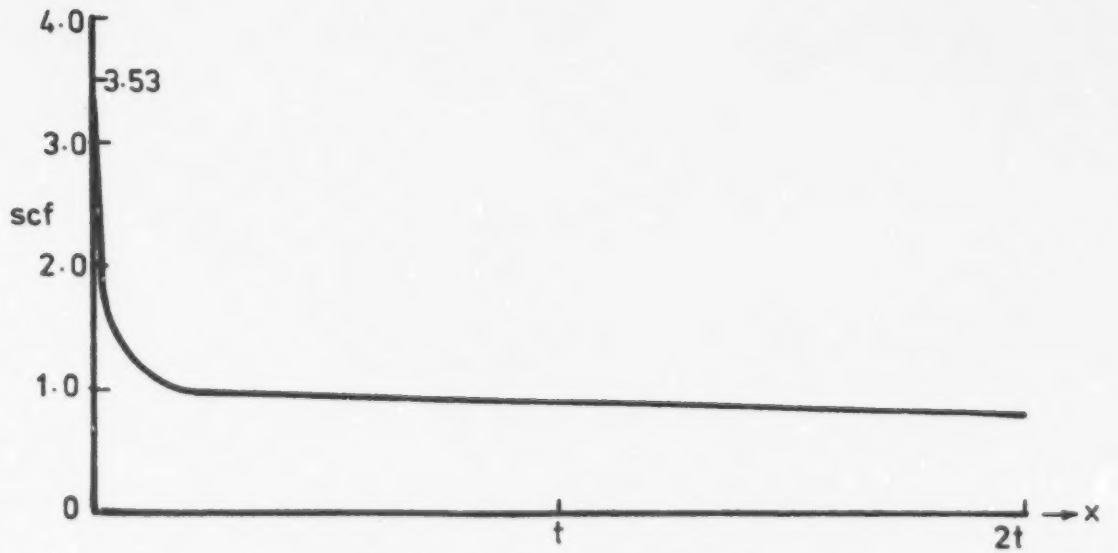

STRESS CONCENTRATION FACTOR AT WELD TOE
VARIATION OF σ_x IN x DIRECTION
WELD ANGLE 60° t = 28 mm

FIG. 4.12

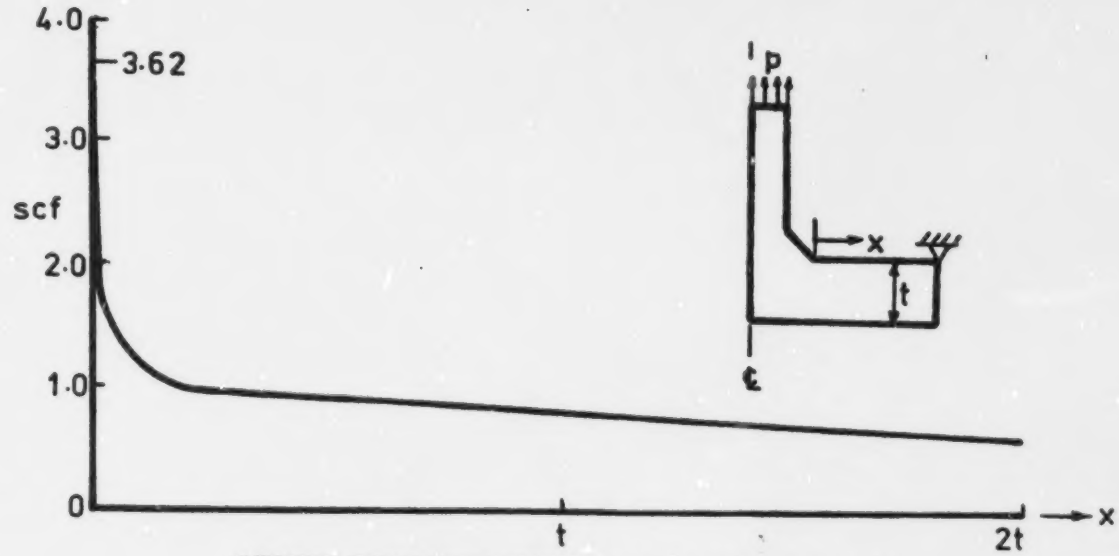

STRESS CONCENTRATION FACTOR AT WELD TOE

VARIATION OF σ_x IN x DIRECTION

WELD ANGLE 60° t = 53 mm

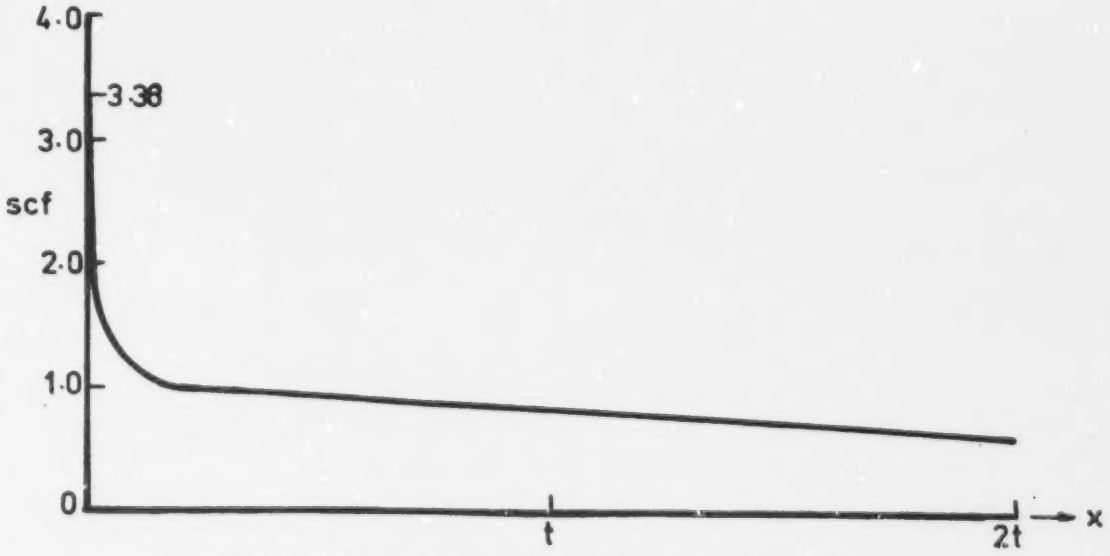

STRESS CONCENTRATION FACTOR AT WELD TOE

VARIATION OF σ_x IN x DIRECTION

WELD ANGLE 45° t = 53 mm

FIG. 4.13

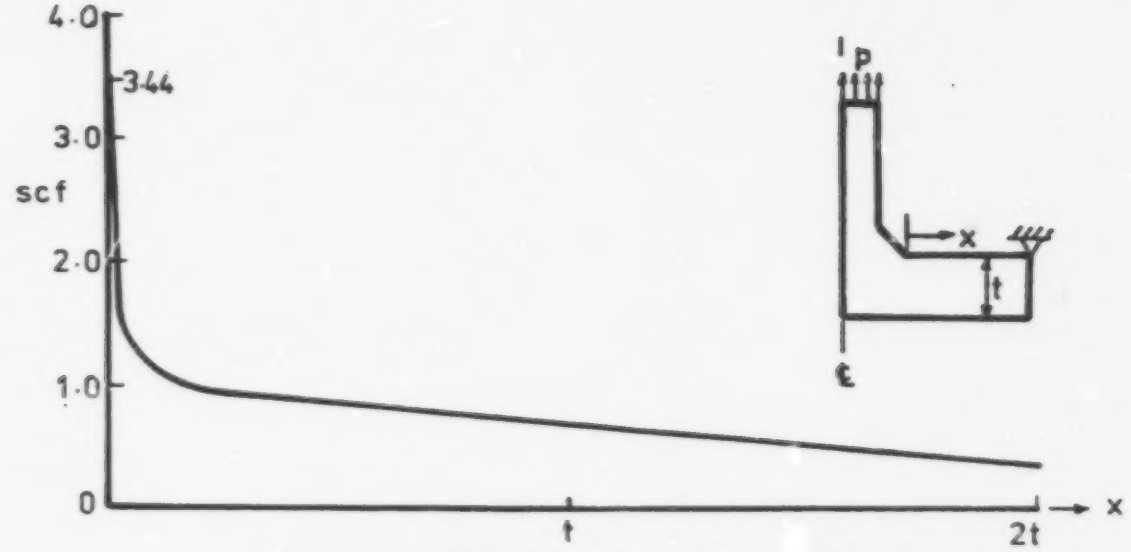

STRESS CONCENTRATION FACTOR AT WELD TOE

VARIATION OF σ_x IN x DIRECTION

WELD ANGLE 45° t = 78 mm

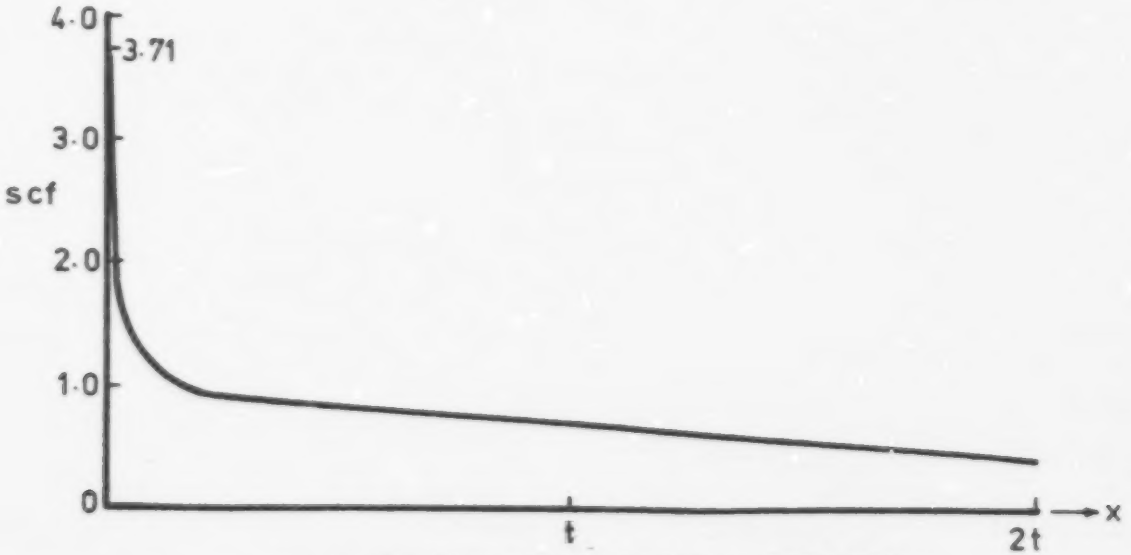

STRESS CONCENTRATION FACTOR AT WELD TOE

VARIATION OF σ_x IN x DIRECTION

WELD ANGLE 60° t = 78 mm

FIG. 4.14

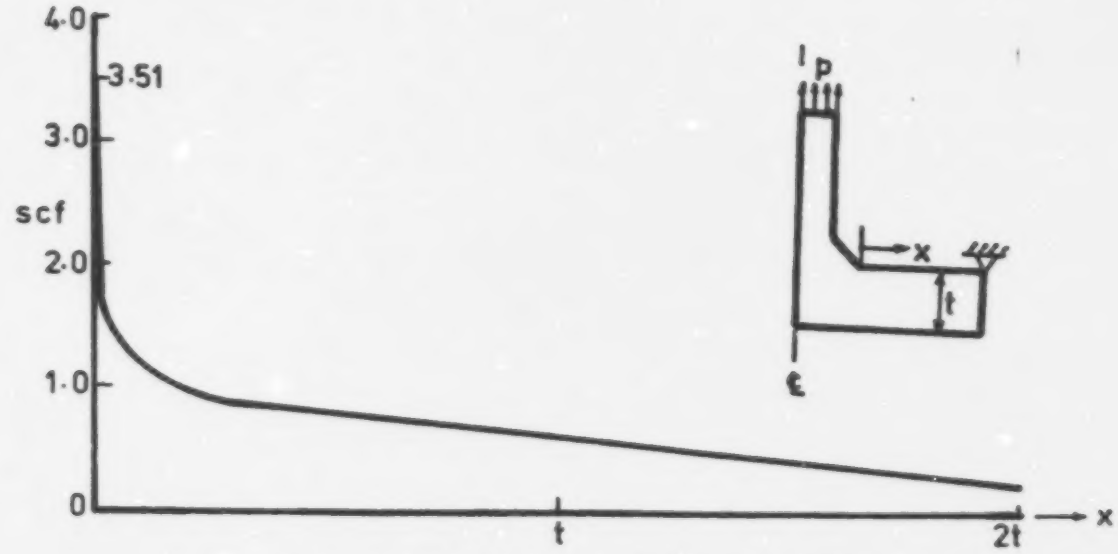

STRESS CONCENTRATION FACTOR AT WELD TOE
VARIATION OF σ_x IN x DIRECTION
WELD ANGLE 45° t = 103 mm

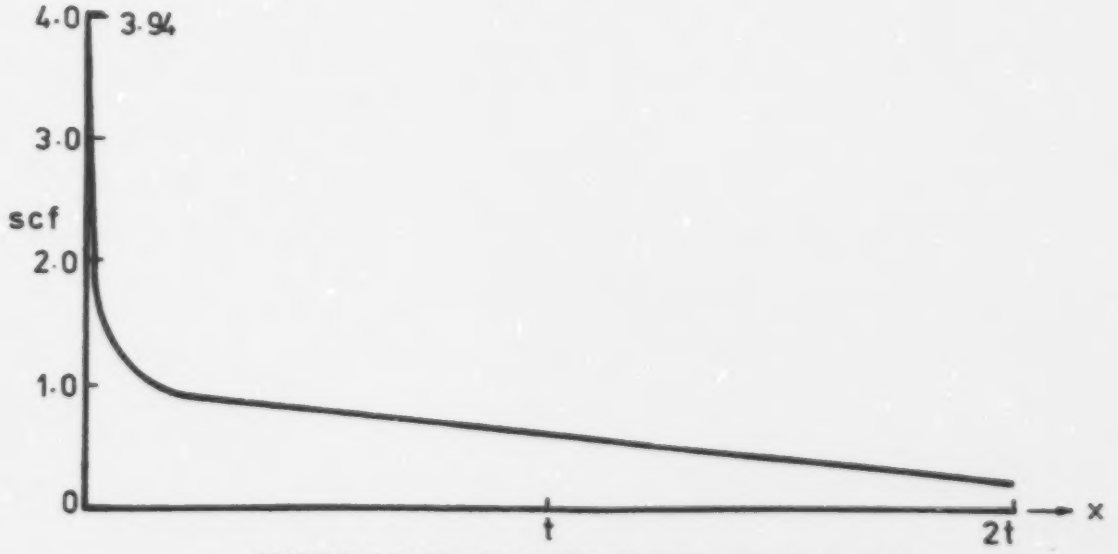

STRESS CONCENTRATION FACTOR AT WELD TOE
VARIATION OF σ_x IN x DIRECTION
WELD ANGLE 60° t = 103 mm

FIG. 4.15

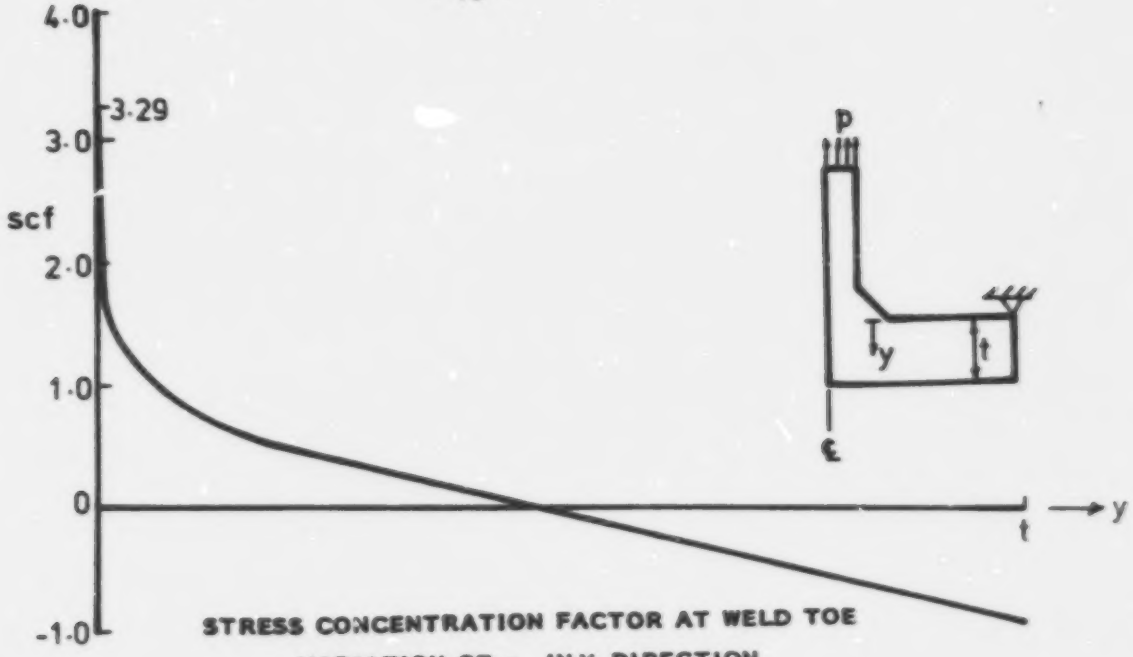

STRESS CONCENTRATION FACTOR AT WELD TOE
VARIATION OF σ_x IN y DIRECTION
WELD ANGLE 45° t = 15 mm

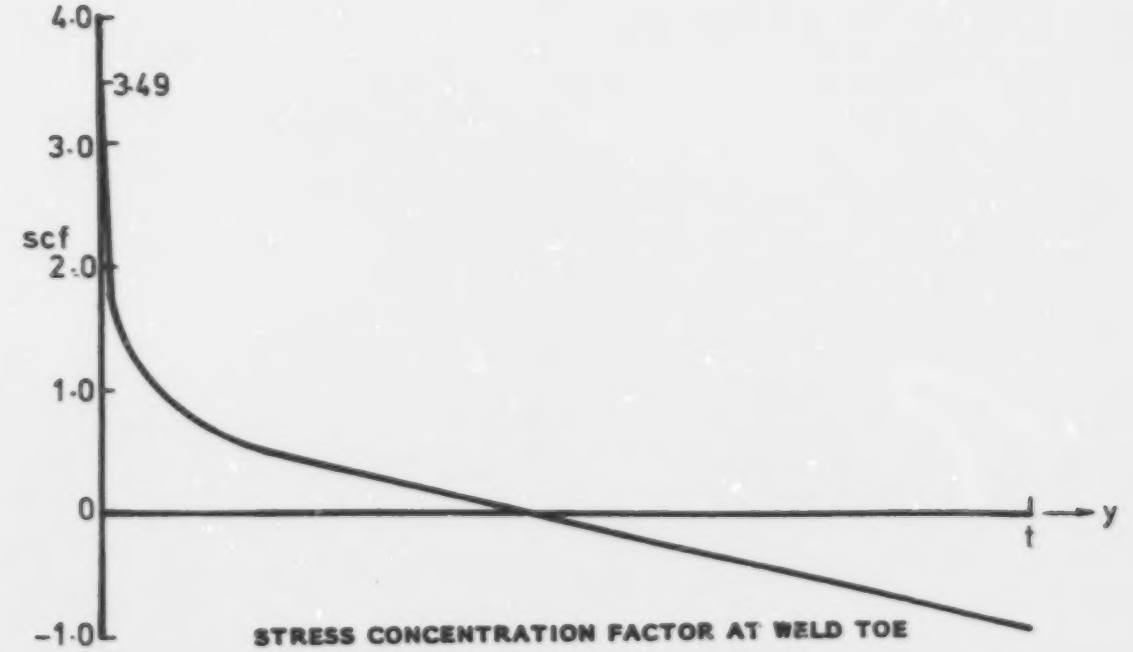

STRESS CONCENTRATION FACTOR AT WELD TOE
VARIATION OF σ_x IN y DIRECTION
WELD ANGLE 60° t = 15 mm

FIG. 4.16

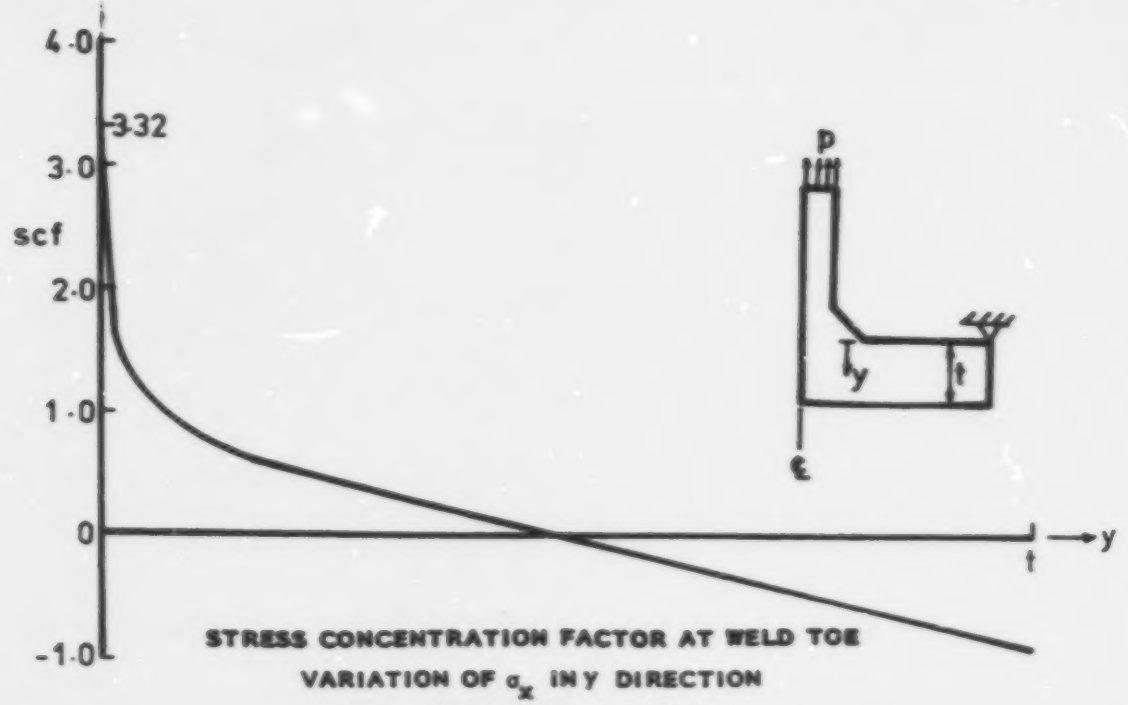

STRESS CONCENTRATION FACTOR AT WELD TOE
VARIATION OF σ_x IN y DIRECTION
WELD ANGLE 45° t = 28 mm

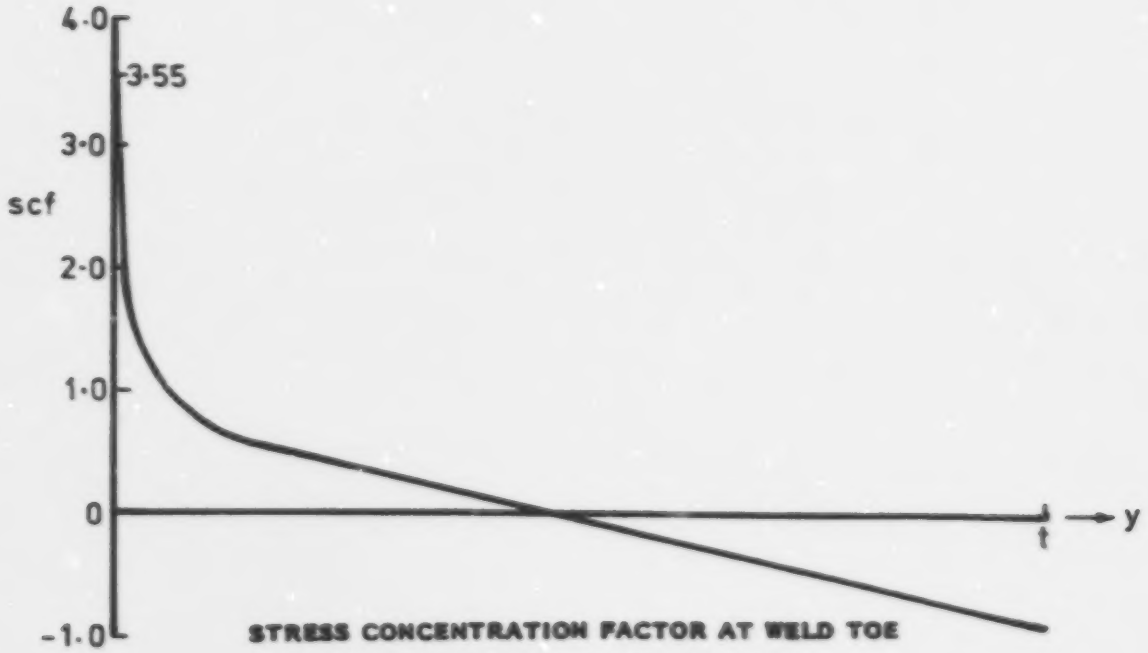

STRESS CONCENTRATION FACTOR AT WELD TOE
VARIATION OF σ_x IN y DIRECTION
WELD ANGLE 60° t = 28 mm

FIG. 4.17

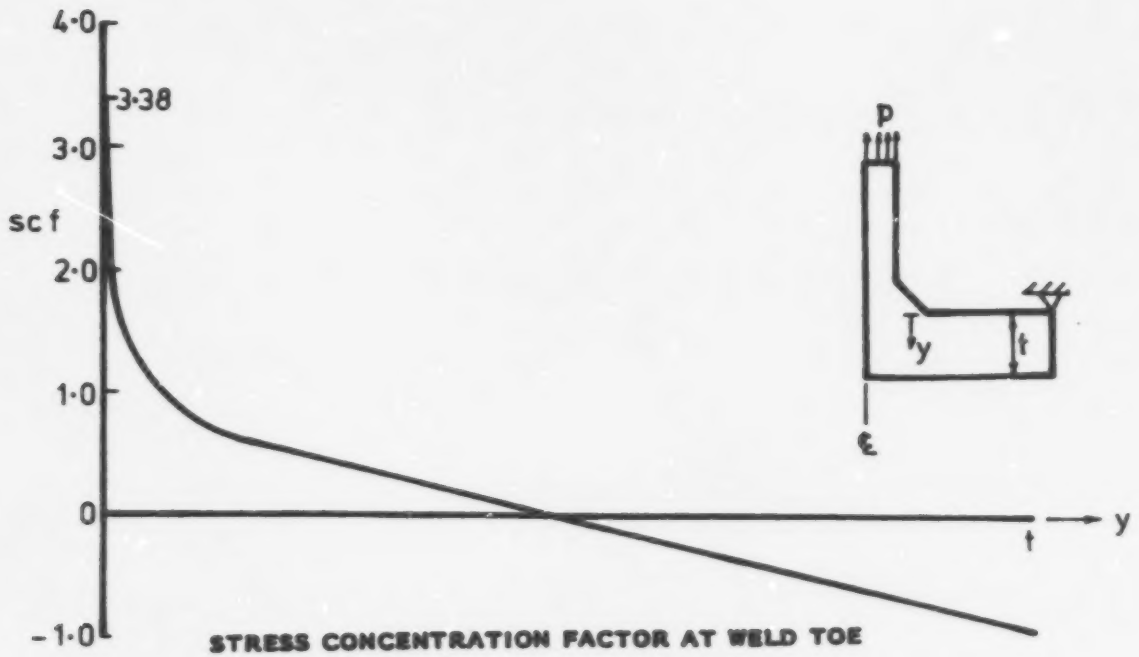

STRESS CONCENTRATION FACTOR AT WELD TOE
VARIATION OF σ_x IN y DIRECTION
WELD ANGLE 45° t = 53 mm

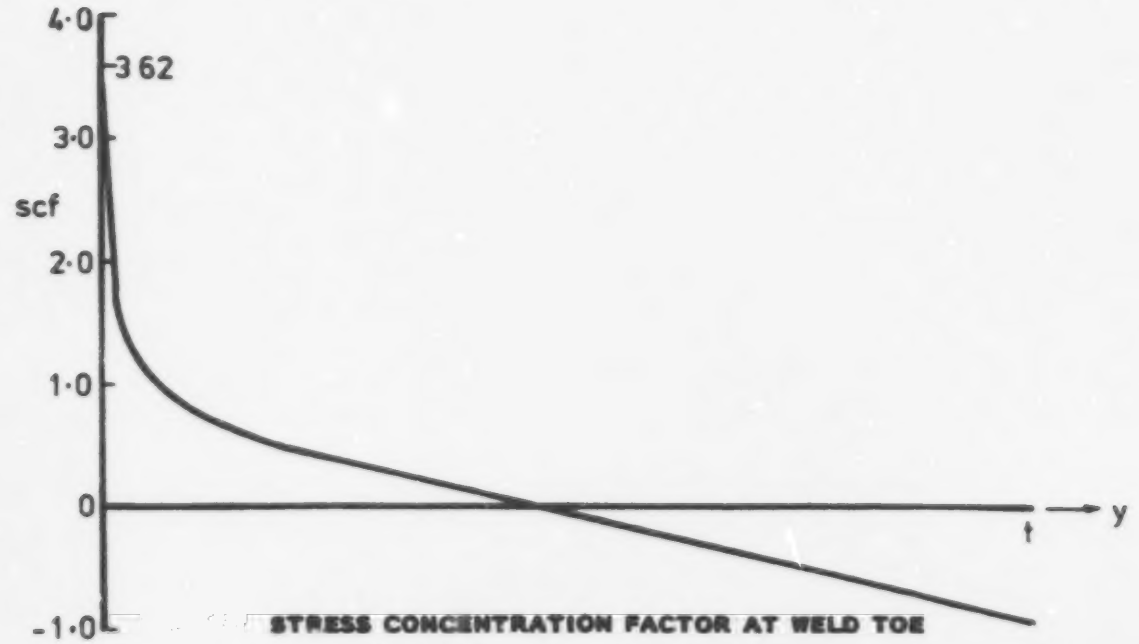

STRESS CONCENTRATION FACTOR AT WELD TOE
VARIATION OF σ_x IN y DIRECTION
WELD ANGLE 60° t = 53 mm

FIG. 4.18

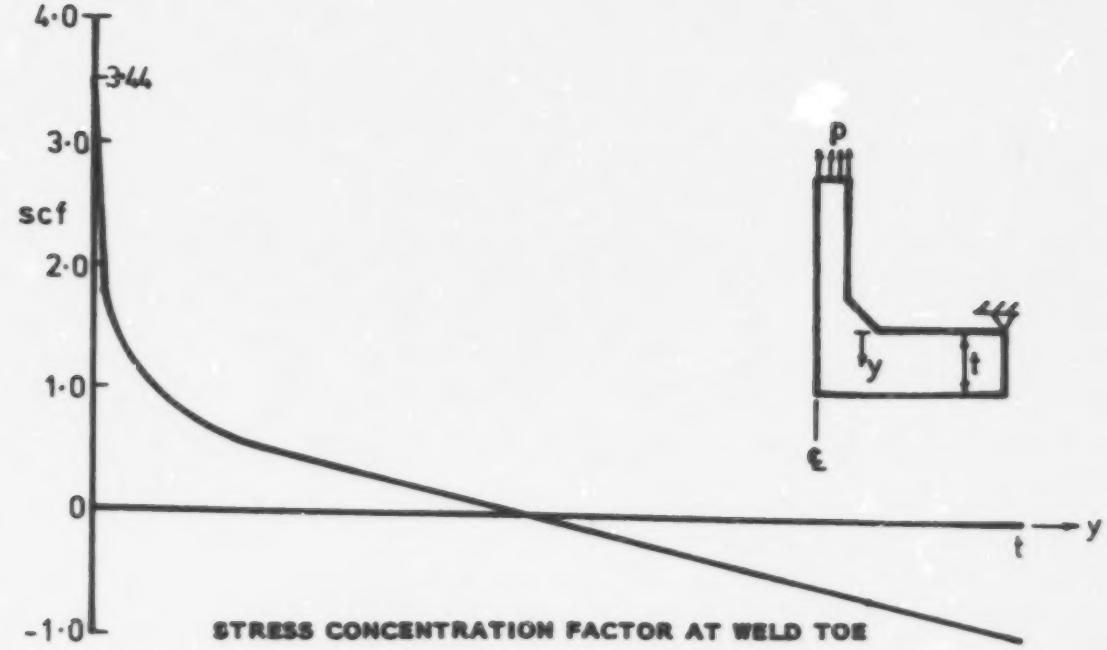

STRESS CONCENTRATION FACTOR AT WELD TOE
VARIATION OF σ_x IN y DIRECTION
WELD ANGLE 45° t = 78 mm

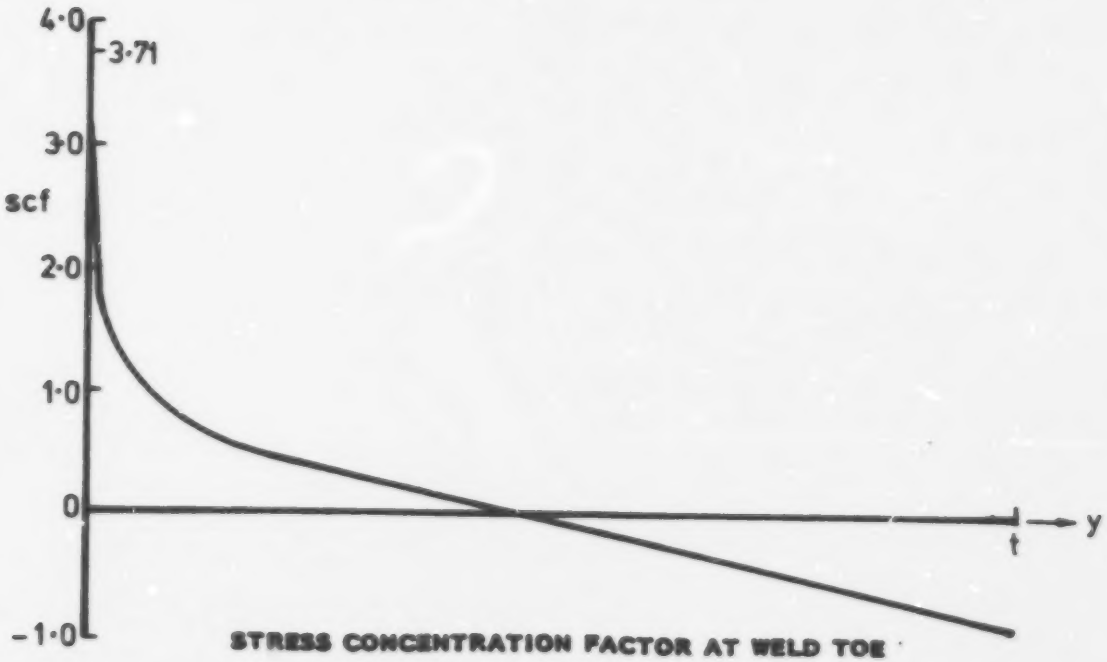

STRESS CONCENTRATION FACTOR AT WELD TOE
VARIATION OF σ_x IN y DIRECTION
WELD ANGLE 60° t = 78 mm

FIG. 4.19

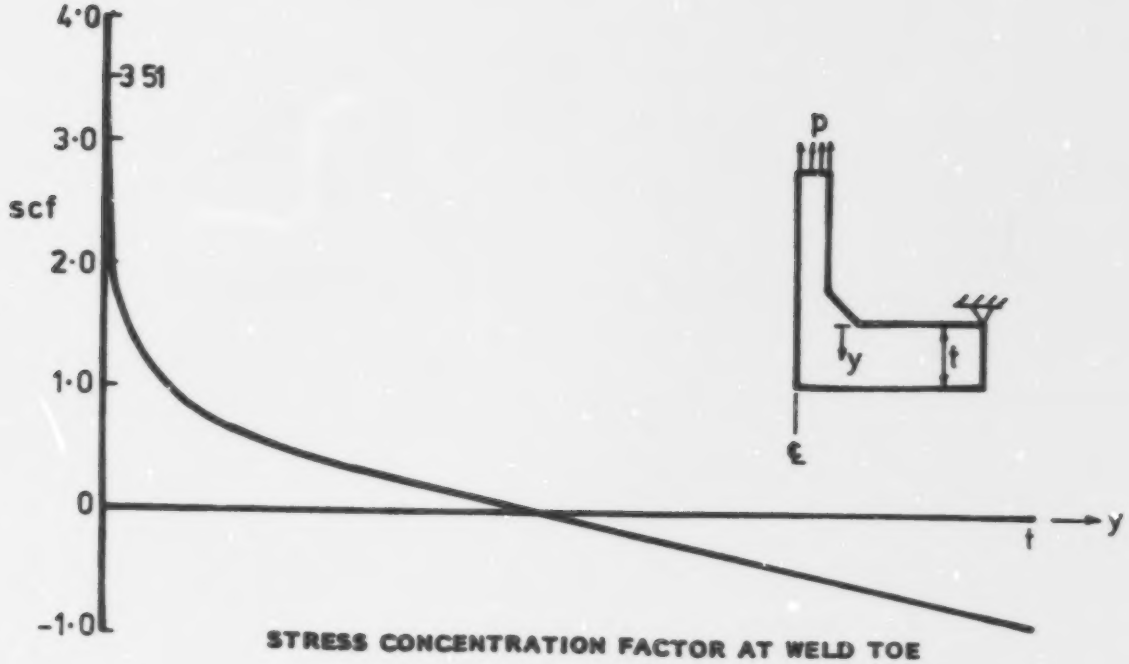

STRESS CONCENTRATION FACTOR AT WELD TOE
VARIATION OF σ_x IN y DIRECTION
WELD ANGLE 45° t = 103 mm

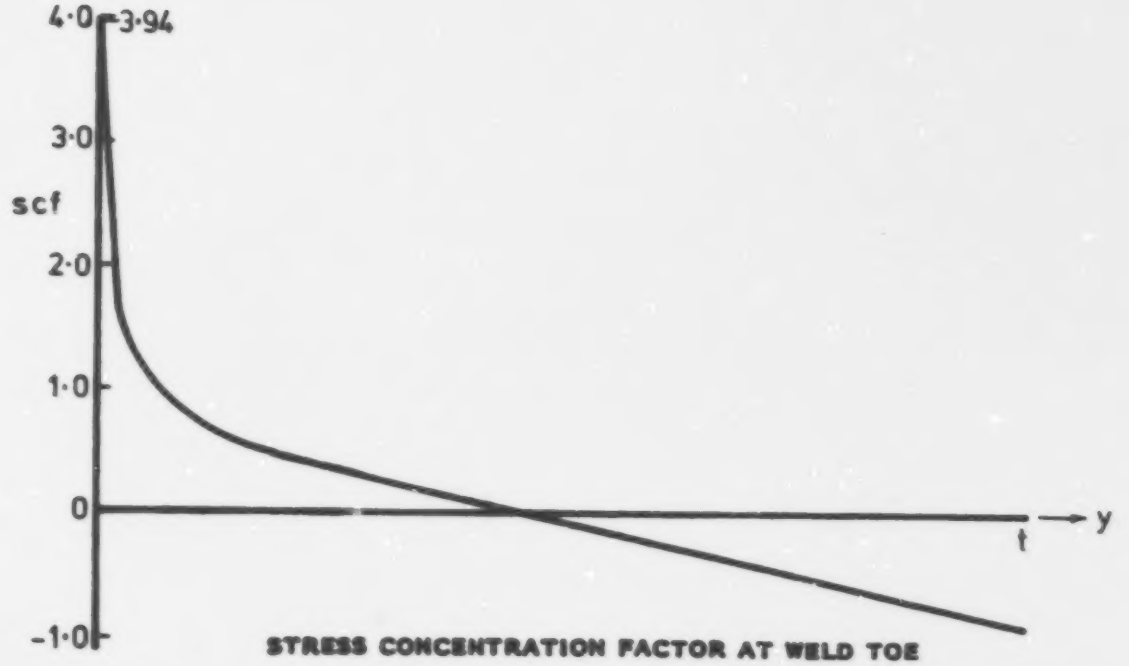

STRESS CONCENTRATION FACTOR AT WELD TOE
VARIATION OF σ_x IN y DIRECTION
WELD ANGLE 60° t = 103 mm

FIG. 4.20

CHAPTER V

3 - DIMENSIONAL STUDIES

5.1 Introduction

This section of the report describes the 3-dimensional FE studies carried out to analyse an elliptical crack at the weld toe of the 'T' specimen. Several preliminary analyses are also reported which were carried out for a surface crack in a tension block to develop an adequate mesh and to assess the accuracy of the 3-dimensional FM capability of ASAS.

5.2 Modelling of Semi-Elliptical Cracks

The modelling of a semi-elliptical surface crack by 3-dimensional finite elements is extensive in time and effort, and the data checking is very tedious. Also, in order to assess the accuracy of the ASAS 3-dimensional crack tip element it was necessary to change the mesh parameters such as number of crack tip elements around the crack, their size and also the crack shape. To facilitate the production of 3-dimensional finite element input data a mesh generator for elliptical cracks was developed at Carleton University which produces input data in ASAS input format.

This mesh generator provides the following advantages:

(i) quick and easy production of 3-dimensional FE meshes

(ii) error free data for ASAS

(iii) a regular mesh which produces a known progression into new meshes so that the accuracy and behaviour of the crack tip elements and the mesh refinement can be carried out in a systematic way.

The major disadvantage with this mesh generator is that the mesh produced is not optimized, therefore the solution times, and thus the costs, are increased. However, it is felt that this disadvantage is acceptable in light of the flexibility that the program provides for the producing and modifying 3-dimensional FE crack meshes quickly, error free and with minimum effort.

The mesh generator operates in the following manner. A two-dimensional crack mesh is input in ASAS format; fig. 5.1 shows the two-dimensional mesh for a surface crack in a tension block. This mesh is then rotated around an elliptical path, of the required a/c ratio, in the z plane in a stepwise fashion to produce the 3-dimensional mesh of the crack region, fig. 5.3. The number of elements along the crack front corresponds to the number of angles ϕ. (fig. 5.2), input to the mesh generator. The values of ϕ are chosen such that the length of each crack tip element along the crack front is equal.

The mesh generator outputs the element connectivity, nodal co-ordinates, nodal suppressions and nodal link data of the 3-dimensional mesh in ASAS input format. This data can be produced in cartesian or polar co-ordinates.

Typically, a 3-dimensional mesh as shown in fig. 5.3 would take approximately two weeks to produce manually. Using the mesh generator a more regular mesh was produced in less than one hour and was error free.

Before attempting to model elliptical weld toe cracks with collapsed isoparametric brick elements it was necessary to check the behaviour of the ASAS version of this element (designated CB15) and to develop the density of the mesh required in the crack tip region to give acceptable results.

To investigate how the crack tip element size and length affects the SIF calculated from ASAS FE results, a cube of side 2540 mm subjected to a unit tensile stress in the y direction was analysed. The dimensions of the cube and the crack are shown in fig. 5.4. This cube approximates an infinite medium to within 1% accuracy (49). The crack shape was chosen as circular, i.e. a/c = 1.0, and the size of the crack compared with the half thickness of the block was a/t = 0.082. The variables in the description of the mesh which are of interest are (i) the number of elements around the crack front (ii) the length of the element perpendicular to the crack front compared to the crack depth, i.e. a/L ratio, and (iii) the length of the element perpendicular to the crack front compared to the length of the element along the crack front, i.e. the m/L ratio. These element dimensions are defined in fig. 5.5.

In the first series of analyses three FE meshes were produced, using the mesh generator, with 2, 4 and 8 elements around the crack front. In all these meshes the crack tip element length L remained constant and the element size m was reduced. These meshes produced had m/L ratios of 4, 2.07 and 1.03 and consisted of 38, 76 and 152 elements respectively. The 76 element mesh is shown in fig. 5.6.

Using the substructuring capability of ASAS to change the boundary suppressions of the quarter cube, it was possible at little extra cost, to obtain the stress intensity factor solution or a semi-circular surface crack in addition to the embedded circular crack.

The results for these two benchmark problems giving the variation of K_I around the crack are given in tables 5.1 and 5.2. These results are also shown in figs. 5.7 and 5.8 compared with the empirical equation of Raju and Newman (50) derived from finite element results. In the calculation of the SIF plane strain conditions were assumed throughout except at the intersection of the crack with the block surface where plane stress conditions were assumed.

The accuracy of the ASAS FE solutions for the embedded crack as compared with the exact solution was 7.6% for 38 element model, 4.6% for the 76 element model and 3.6% for the 152 element model. The accuracy of the SIF variation for the surface crack compared with calculations using the Raju and Newman equation were within 2% as shown in table 5.3.

In a second series of tests the number of elements along the crack front was kept constant at four and the length L of the element was varied. Three analyses were completed with a/L ratios of approximately 2.5, 5 and 10. The results of these analyses, showing the variation of K_I along the crack front, compared with the equation. of Raju and Newman are shown in fig. 5.9.

From the above series of tests the experience of modelling the crack tip region was developed. It can be concluded that in order to compromise between the computing cost and accuracy the crack tip mesh should be constructed using a minimum of four crack tip elements around the crack and the dimensions of these elements should have approximately a/L = 2 and a/L = 5.

5.3 3-D Modelling of Weld Toe Crack

In order to produce the 3-dimensional FE model of the cracked 'T' specimen joint the mesh generator, described in the previous section, and multilevel substructuring capability of the ASAS FE program was used extensively. Due to symmetry only 1/4 of the total joint was considered. Referring to fig. 5.10 the joint was modelled as follows: the mesh for the substructure SECA was produced using the mesh generator from a two dimensional mesh of the x-z plane. SECA was then mirrored about the plane of the crack to form substructure SECB. The mesh SECC was also produced from a 2-dimensional mesh using the mesh generator. The mesh generator program also produces the correct linking nodes, linking sequence and boundary conditions for these model components. The substructures WELD1, WELD2 and WELD3 representing the 30^{o}, 45^{o} and 70^{o} weld shapes, as shown in fig. 4.4 were produced manually. The substructures were combined in global analyses to form the complete structures with different weld shapes.

It is also possible in the above substructuring procedure to apply a series of loading and boundary conditions so that three different load cases can be analysed for each crack shape at the weld toe. These three load cases are (i) axial tension, i.e. a non-load-carrying weld, (ii) pure bending, and (iii) three point bending, i.e., a load carrying weld. This procedure enables nine load and weld cases to be analysed for each crack shape which resulted in a substantial cost reduction for each case considered.

In order to check the above modelling procedure and the accuracy of the results, a structure was produced with no weld substructures included. This case is therefore equivalent to a plate with a semi-circular surface crack (a/c = 1.0 and a/t = 0.1) loaded in tension and pure bending. The results are shown in figs. 5.11 - 5.12 compared with the results of Newman and Raju, and demonstrate the accuracy of the modelling procedure.

5.4 3-D Weld Toe Crack Results

The 3-D weld toe crack cases considered in this work are given in Table 5.4. In each case three weld angles were considered as described in a previous section of this report. The physical dimensions of the model are given in Figure 5.13. Due to symmetry only one quarter of the 'T' specimen was modelled and the FE input for the substructure analysis was produced as described in section 5.3. In each FE model there were four crack tip elements along the crack front and three different loadcases were analysed for each crack shape and weld shape considered. In each case the loading was adjusted so that the axial stress σ_x at the weld toe had unit value. In all 90 different cases of crack shape, weld shape and loading were considered.

The results for the crack geometries considered showing the variation of K_1, non dimensionalized with respect to an embedded circular crack, as θ varies from 0 to 90^o are given in figures 5.14 to 5.44. In these plots $\theta = 0^o$ is the deepest point of the crack and $\theta = 90^o$ is the point where the crack intersects the surface of the plate (i.e. the weld toe).

In every case considered the 3-point bending results were greater than or equal to the 4-point bending results. The greatest differences between the 3-point and 4-point bending results occurred at the weld toe, ($\theta = 90^o$). For the crack shapes of a/c = 1.0 and 0.5 the stress intensity factor (SIF) is a minimum at the deepest point, ($\theta = 0^o$) and increases to a maximum at the weld toe, but the magnitude of this variation decreases with increasing crack depth.

The effect of weld angle on the SIF can be seen from the results with the SIF increasing with increasing weld angle. As expected the influence of the weld angle on the SIF decreases with increasing crack depth. For example the increase in SIF at the weld toe between the 30^{o} and 70^{o} weld shapes for a/c = 1.0 is 24% at a crack depth of 0.05 and at a crack depth of 0.2 this difference is reduced to 7%. For the cases considered at the deepest point of the crack front the tension case results are lower than the bending results for shallow cracks, but as expected, as the crack depth increases the tension case results become higher.

In contrast to the above results the SIF at the weld toe of the a/c = 0.25 crack shape and 30^{o} weld profile is less than the SIF at the deepest point of the crack front. For the 45^{o} weld shape the variation of the SIF around the crack front is almost constant and for the 70^{o} weld shape the SIF at the weld is again greater than the SIF at the deepest point. This observation only applies to the two shallow crack depths considered and further numerical studies should be carried out for this crack shape and for crack shapes with a/c less than 0.25.

TABLE 5.1

K_I for an Embedded Crack in a Tension Block

$$\text{Exact Solution } \frac{K_I}{\sigma\sqrt{\frac{4a}{\pi}}} = 1.0$$

$a/L = 5.263 \quad a/c = 1.0$

θ	TB1 (38 elements)	TB2 (76 elements)	TB3 (152 elements)
	$K_I/\sigma\sqrt{\frac{4a}{\pi}}$	$K_I/\sigma\sqrt{\frac{4a}{\pi}}$	$K_I/\sigma\sqrt{\frac{4a}{\pi}}$
0	1.078	1.047	1.037
5.625			1.037
11.25		1.048	1.037
16.875			1.037
22.5	1.081	1.047	1.037
28.125			1.037
33.75		1.048	1.037
39.375			1.037
45	1.077	1.047	1.037
50.625			1.037
56.25		1.048	1.037
61.875			1.037
67.5	1.081	1.047	1.036
73.125			1.037
78.75		1.048	1.037
84.375			1.037
90.0	1.077	1.047	1.037

TABLE 5.2

K_I for a Surface Crack in a Tension Block

$a/L = 5.263 \quad a/c = 1.0 \quad Q = \frac{\pi^2}{4}$

	TB1 (38 elements)	TB2 (76 elements)	TB3 (152 elements)
θ	$K_I/\sigma\sqrt{\pi a}$ / Q	$K_I/\sigma\sqrt{\pi a}$ / Q	$K_I/\sigma\sqrt{\pi a}$ / Q
0	1.10	1.07	1.059
5.625			1.06
11.25		1.072	1.061
16.875			1.062
22.5	1.11	1.074	1.064
28.125			1.065
33.75		1.078	1.067
39.375			1.068
45	1.12	1.085	1.074
50.625			1.078
56.25		1.094	1.085
61.875			1.092
67.5	1.145	1.11	1.103
73.125			1.114
78.75		1.149	1.134
84.375			1.180
90.0	1.15	1.134	1.143

TABLE 5.3

COMPARISON OF ASAS FE RESULTS
WITH THE EQUATION OF NEWMAN AND RAJU
FOR A CRACK WITH

$a/c = 1.0 \quad a/t = 0.082 \quad a/L = 5.263 \quad Q = \frac{\pi^2}{4}$

θ	$\frac{K_I}{\sigma\sqrt{\pi a/Q}}$		
	ASAS FE	NEWMAN & RAJU EQUATION	ERROR %
0	1.059	1.042	1.63
11.25	1.061	1.0425	1.77
22.5	1.064	1.043	2.01
33.75	1.067	1.0455	2.06
45.0	1.074	1.0516	2.13
56.25	1.085	1.0635	2.02
67.5	1.103	1.0831	1.84
78.75	1.134	1.1115	2.02
90.0	1.143	1.1491	0.5

TABLE 5.4

WELD TOE CRACK GEOMETRIES

a/c	a/t
1.0	0.05
	0.1
	0.2
	0.4
0.5	0.025
	0.05
	0.1
	0.2
0.25	0.025
	0.05

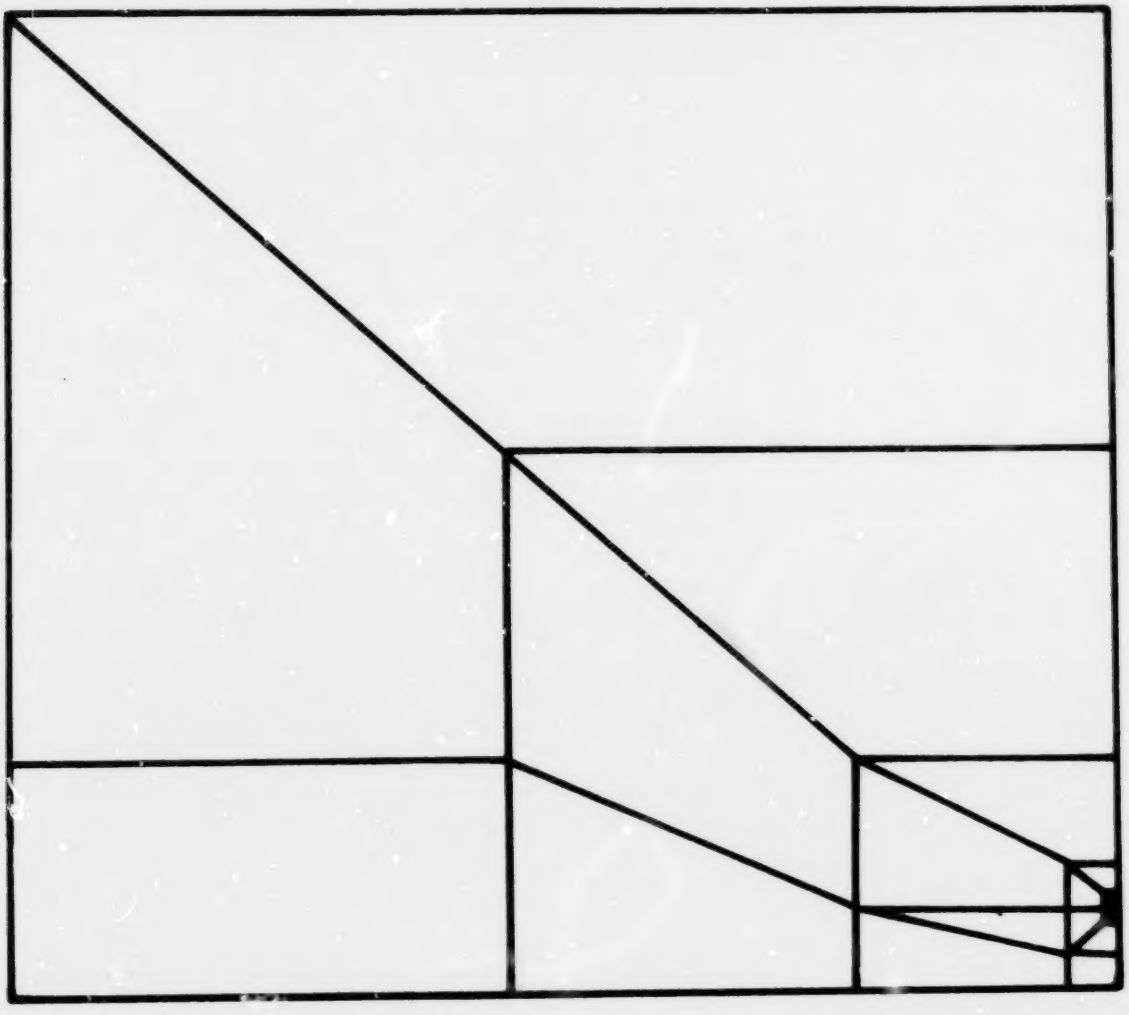

2-D MESH FOR TENSION BLOCK

FIG. 5.1

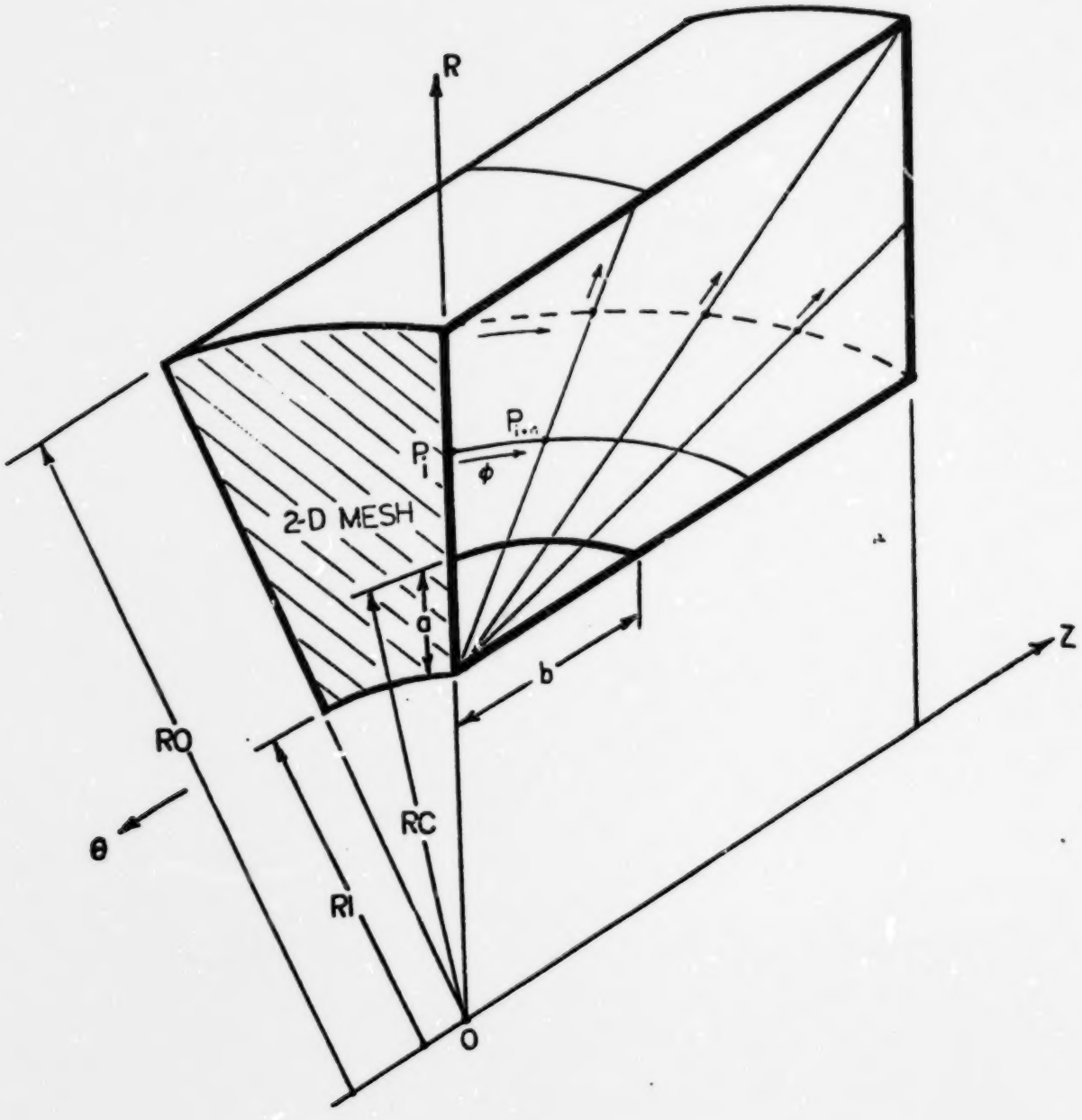

SCHEMATIC OF 3-D MESH GENERATION PROCESS

FIG. 5.2

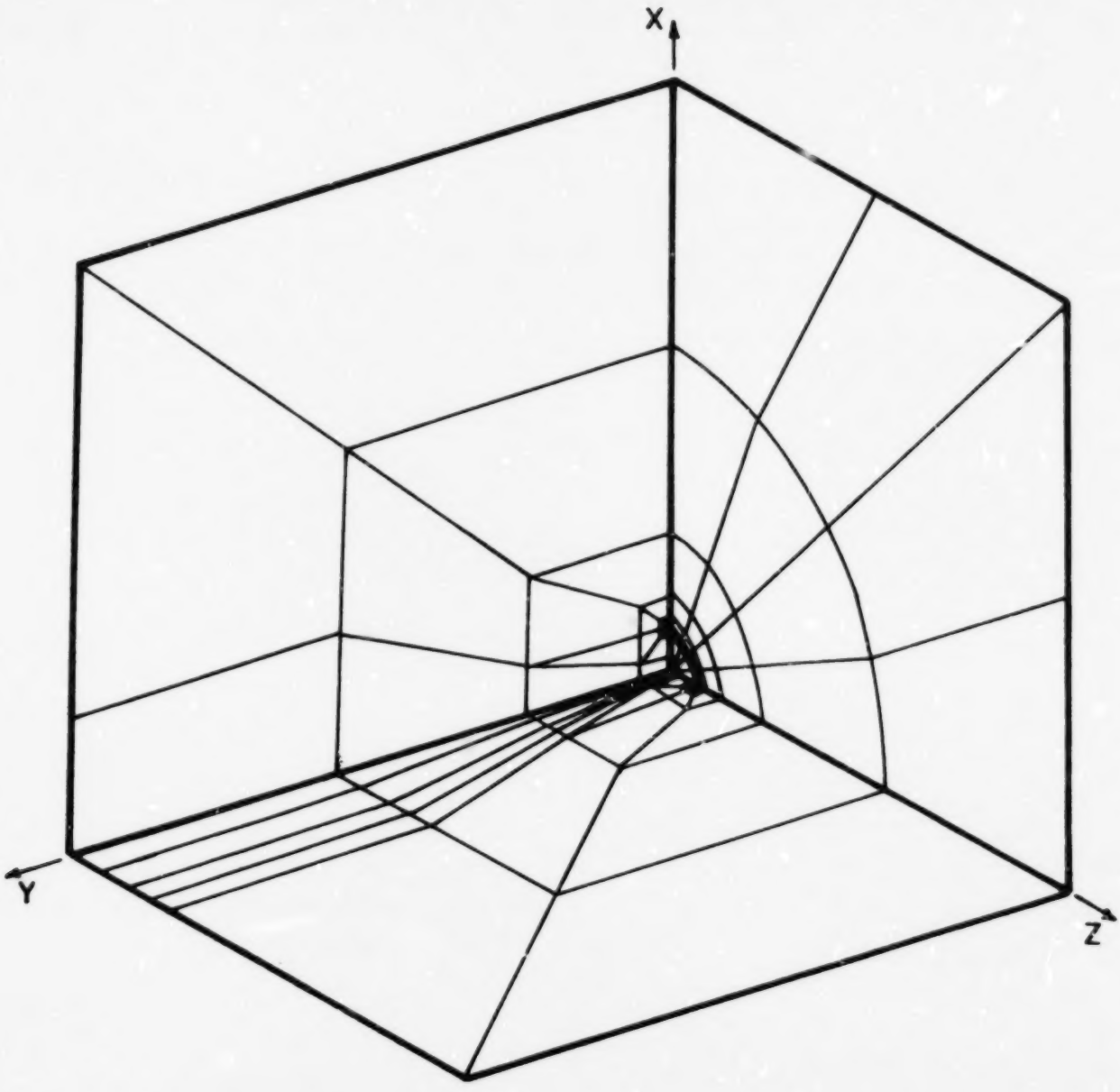

3-D MESH FOR TENSION BLOCK
PRODUCED BY MESH GENERATOR

FIG. 5.3

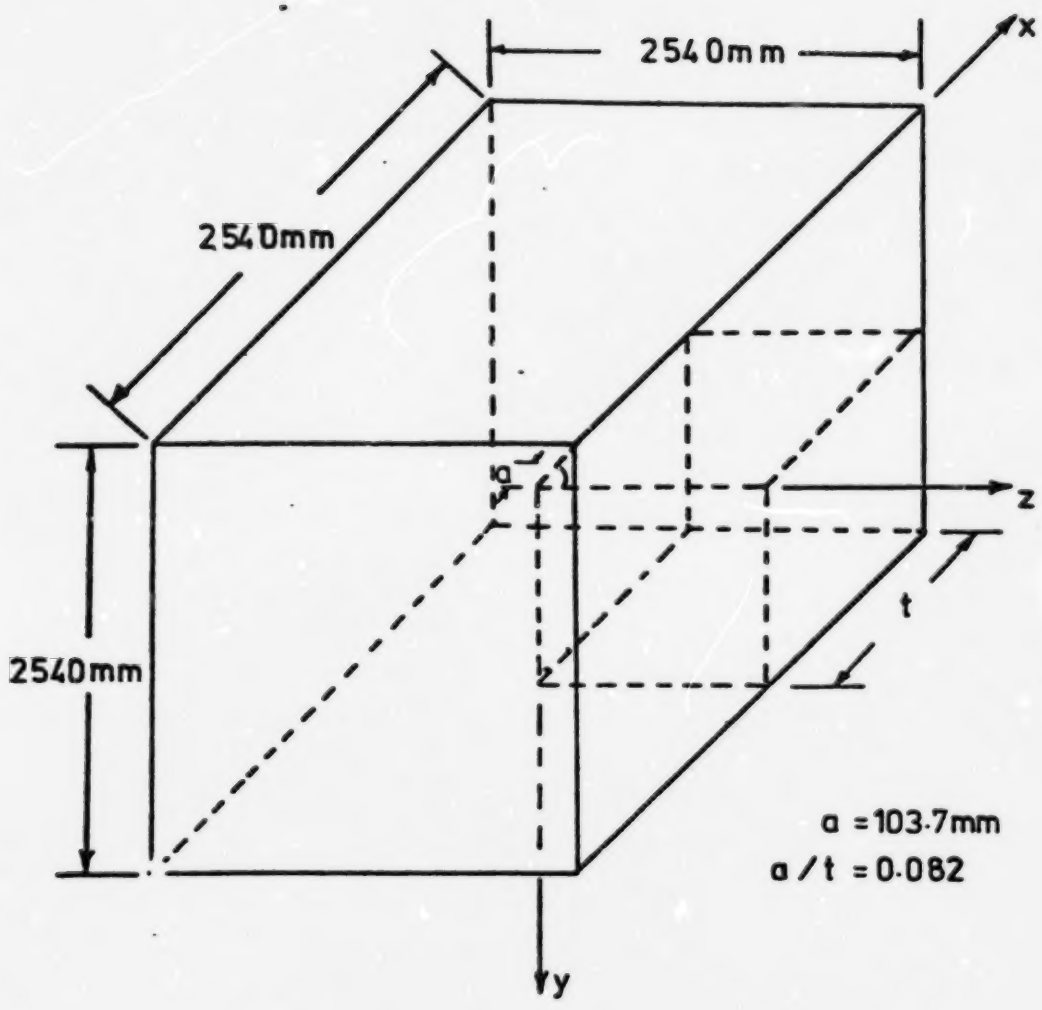

TENSION BLOCK GEOMETRY

FIG. 5.4

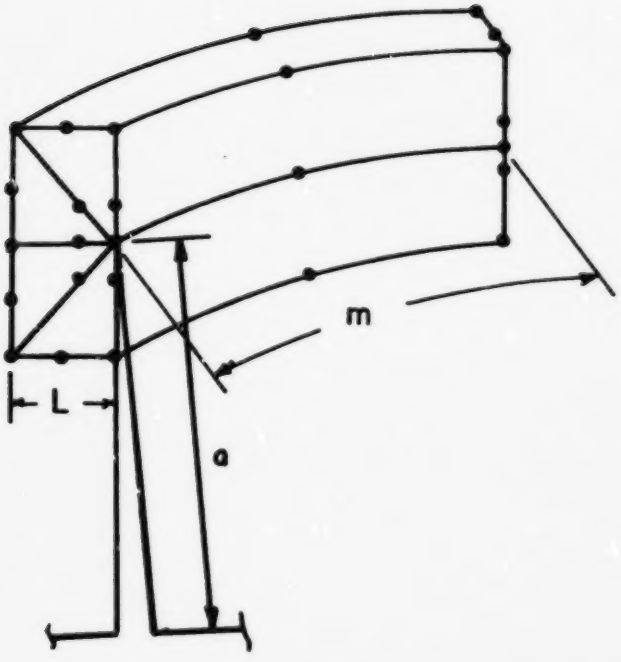

DEFINITION OF M/L RATIO

FIG. 5.5

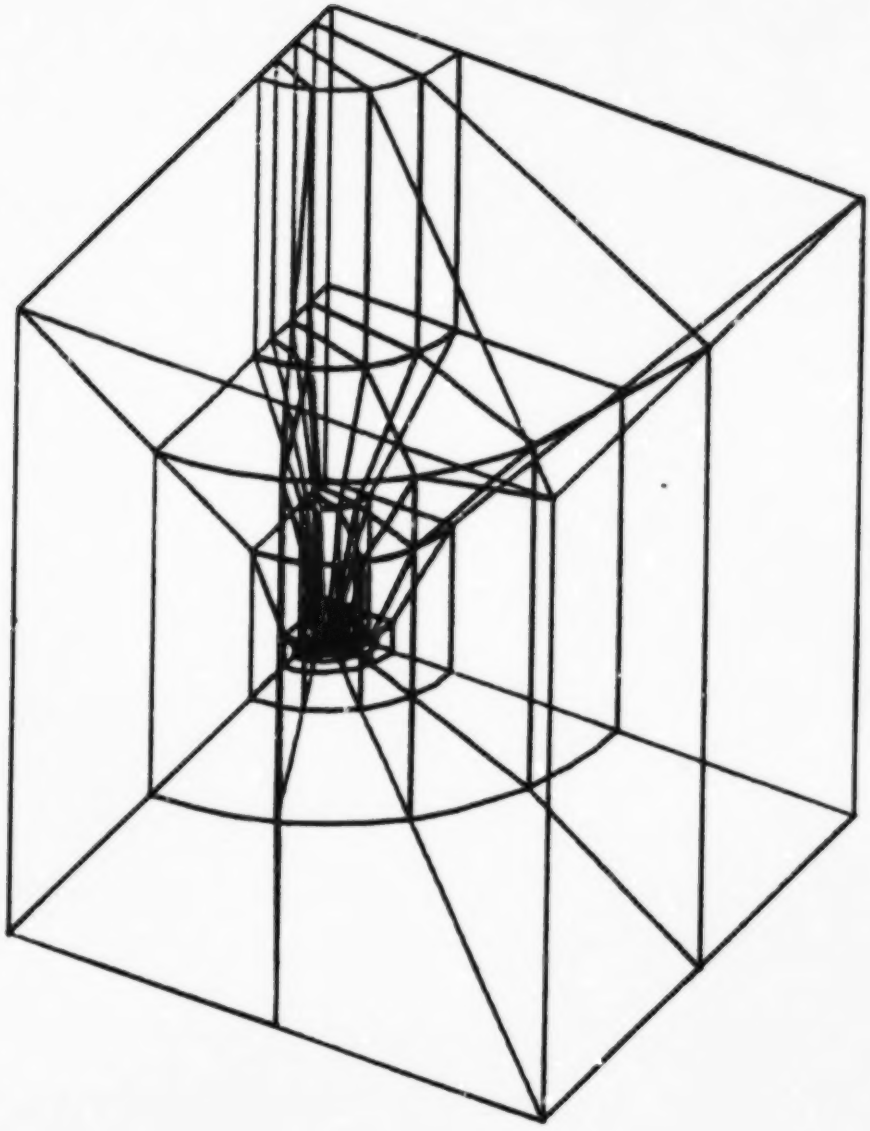

3-D MESH WITH 76 ELEMENTS FOR EMBEDDED AND SURFACE CRACK PROBLEMS

FIG. 5.6

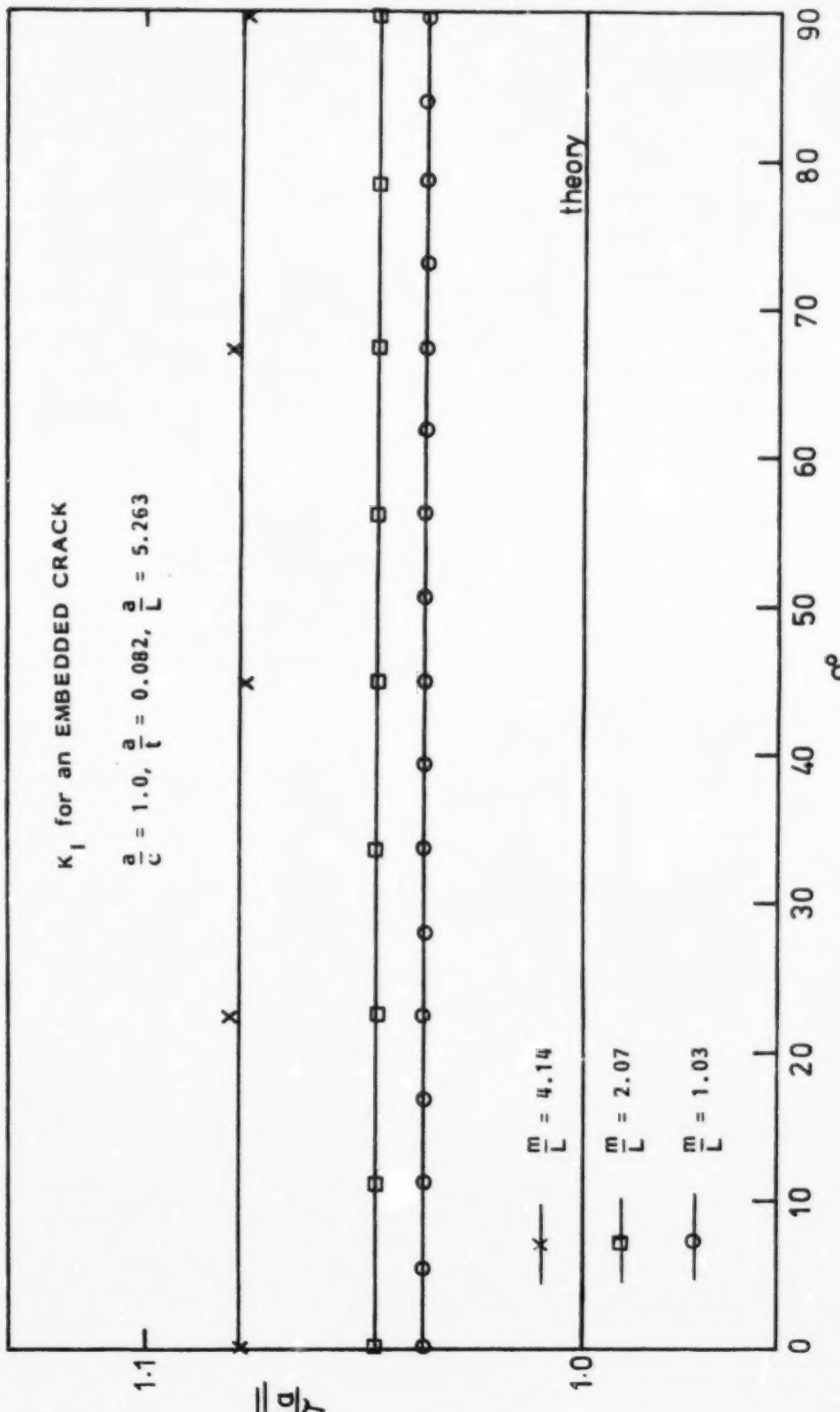
K_I for an EMBEDDED CRACK
a/c = 1.0, a/t = 0.082, a/L = 5.263
K_I / σ√(πa/Q)
1.1
1.0
0
10
20
30
40
50
60
70
80
90
θ°
theory
m/L = 4.14
m/L = 2.07
m/L = 1.03

FIG. 5.7

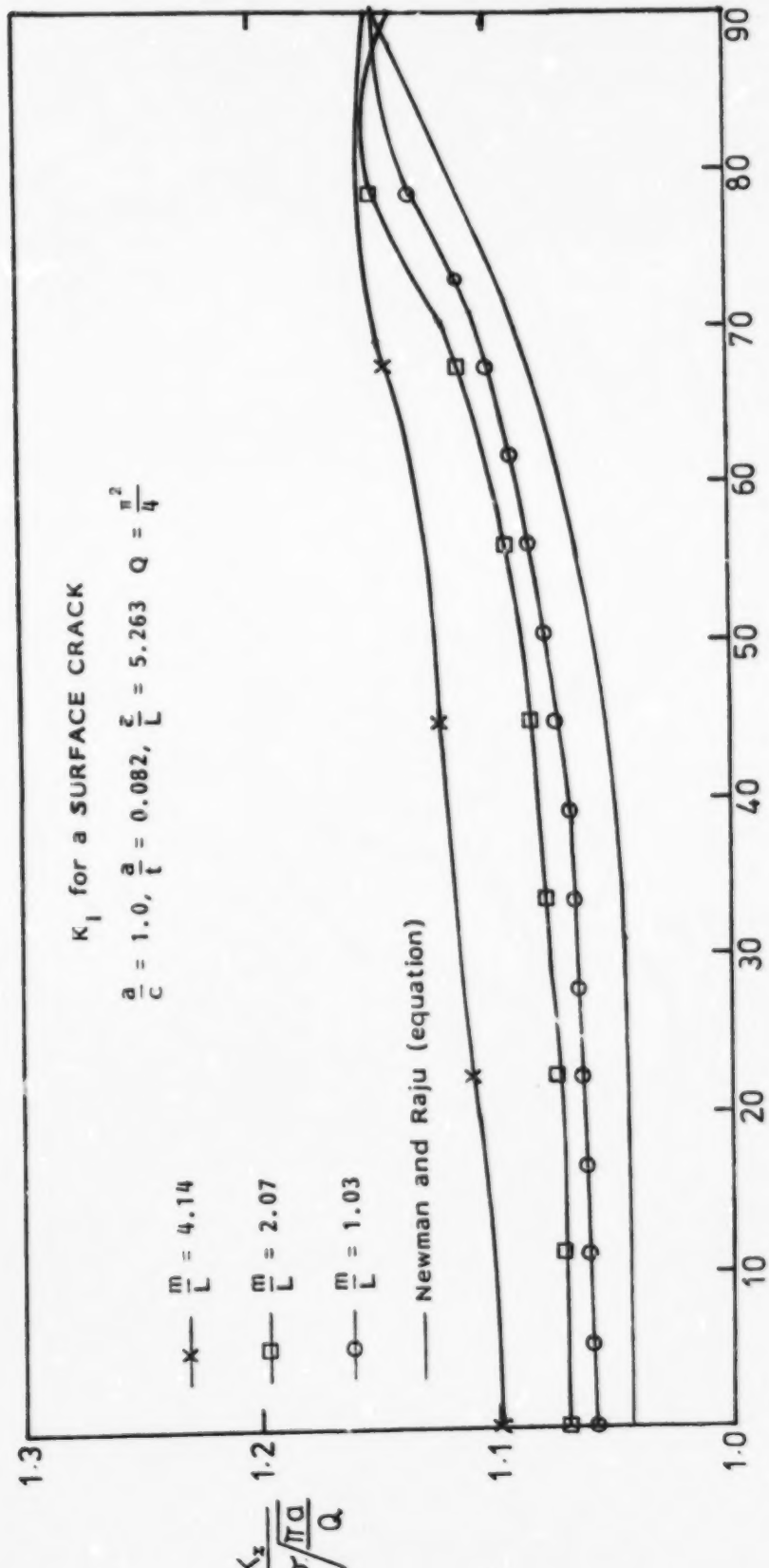
K_I for a SURFACE CRACK
$\frac{a}{c} = 1.0$, $\frac{a}{t} = 0.082$, $\frac{\ell}{L} = 5.263$ $Q = \frac{\pi^2}{4}$
$\frac{m}{L} = 4.14$
$\frac{m}{L} = 2.07$
$\frac{m}{L} = 1.03$
Newman and Raju (equation)
$\frac{K_I}{\sigma\sqrt{\pi a}/Q}$
1.3
1.2
1.1
1.0
10
20
30
40
50
60
70
80
90
θ°

FIG. 5.8

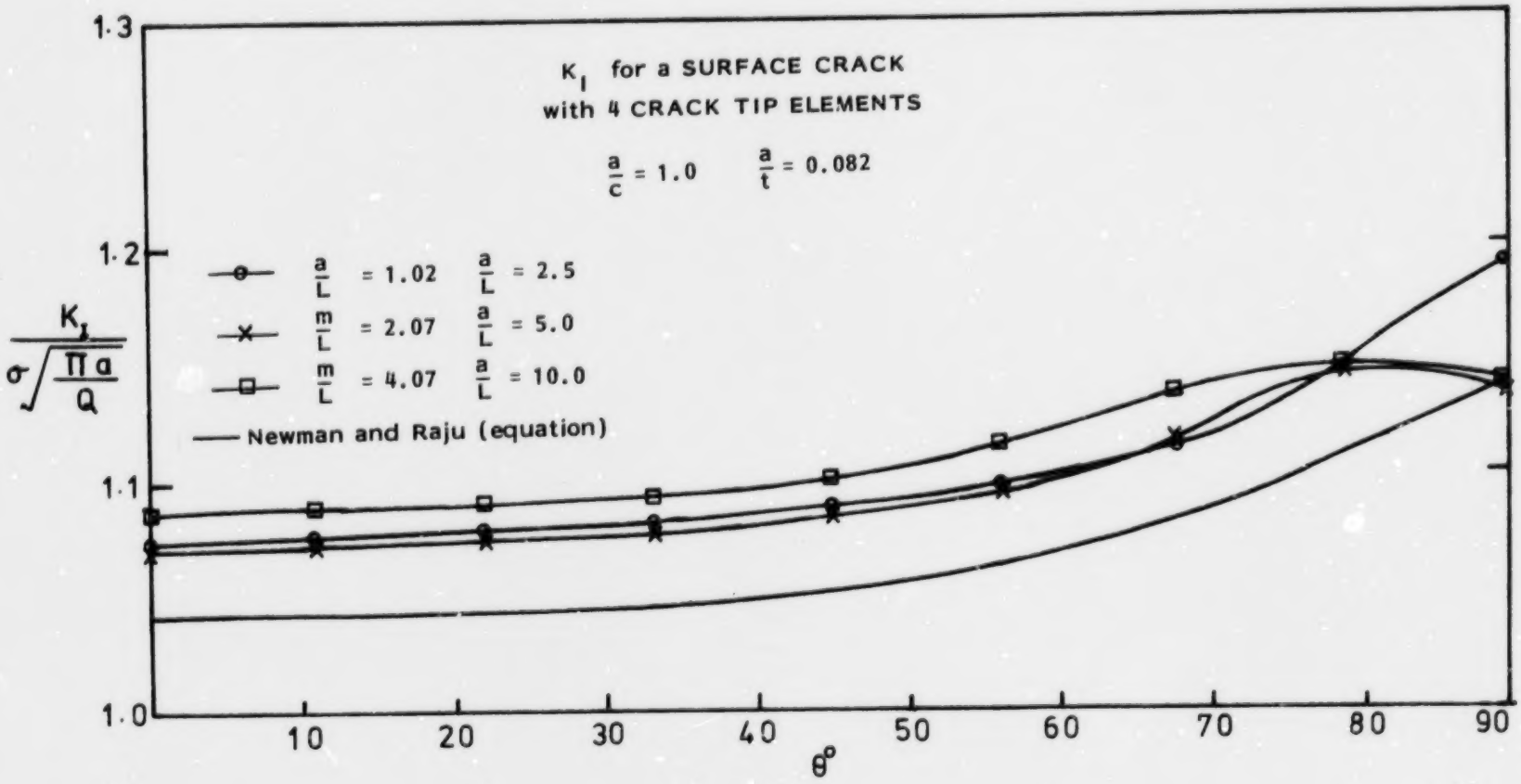
K_I for a SURFACE CRACK
with 4 CRACK TIP ELEMENTS
$\frac{a}{c} = 1.0$ $\frac{a}{t} = 0.082$
$\frac{a}{L} = 1.02$ $\frac{a}{L} = 2.5$
$\frac{m}{L} = 2.07$ $\frac{a}{L} = 5.0$
$\frac{m}{L} = 4.07$ $\frac{a}{L} = 10.0$
Newman and Raju (equation)
$\frac{K_I}{\sigma\sqrt{\frac{\pi a}{Q}}}$
1.3
1.2
1.1
1.0
10
20
30
40
50
60
70
80
90
θ°

FIG. 5.9

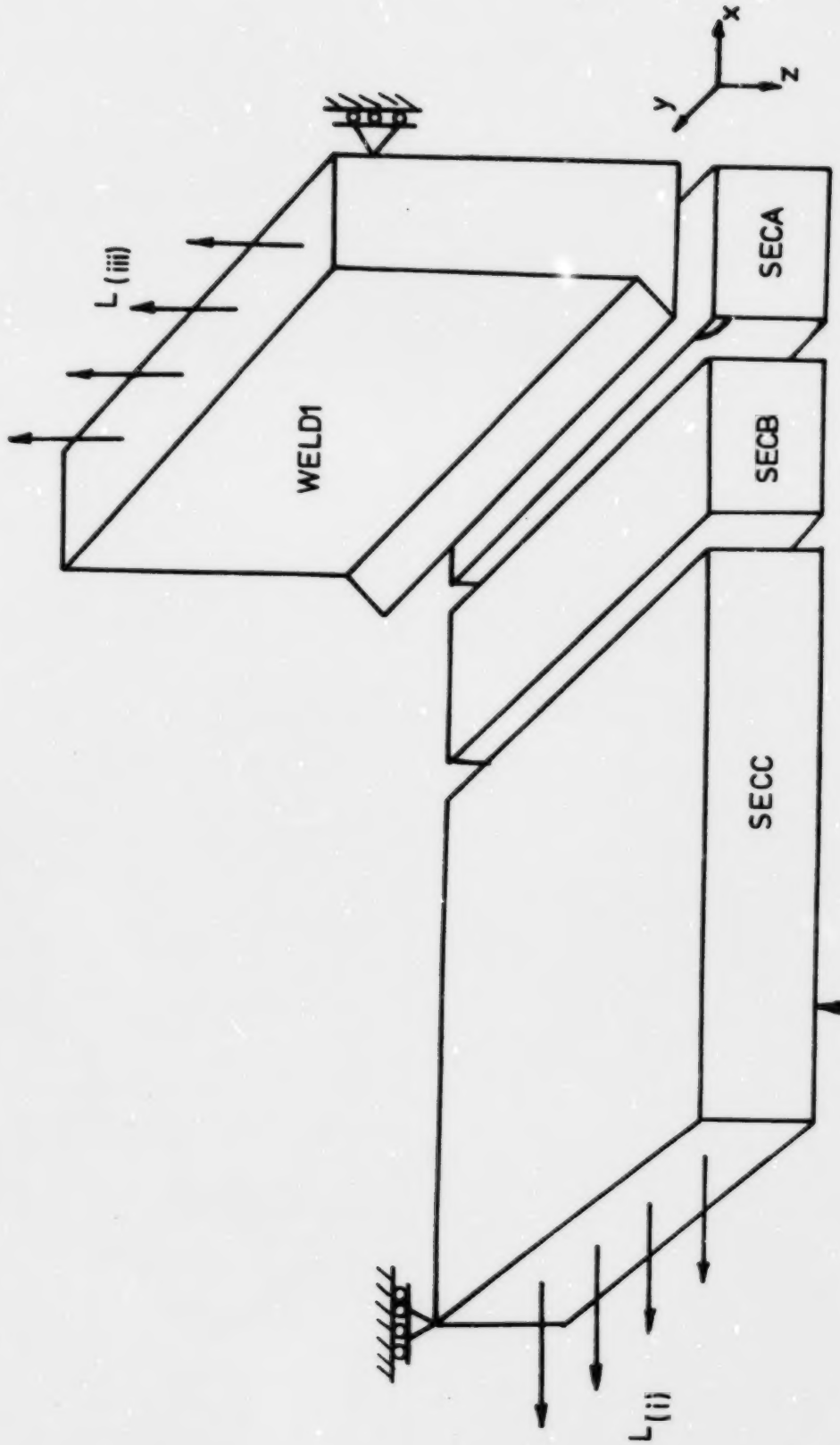

FIG. 5.10

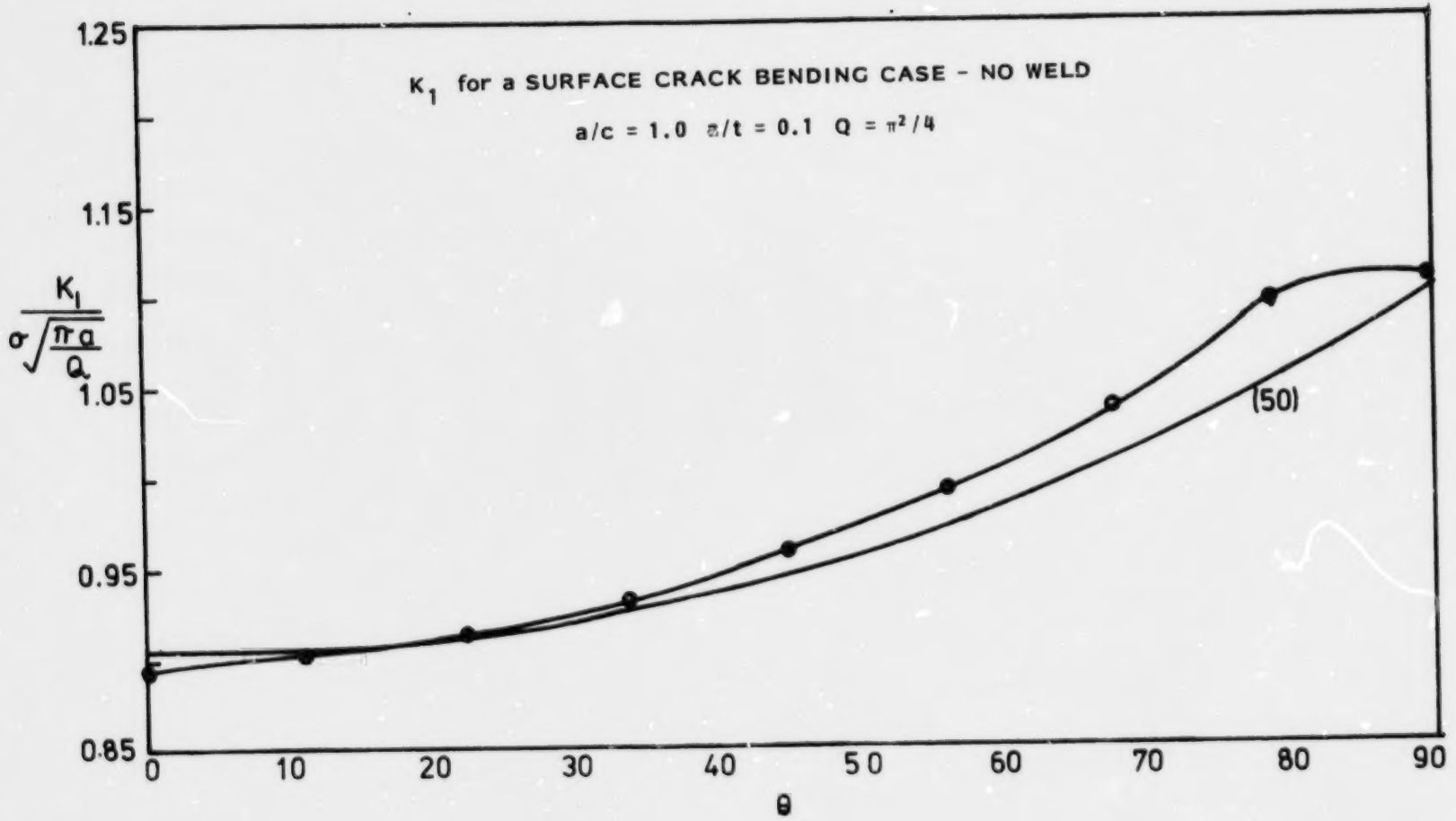
K_1 for a SURFACE CRACK BENDING CASE - NO WELD
a/c = 1.0 a/t = 0.1 Q = π²/4
1.25
1.15
1.05
0.95
0.85
$\frac{K_1}{\sigma\sqrt{\frac{\pi a}{Q}}}$
0
10
20
30
40
50
60
70
80
90
θ
(50)

FIG. 5.11

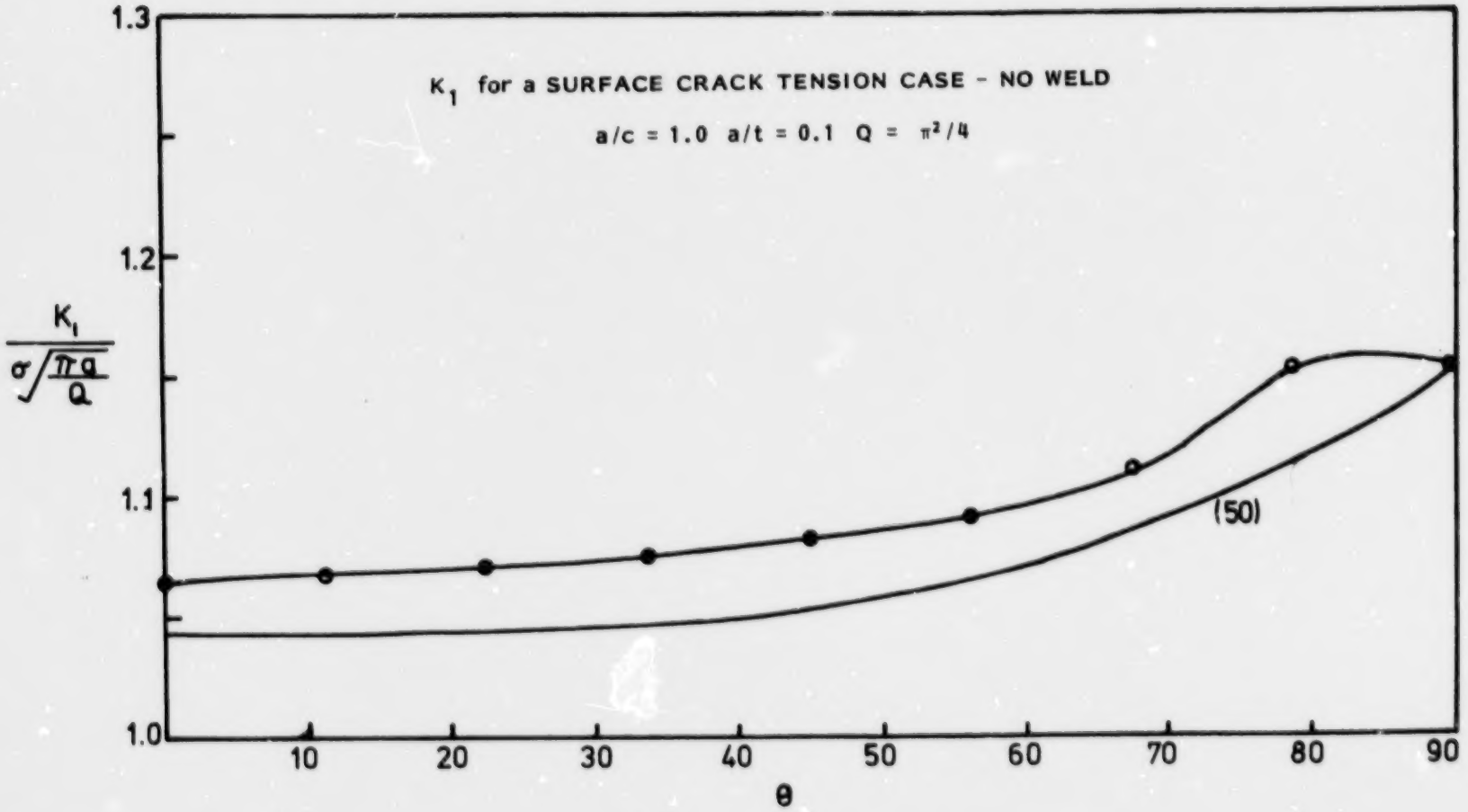
K_1 for a SURFACE CRACK TENSION CASE - NO WELD
a/c = 1.0 a/t = 0.1 Q = $\pi^2/4$
$\frac{K_1}{\sigma\sqrt{\frac{\pi a}{Q}}}$
1.3
1.2
1.1
1.0
10
20
30
40
50
60
70
80
90
θ
(50)

FIG. 5.12

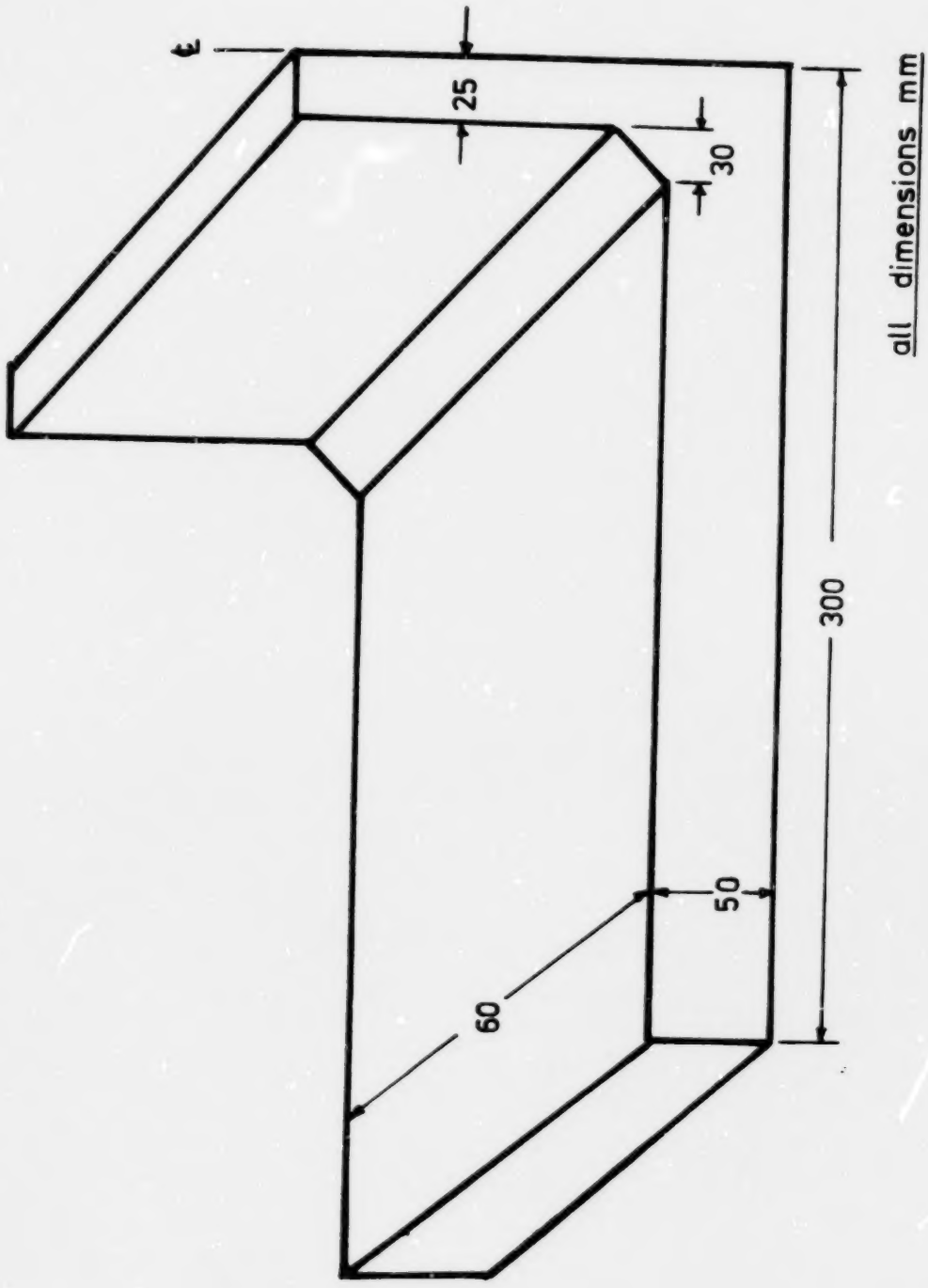

FIG. 5.13

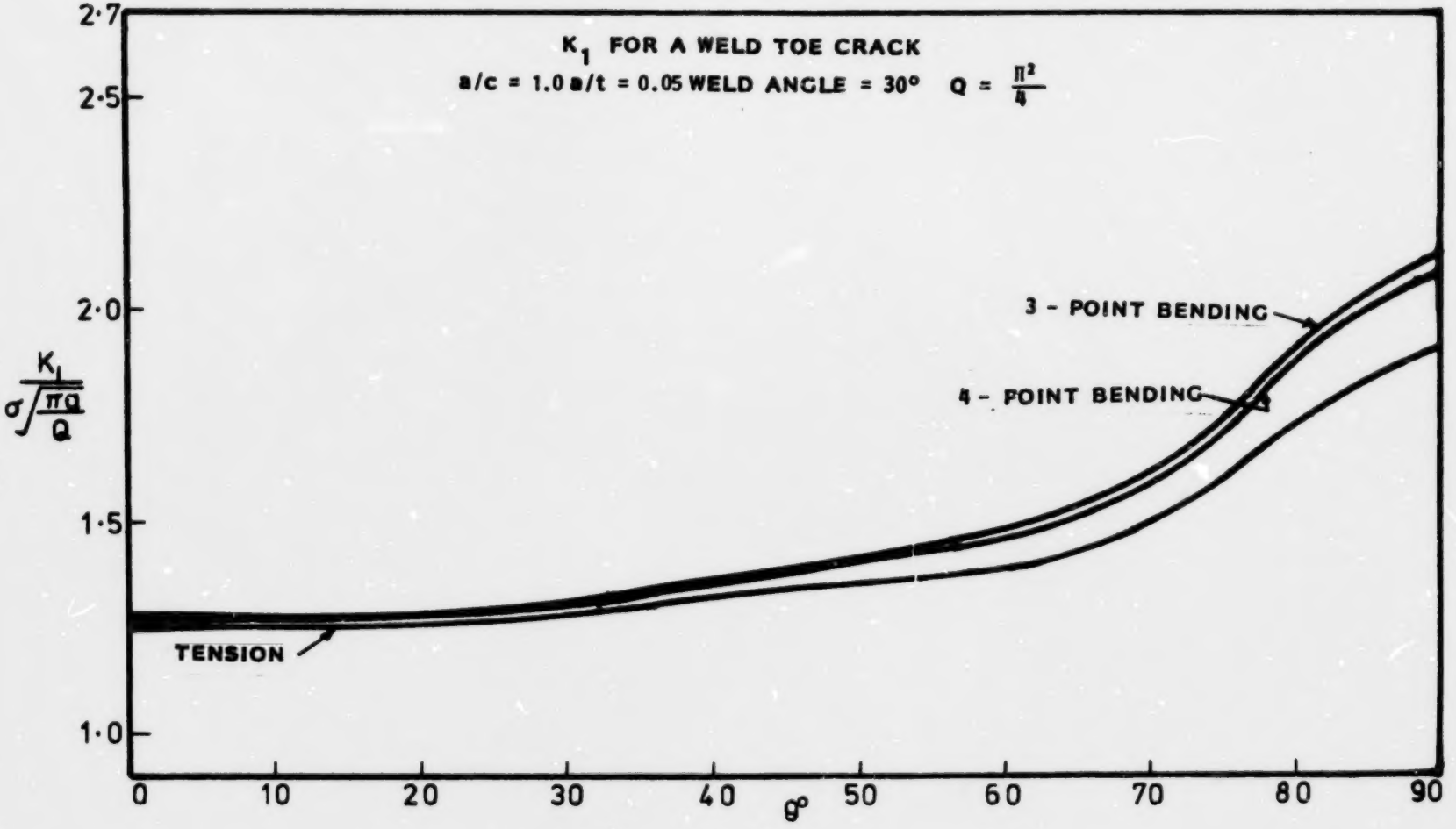
K_1 FOR A WELD TOE CRACK
a/c = 1.0 a/t = 0.05 WELD ANGLE = 30° Q = $\frac{\pi^2}{4}$
$\frac{K_1}{\sigma\sqrt{\frac{\pi a}{Q}}}$
2·7
2·5
2·0
1·5
1·0
3 - POINT BENDING
4 - POINT BENDING
TENSION
0
10
20
30
40
50
60
70
80
90
g°

FIG. 5.14

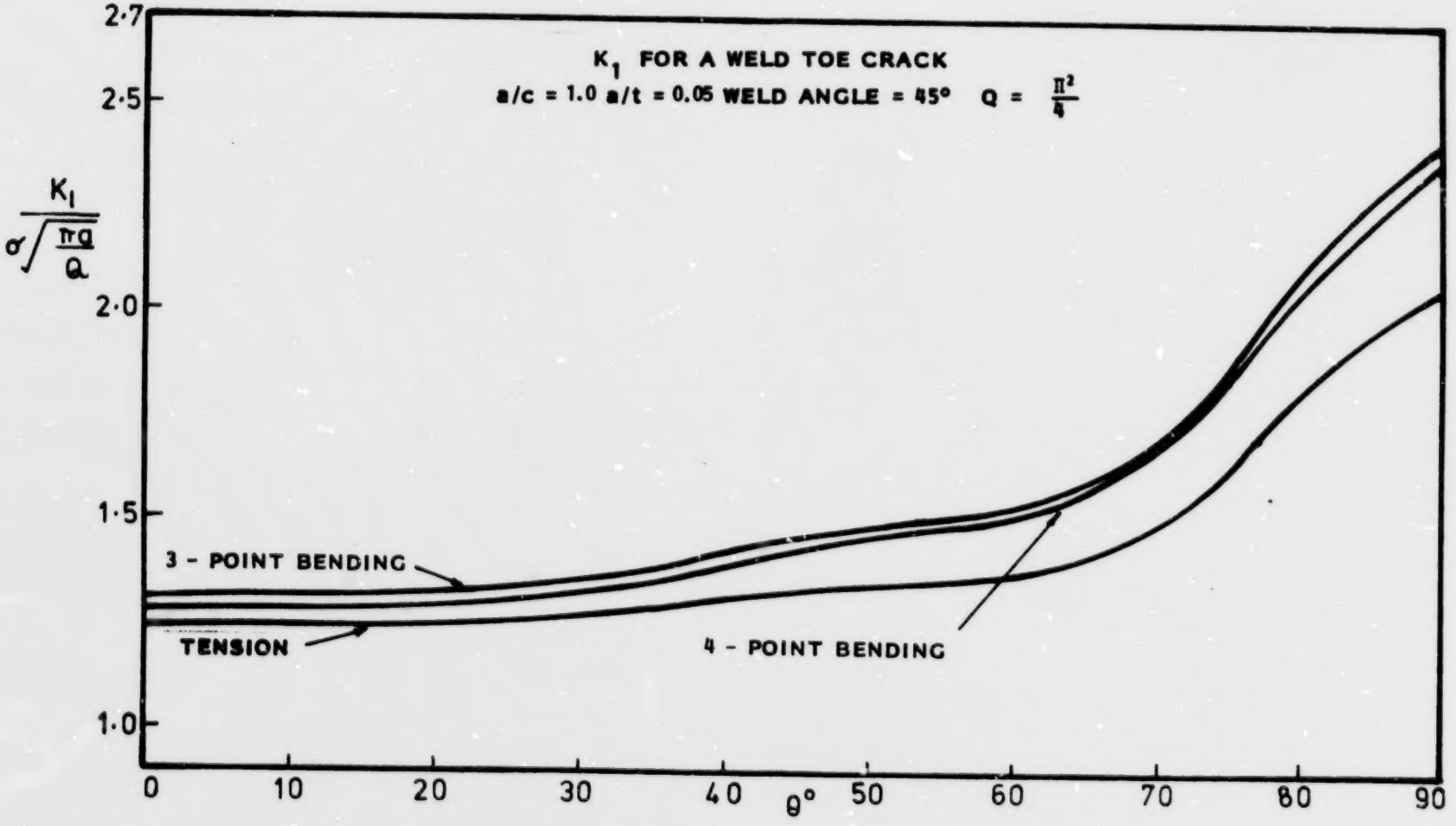
K_1 FOR A WELD TOE CRACK
a/c = 1.0 a/t = 0.05 WELD ANGLE = 45° Q = $\frac{\Pi^2}{4}$
$\frac{K_1}{\sigma\sqrt{\frac{\pi a}{Q}}}$
2·7
2·5
2·0
1·5
1·0
3 - POINT BENDING
TENSION
4 - POINT BENDING
0
10
20
30
40
θ°
50
60
70
80
90

FIG. 5.15

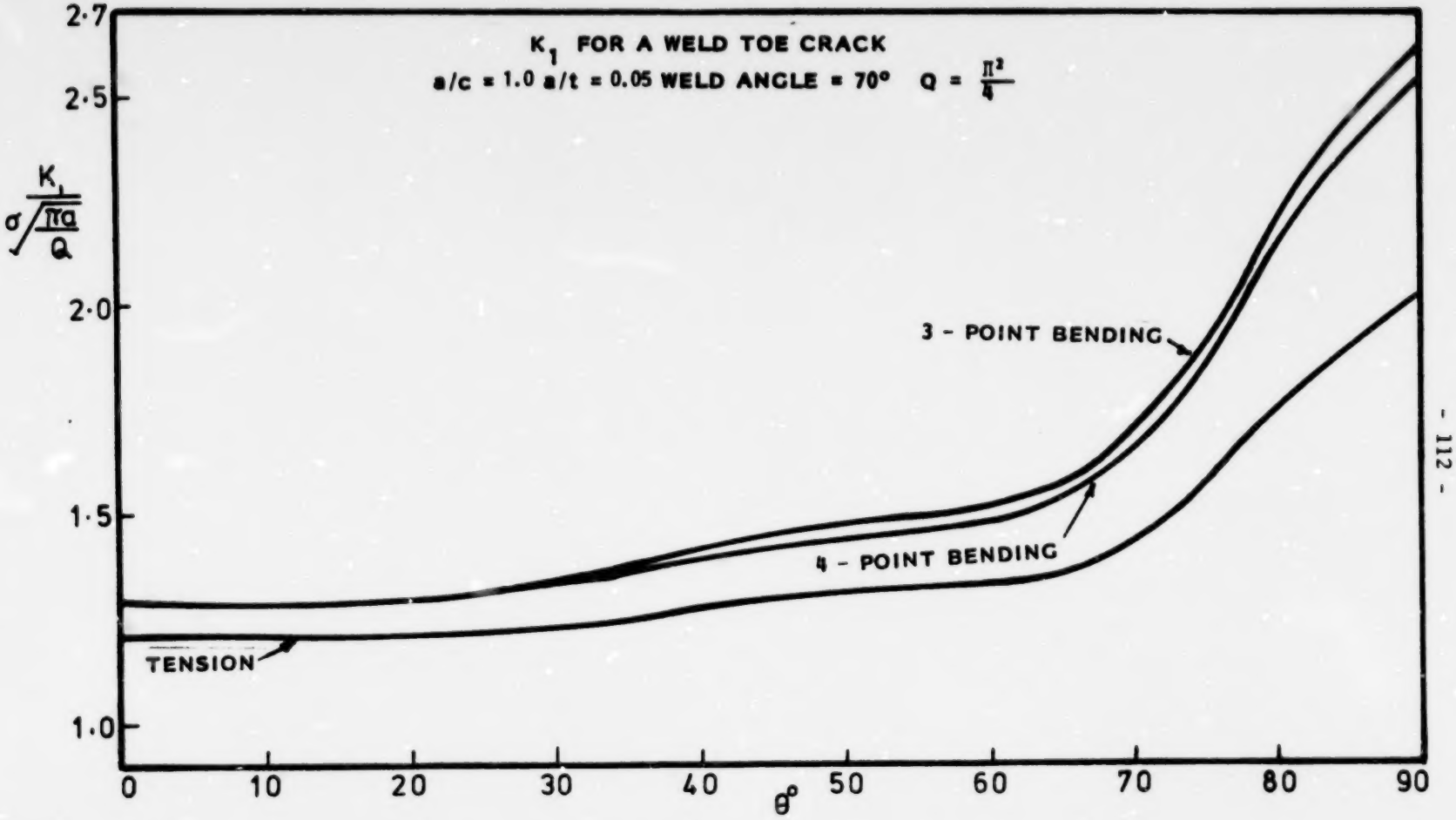
K_1 FOR A WELD TOE CRACK
a/c = 1.0 a/t = 0.05 WELD ANGLE = 70° Q = $\frac{\pi^2}{4}$
$\frac{K_1}{\sigma\sqrt{\frac{\pi a}{Q}}}$
2·7
2·5
2·0
1·5
1·0
3 - POINT BENDING
4 - POINT BENDING
TENSION
0
10
20
30
40
θ°
50
60
70
80
90

FIG. 5.16

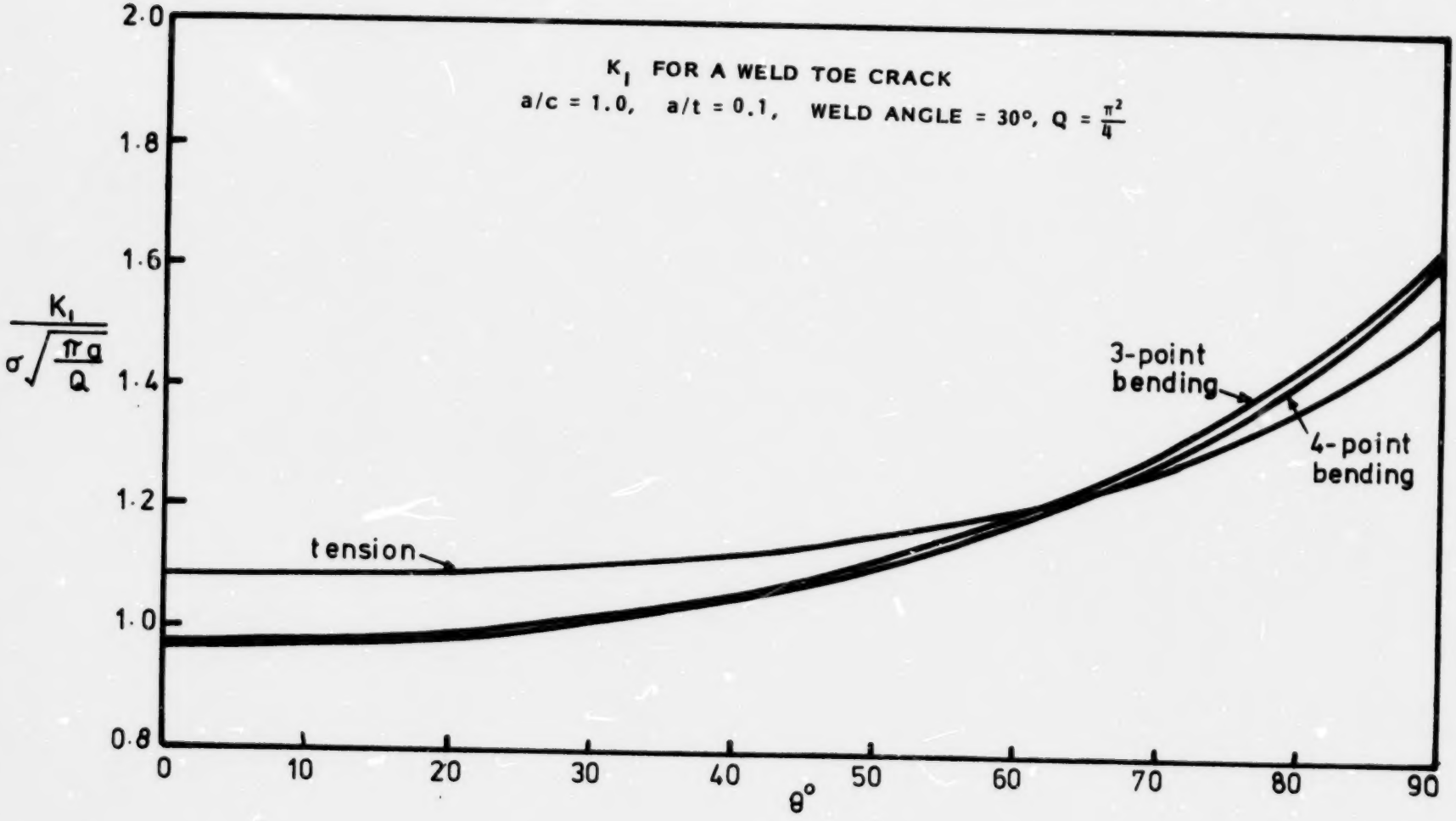
K_I FOR A WELD TOE CRACK
a/c = 1.0, a/t = 0.1, WELD ANGLE = 30°, Q = $\frac{\pi^2}{4}$
$\frac{K_I}{\sigma\sqrt{\frac{\pi a}{Q}}}$
2·0
1·8
1·6
1·4
1·2
1·0
0·8
0
10
20
30
40
50
60
70
80
90
θ°
3-point bending
4-point bending
tension

FIG. 5.17

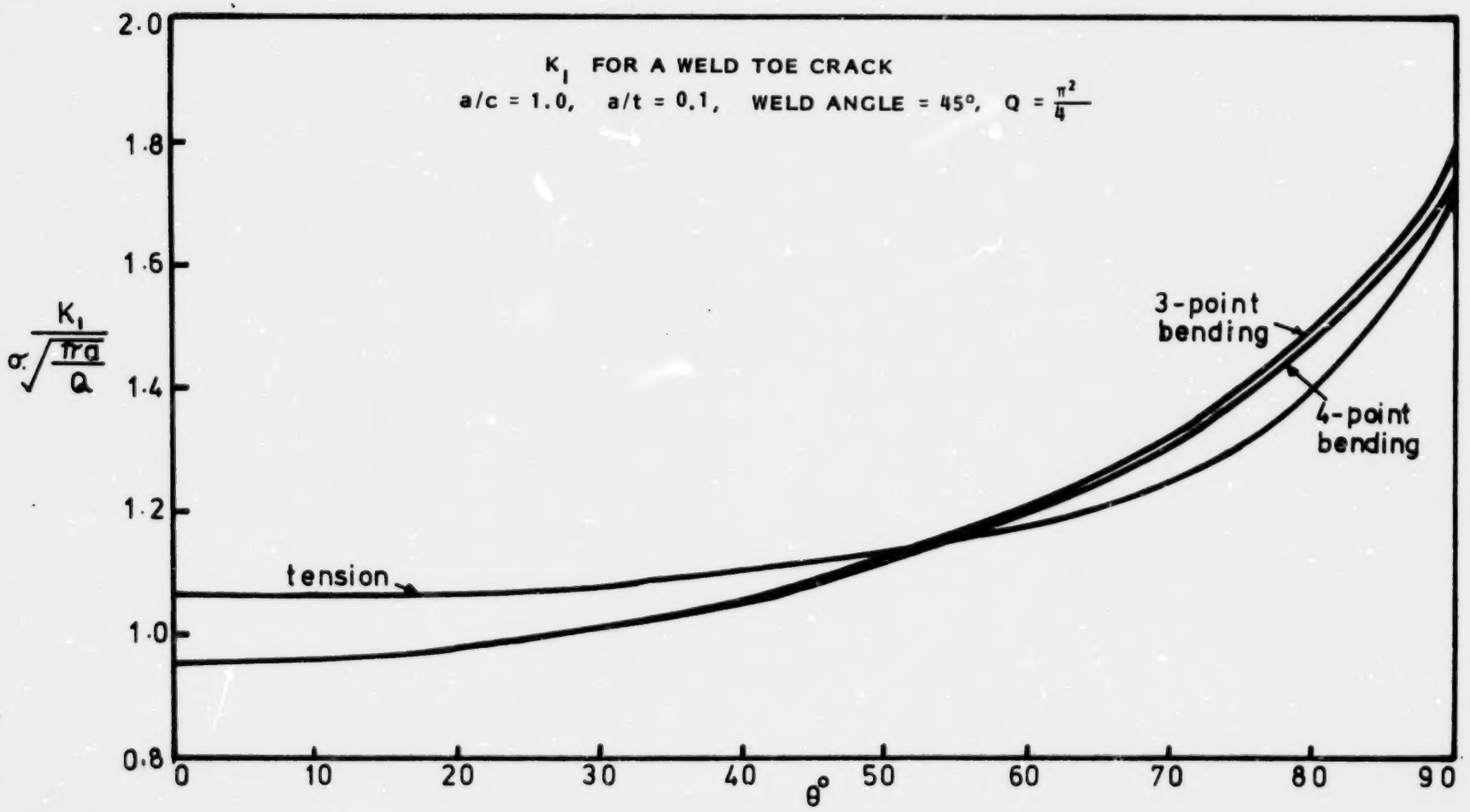
K_I FOR A WELD TOE CRACK
a/c = 1.0, a/t = 0.1, WELD ANGLE = 45°, $Q = \frac{\pi^2}{4}$
$\frac{K_I}{\sigma\sqrt{\frac{\pi a}{Q}}}$
2.0
1.8
1.6
1.4
1.2
1.0
0.8
0
10
20
30
40
θ°
50
60
70
80
90
3-point bending
4-point bending
tension

FIG. 5.18

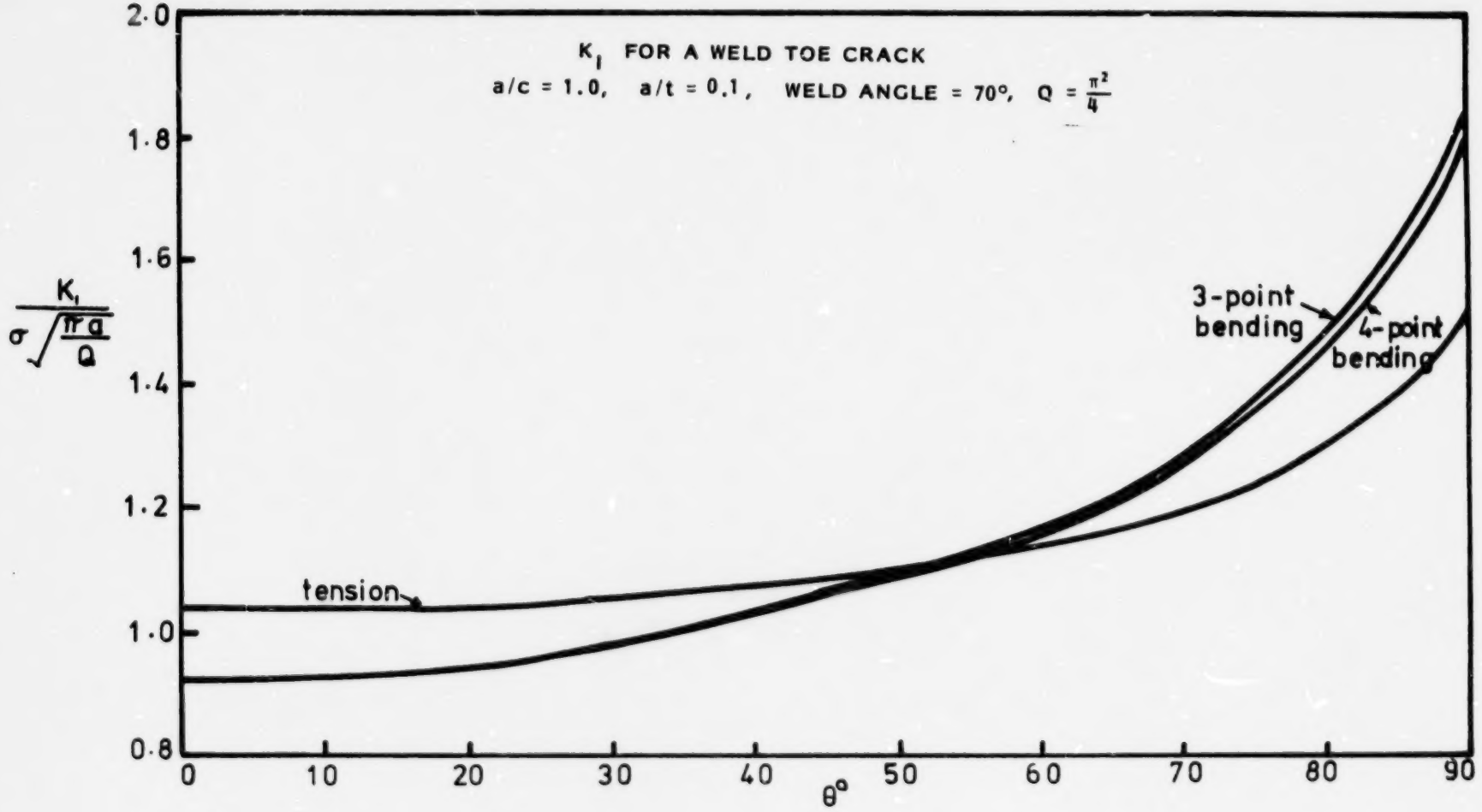
K_I FOR A WELD TOE CRACK
a/c = 1.0, a/t = 0.1, WELD ANGLE = 70°, Q = $\frac{\pi^2}{4}$
$\frac{K_I}{\sigma\sqrt{\frac{\pi a}{Q}}}$
2·0
1·8
1·6
1·4
1·2
1·0
0·8
0
10
20
30
40
50
60
70
80
90
θ°
3-point bending
4-point bending
tension

FIG. 5.19

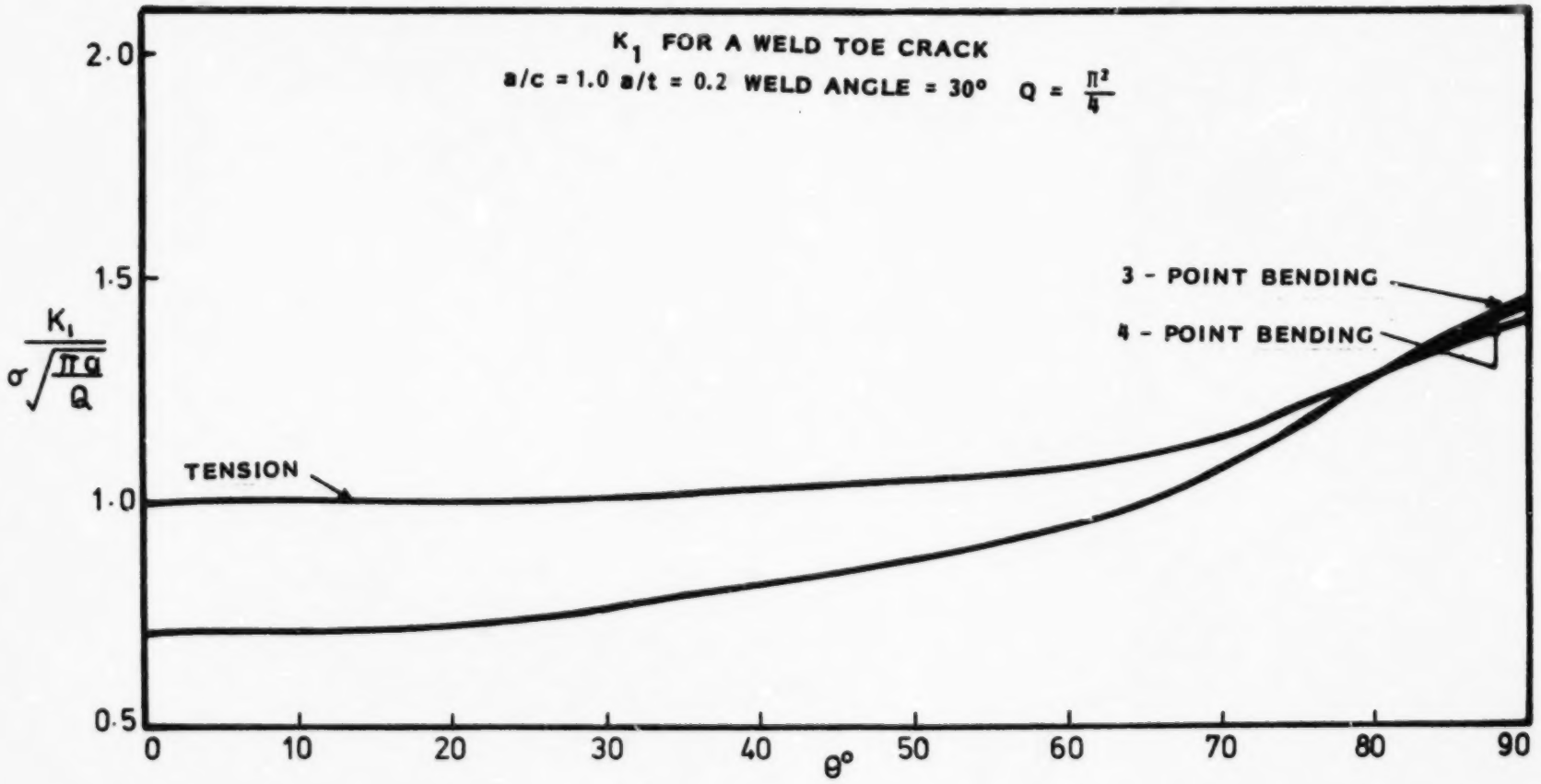
K_1 FOR A WELD TOE CRACK
a/c = 1.0 a/t = 0.2 WELD ANGLE = 30° Q = $\frac{\pi^2}{4}$
2·0
1·5
1·0
0·5
$\frac{K_1}{\sigma\sqrt{\frac{\pi a}{Q}}}$
3 - POINT BENDING
4 - POINT BENDING
TENSION
0
10
20
30
40
θ°
50
60
70
80
90

FIG. 5.20

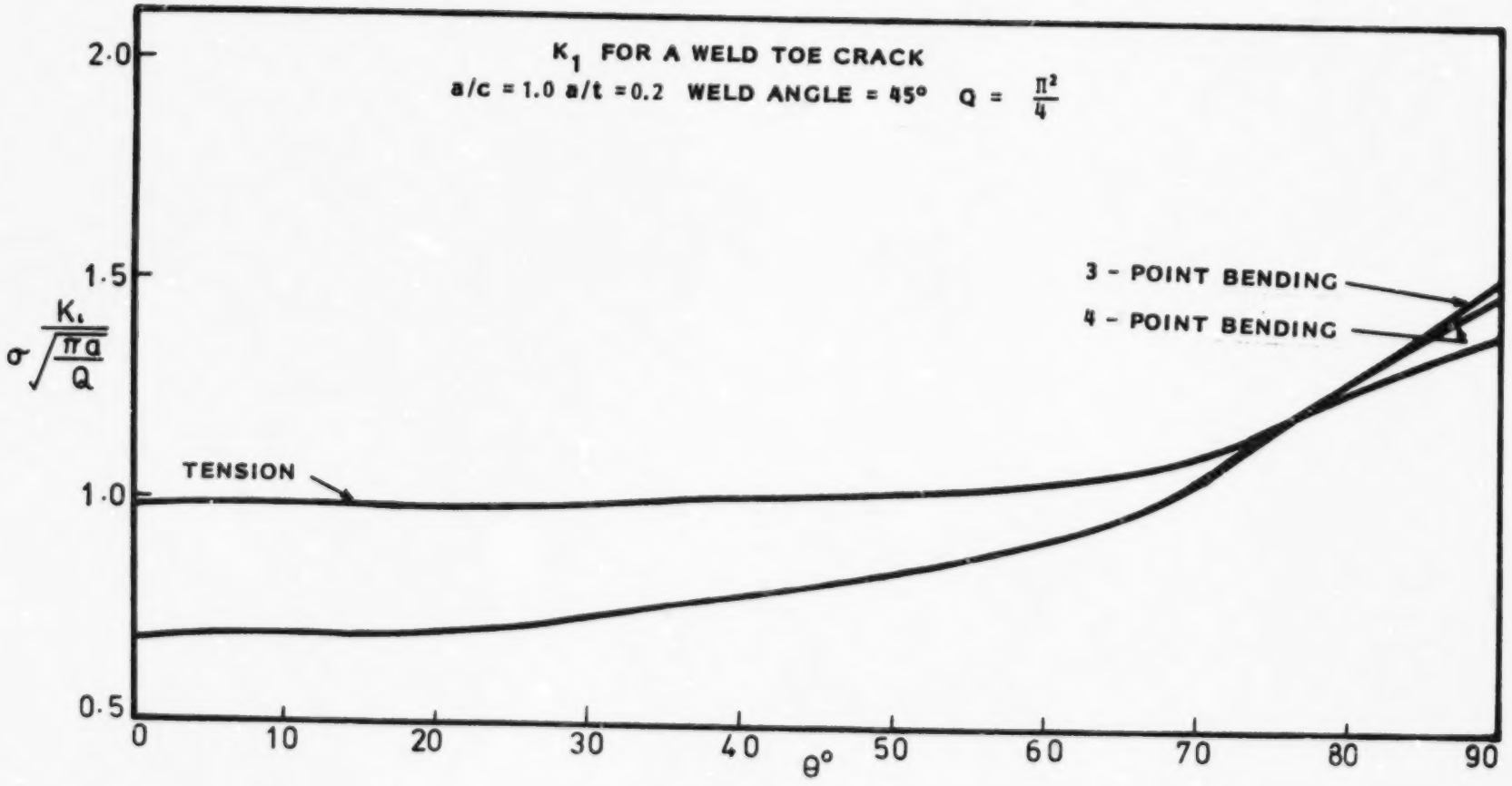
K_1 FOR A WELD TOE CRACK
a/c = 1.0 a/t = 0.2 WELD ANGLE = 45° Q = $\frac{\pi^2}{4}$
3 - POINT BENDING
4 - POINT BENDING
TENSION
$\sigma\sqrt{\frac{\pi a}{Q}}$
2·0
1·5
1·0
0·5
0
10
20
30
40
θ°
50
60
70
80
90

FIG. 5.21

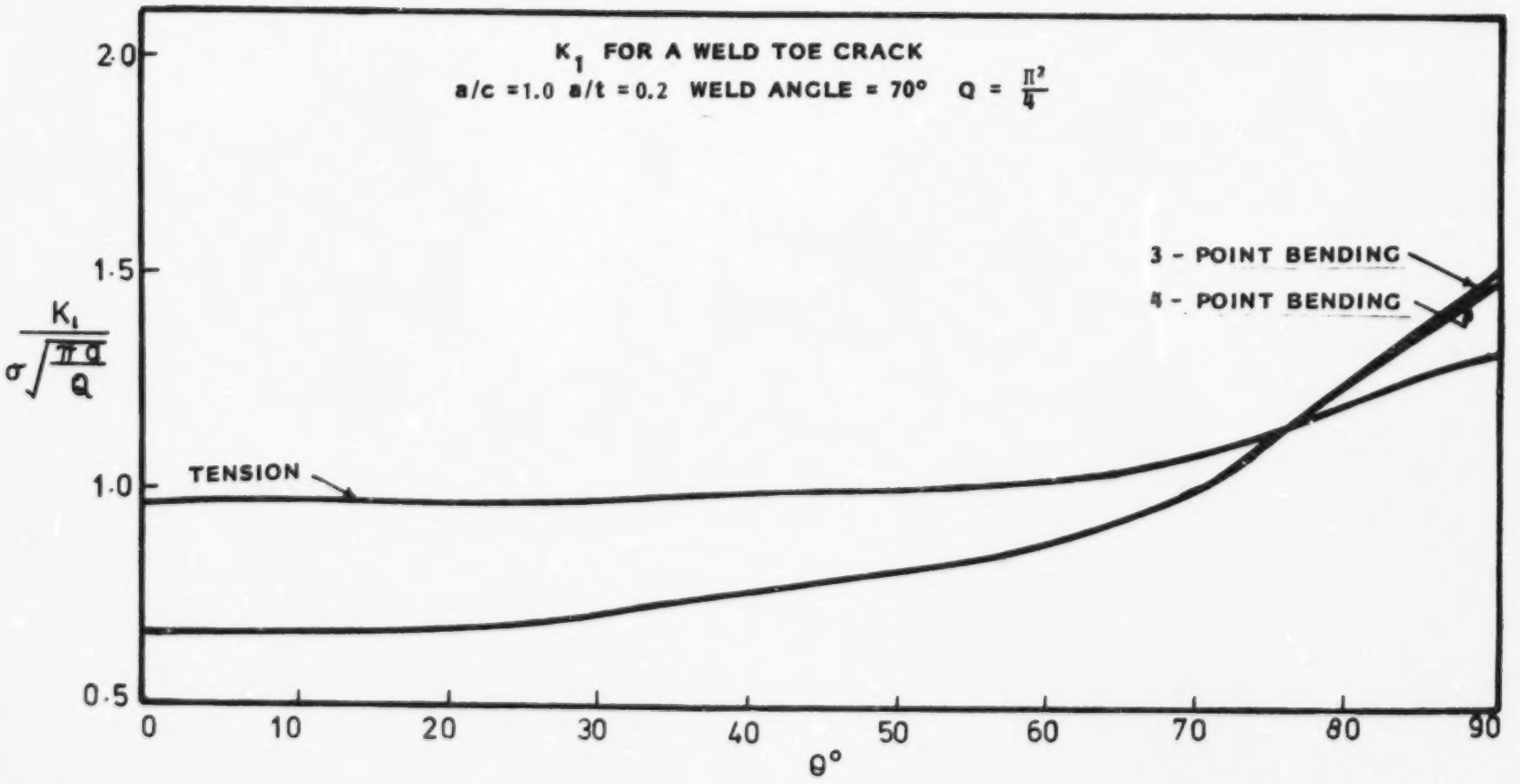
K_1 FOR A WELD TOE CRACK
a/c =1.0 a/t = 0.2 WELD ANGLE = 70° Q = $\frac{\pi^2}{4}$
3 - POINT BENDING
4 - POINT BENDING
TENSION
$\frac{K_1}{\sigma\sqrt{\frac{\pi a}{Q}}}$
2·0
1·5
1·0
0·5
0
10
20
30
40
50
60
70
80
90
θ°

FIG. 5.22

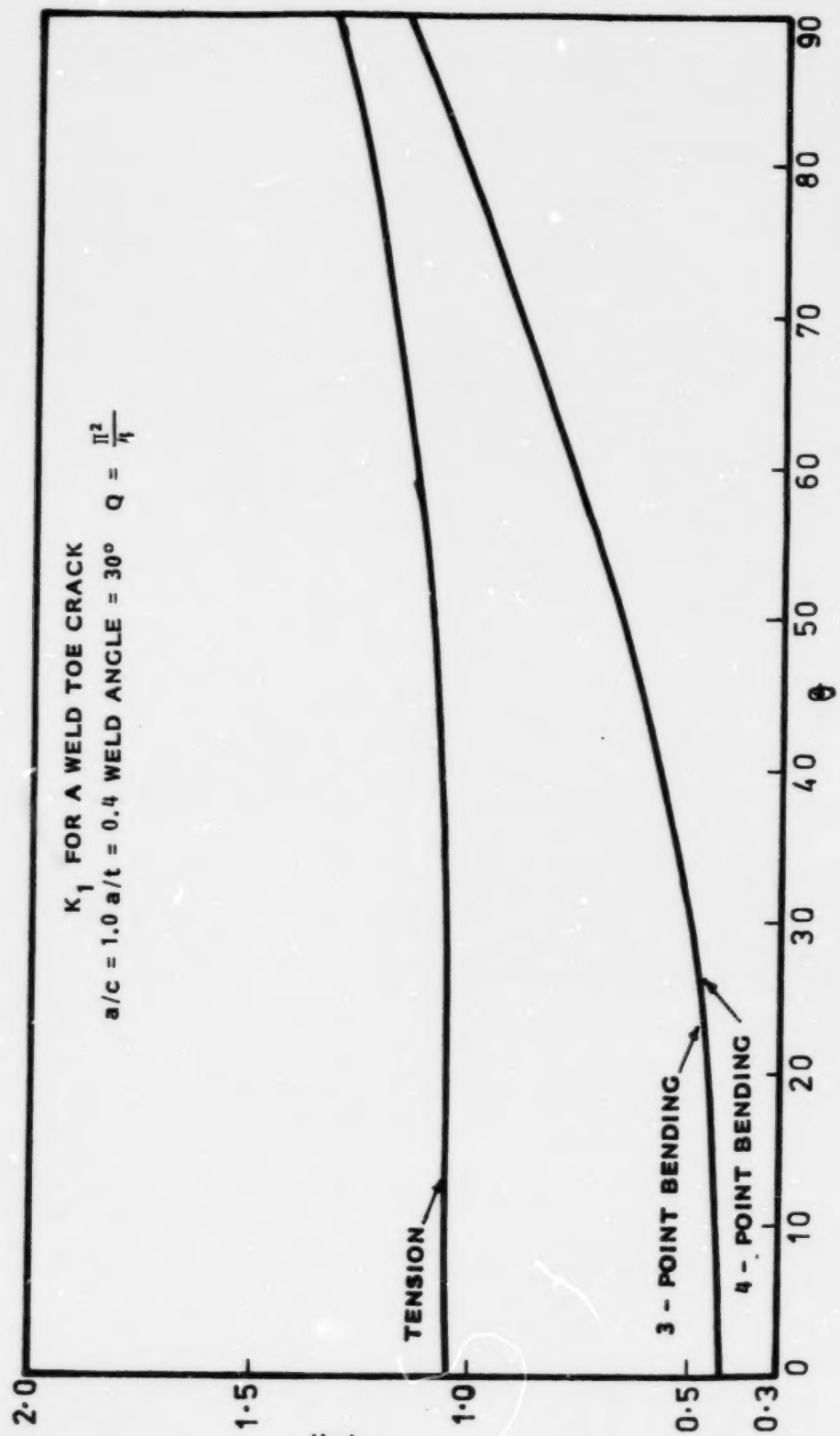
K_1 FOR A WELD TOE CRACK
a/c = 1.0 a/t = 0.4 WELD ANGLE = 30° Q = $\frac{\Pi^2}{4}$
$\frac{K_1}{\sigma\sqrt{\frac{\Pi a}{Q}}}$
2·0
1·5
1·0
0·5
0·3
0
10
20
30
40
50
60
70
80
90
θ
TENSION
3 - POINT BENDING
4 - POINT BENDING

FIG. 5.23

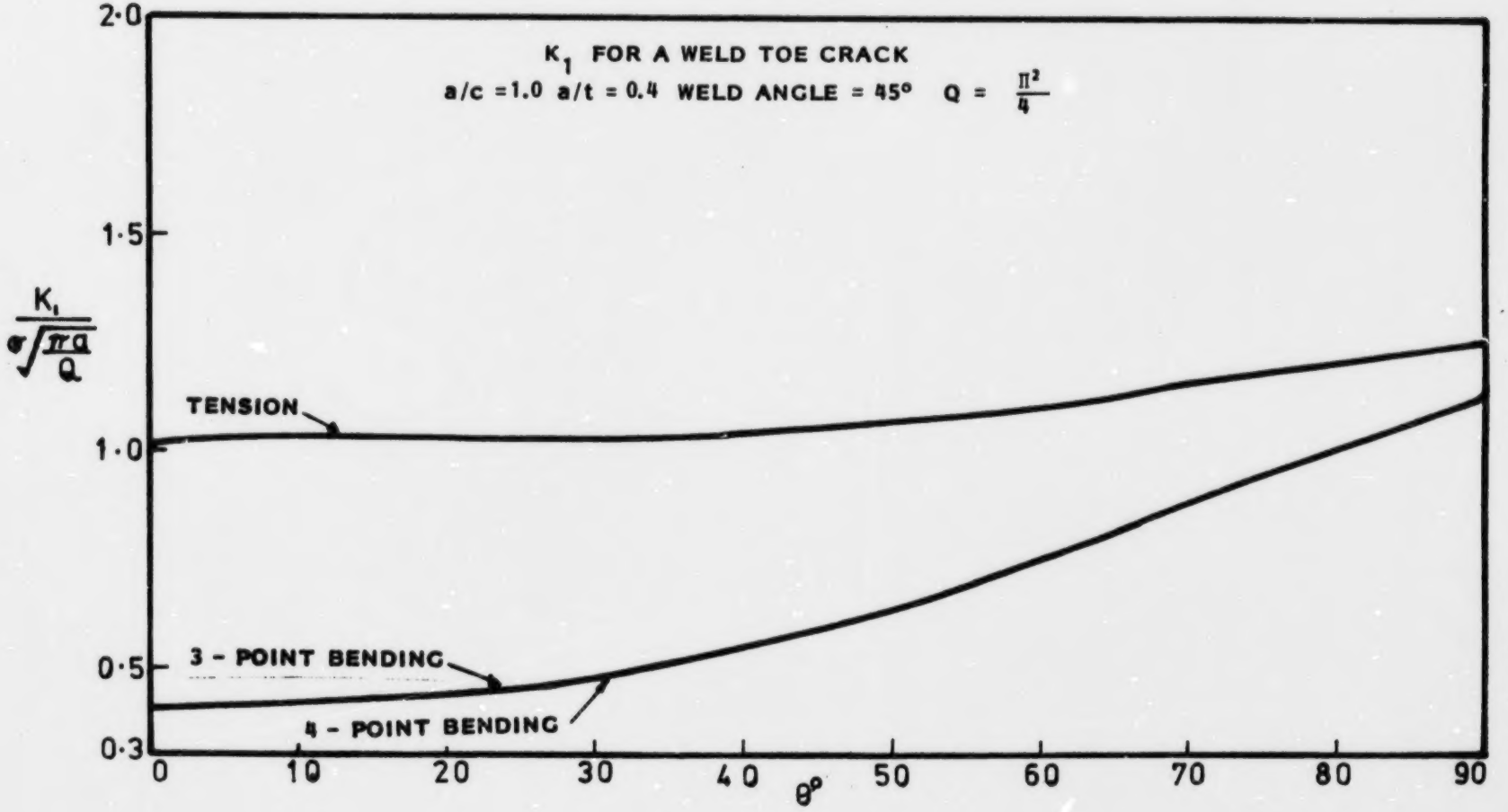
K_1 FOR A WELD TOE CRACK
a/c =1.0 a/t = 0.4 WELD ANGLE = 45° Q = $\frac{\pi^2}{4}$
$\frac{K_1}{\sigma\sqrt{\frac{\pi a}{Q}}}$
2·0
1·5
1·0
0·5
0·3
TENSION
3 - POINT BENDING
4 - POINT BENDING
0
10
20
30
40
θ°
50
60
70
80
90

FIG. 5.24

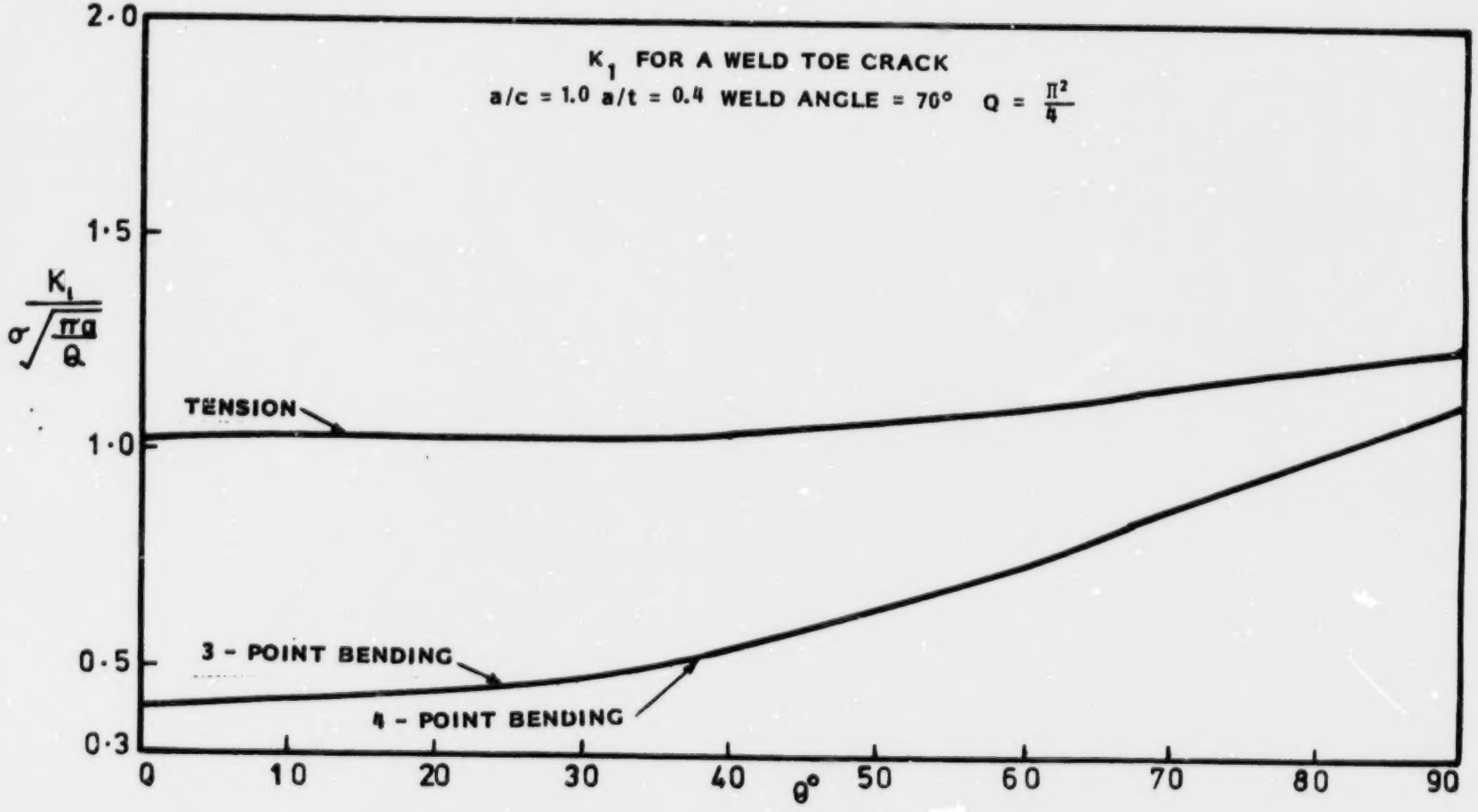
K_1 FOR A WELD TOE CRACK
a/c = 1.0 a/t = 0.4 WELD ANGLE = 70° Q = $\frac{\Pi^2}{4}$
$\frac{K_1}{\sigma\sqrt{\frac{\pi a}{Q}}}$
2·0
1·5
1·0
0·5
0·3
TENSION
3 - POINT BENDING
4 - POINT BENDING
0
10
20
30
40
θ°
50
60
70
80
90

FIG. 5.25

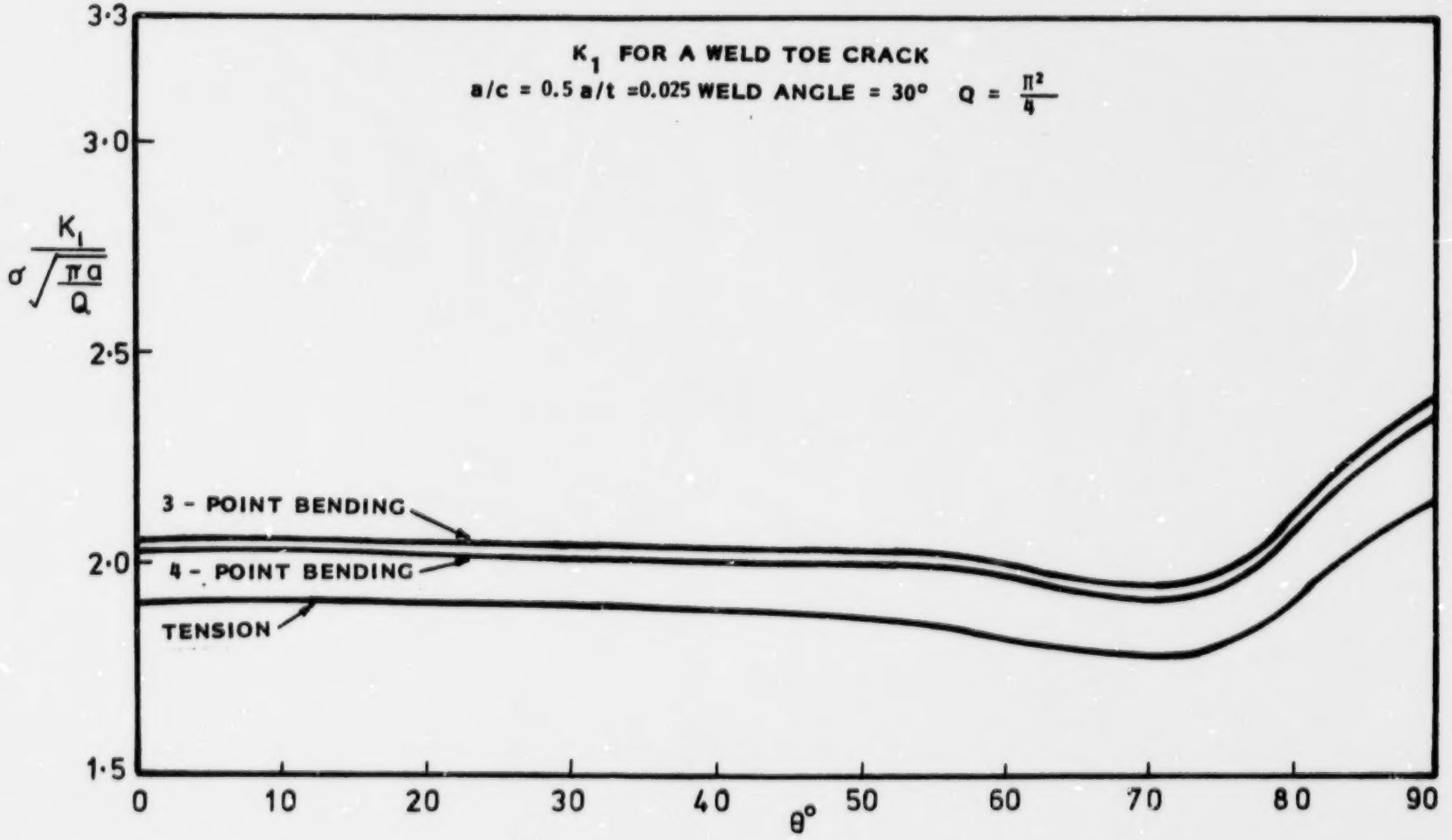
K_1 FOR A WELD TOE CRACK
a/c = 0.5 a/t =0.025 WELD ANGLE = 30° Q = $\frac{\pi^2}{4}$
$\sigma\sqrt{\frac{\pi a}{Q}}$
3·3
3·0
2·5
2·0
1·5
3 - POINT BENDING
4 - POINT BENDING
TENSION
0
10
20
30
40
50
60
70
80
90
θ°

FIG. 5.26

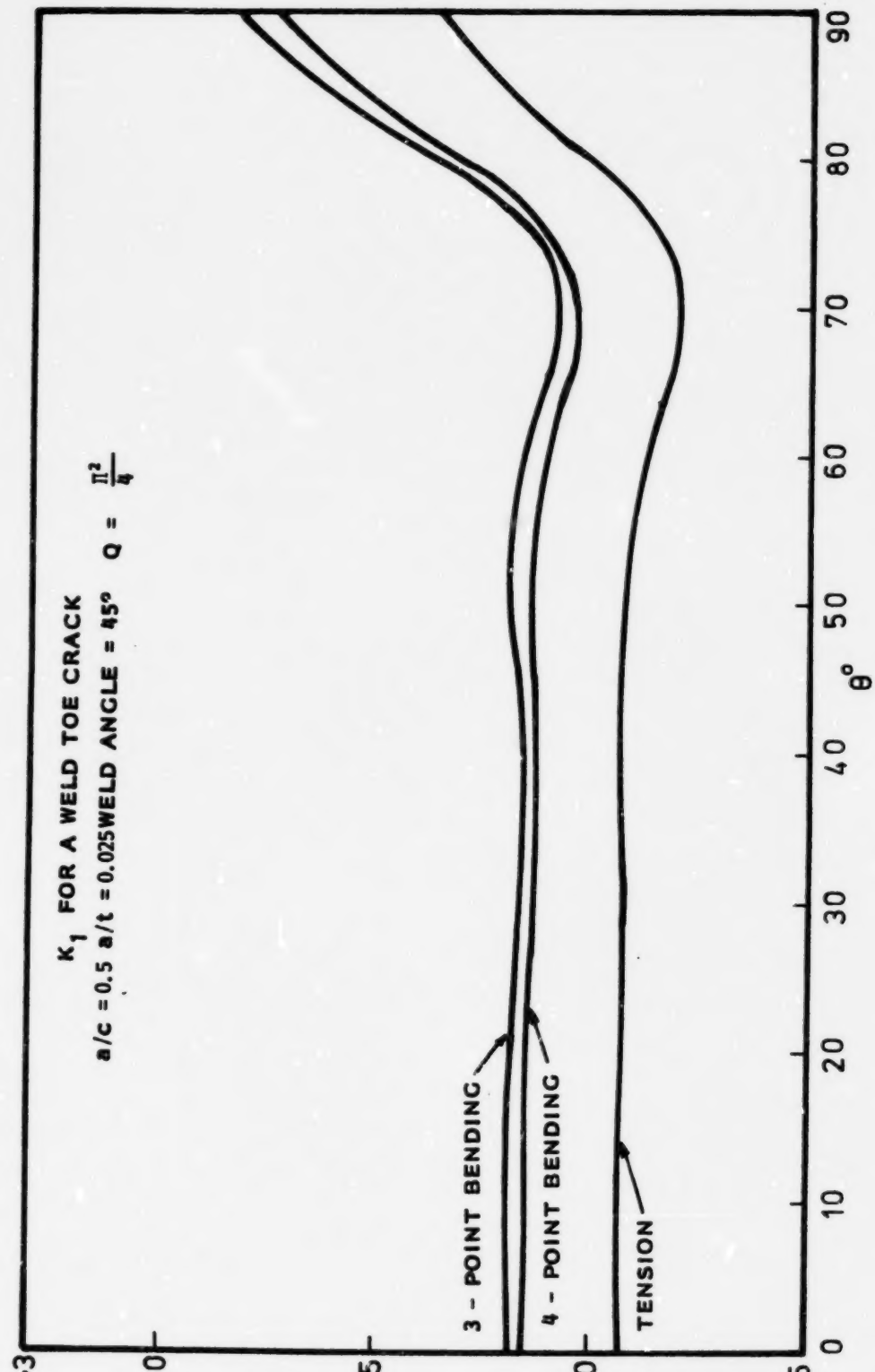
K_1 FOR A WELD TOE CRACK
a/c = 0.5 a/t = 0.025 WELD ANGLE = 45° Q = $\frac{\Pi^2}{4}$
3 - POINT BENDING
4 - POINT BENDING
TENSION
$\frac{K_1}{\sigma\sqrt{\frac{\Pi a}{Q}}}$
3·3
3·0
2·5
2·0
1·5
0
10
20
30
40
50
60
70
80
90
θ°

FIG. 5.27

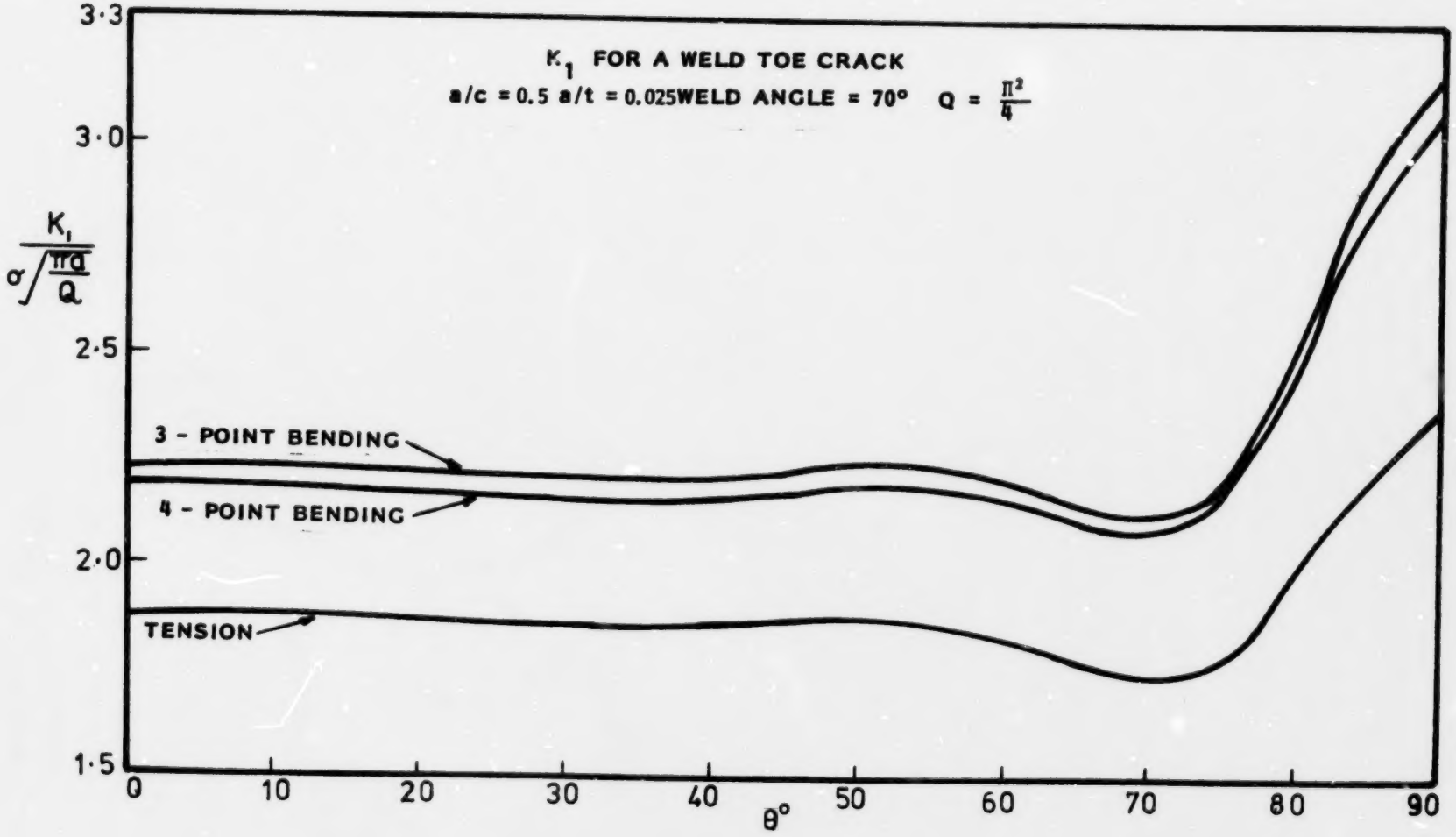
K_1 FOR A WELD TOE CRACK
a/c = 0.5 a/t = 0.025 WELD ANGLE = 70° Q = $\frac{\pi^2}{4}$
$\frac{K_1}{\sigma\sqrt{\frac{\pi a}{Q}}}$
3·3
3·0
2·5
2·0
1·5
3 - POINT BENDING
4 - POINT BENDING
TENSION
0
10
20
30
40
50
60
70
80
90
θ°

FIG. 5.28

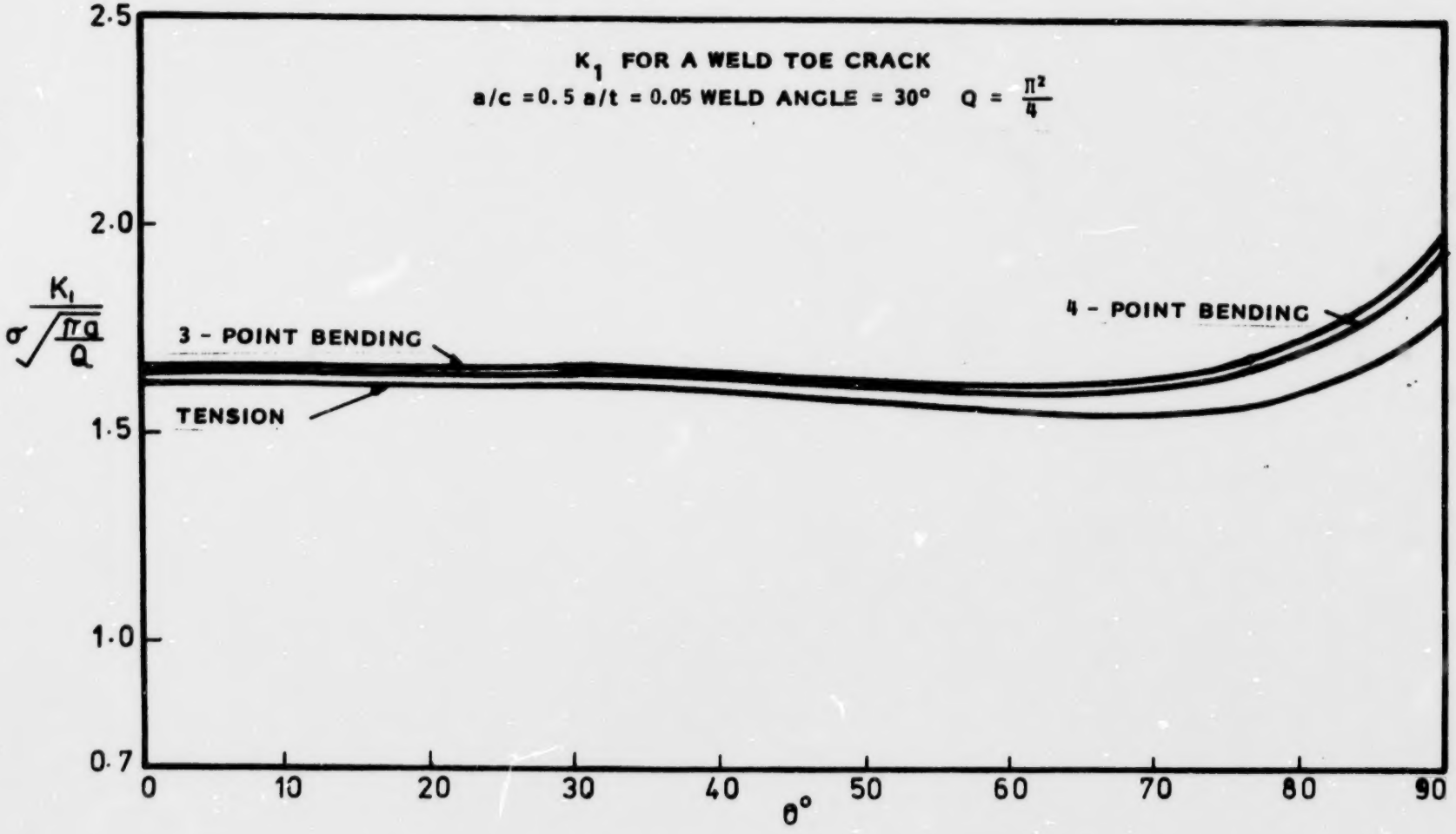
K_1 FOR A WELD TOE CRACK
a/c = 0.5 a/t = 0.05 WELD ANGLE = 30° Q = $\frac{\pi^2}{4}$
$\frac{K_1}{\sigma\sqrt{\frac{\pi a}{Q}}}$
2.5
2.0
1.5
1.0
0.7
3 - POINT BENDING
4 - POINT BENDING
TENSION
0
10
20
30
40
50
60
70
80
90
θ°

FIG. 5.29

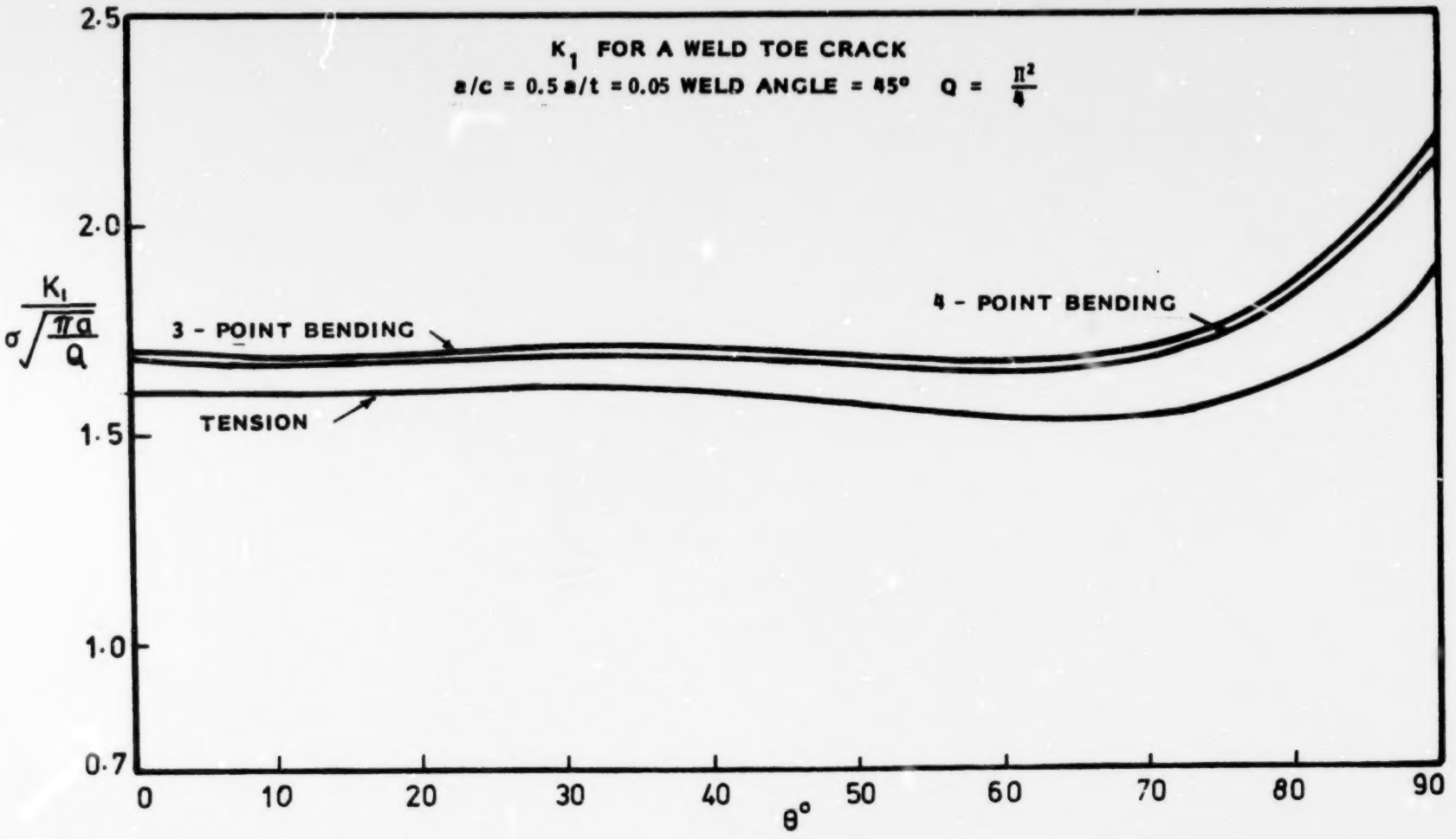
K_1 FOR A WELD TOE CRACK
a/c = 0.5 a/t = 0.05 WELD ANGLE = 45° Q = $\frac{\pi^2}{4}$
$\frac{K_1}{\sigma\sqrt{\frac{\pi a}{Q}}}$
2·5
2·0
1·5
1·0
0·7
3 - POINT BENDING
4 - POINT BENDING
TENSION
0
10
20
30
40
50
60
70
80
90
θ°

FIG. 5.30

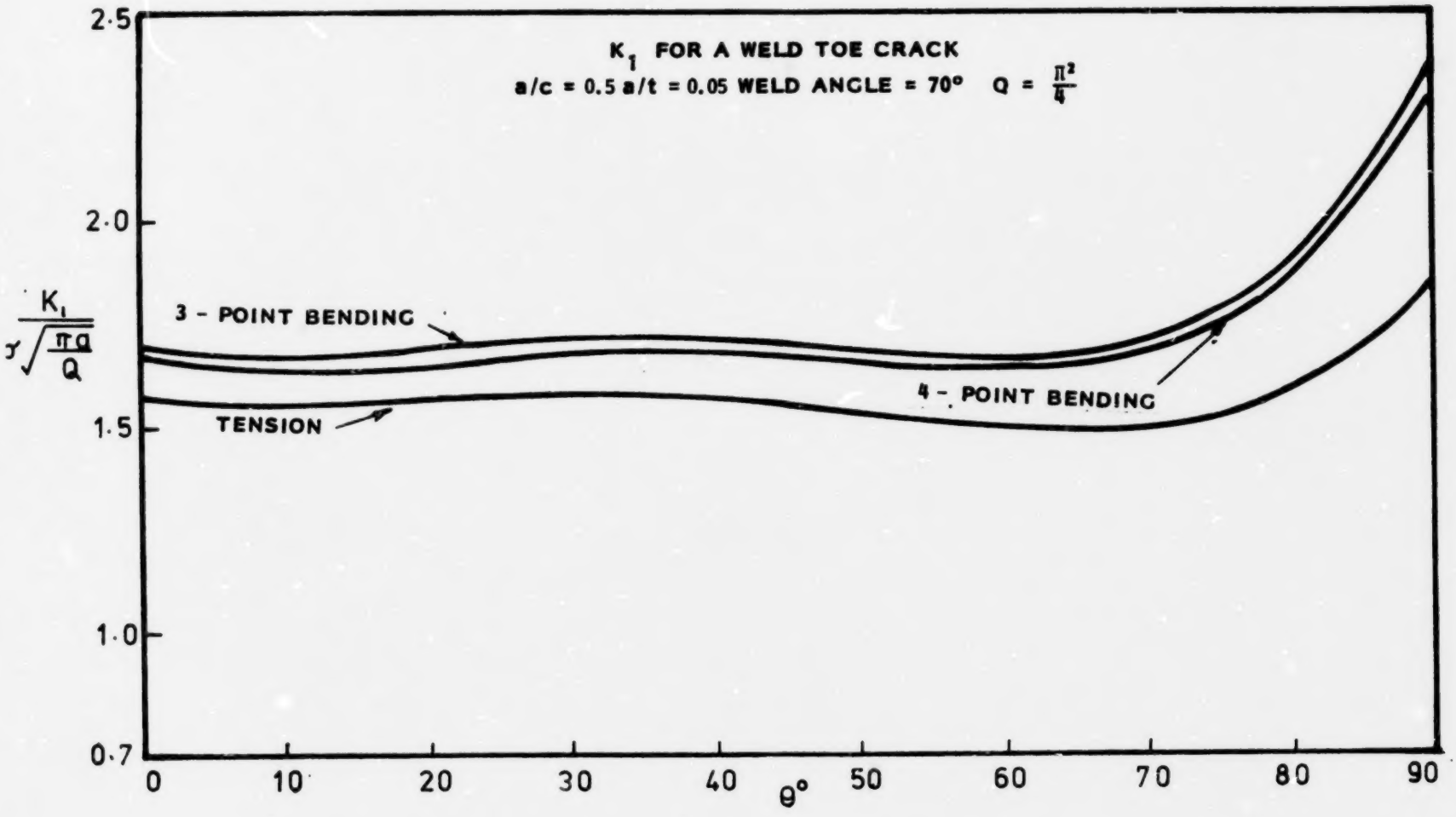
K_1 FOR A WELD TOE CRACK
a/c = 0.5 a/t = 0.05 WELD ANGLE = 70° Q = $\frac{\pi^2}{4}$
$\frac{K_1}{\sigma\sqrt{\frac{\pi a}{Q}}}$
3 - POINT BENDING
4 - POINT BENDING
TENSION
2·5
2·0
1·5
1·0
0·7
0
10
20
30
40
θ°
50
60
70
80
90

FIG. 5.31

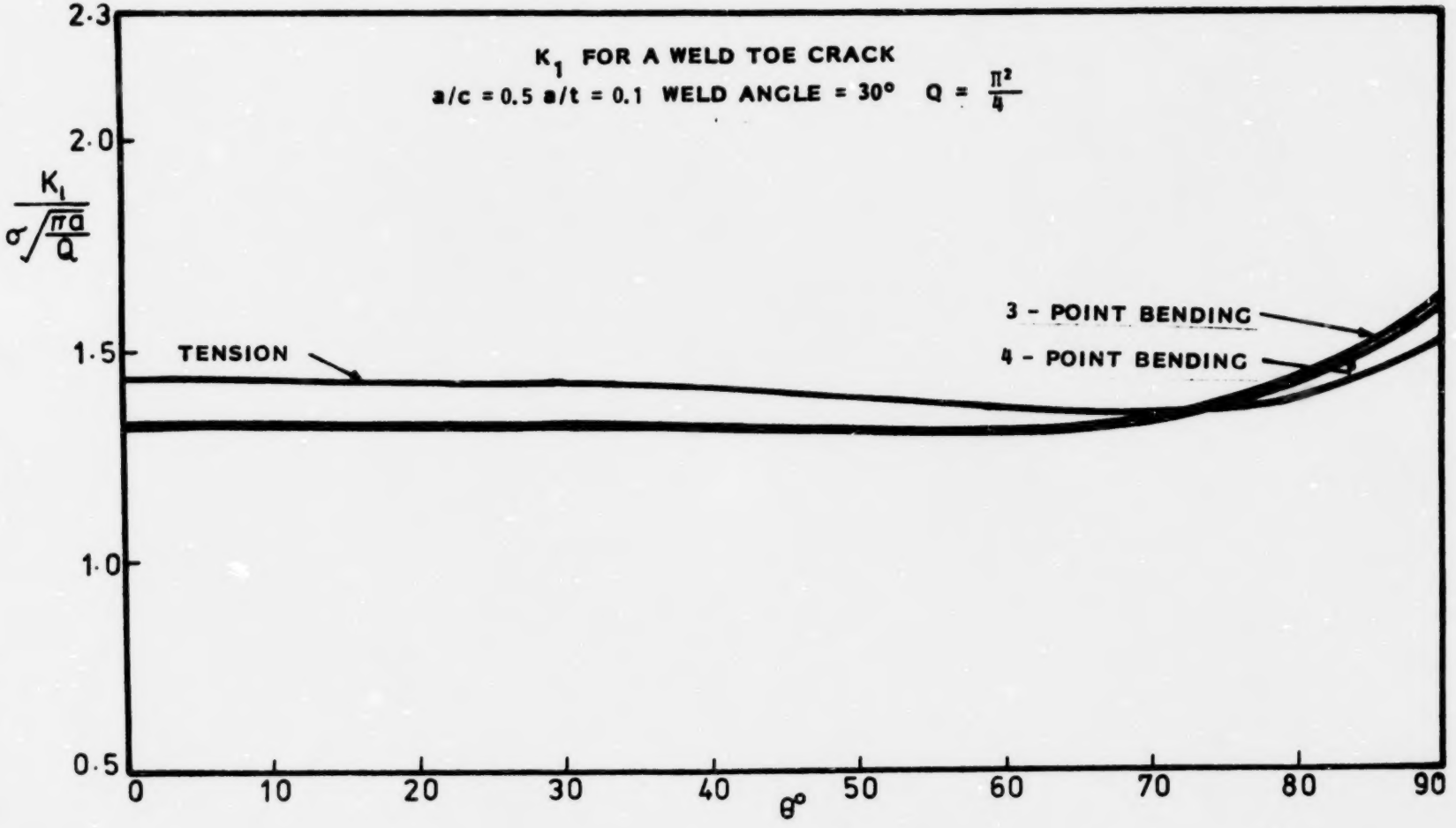
K_1 FOR A WELD TOE CRACK
a/c = 0.5 a/t = 0.1 WELD ANGLE = 30° Q = $\frac{\Pi^2}{4}$
$\frac{K_1}{\sigma\sqrt{\frac{\pi a}{Q}}}$
2·3
2·0
1·5
1·0
0·5
TENSION
3 - POINT BENDING
4 - POINT BENDING
0
10
20
30
40
50
60
70
80
90
θ°

FIG. 5.32

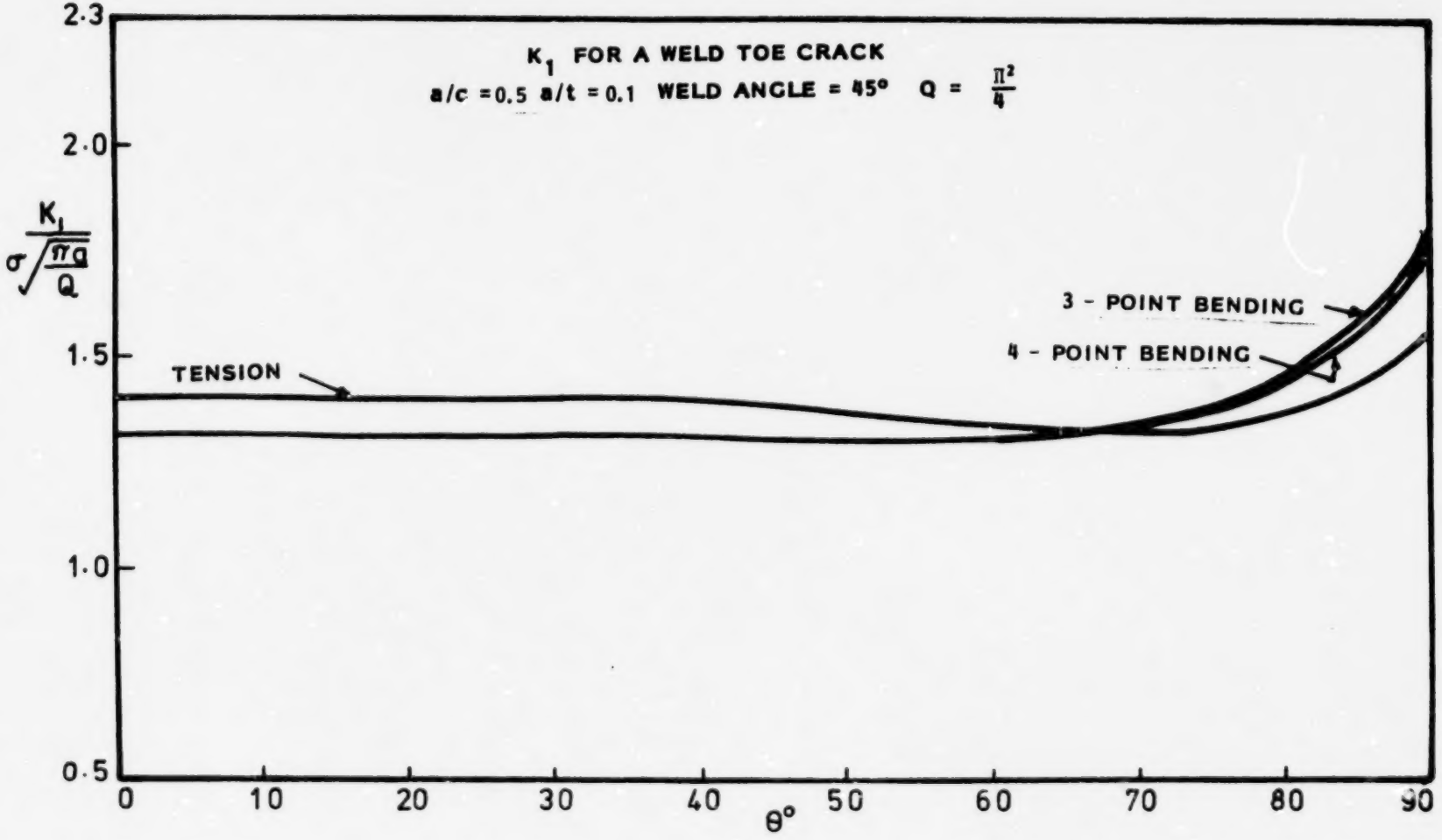
K_1 FOR A WELD TOE CRACK
a/c = 0.5 a/t = 0.1 WELD ANGLE = 45° Q = $\frac{\Pi^2}{4}$
$\frac{K_1}{\sigma\sqrt{\frac{\pi a}{Q}}}$
2·3
2·0
1·5
1·0
0·5
TENSION
3 - POINT BENDING
4 - POINT BENDING
0
10
20
30
40
θ°
50
60
70
80
90

FIG. 5.33

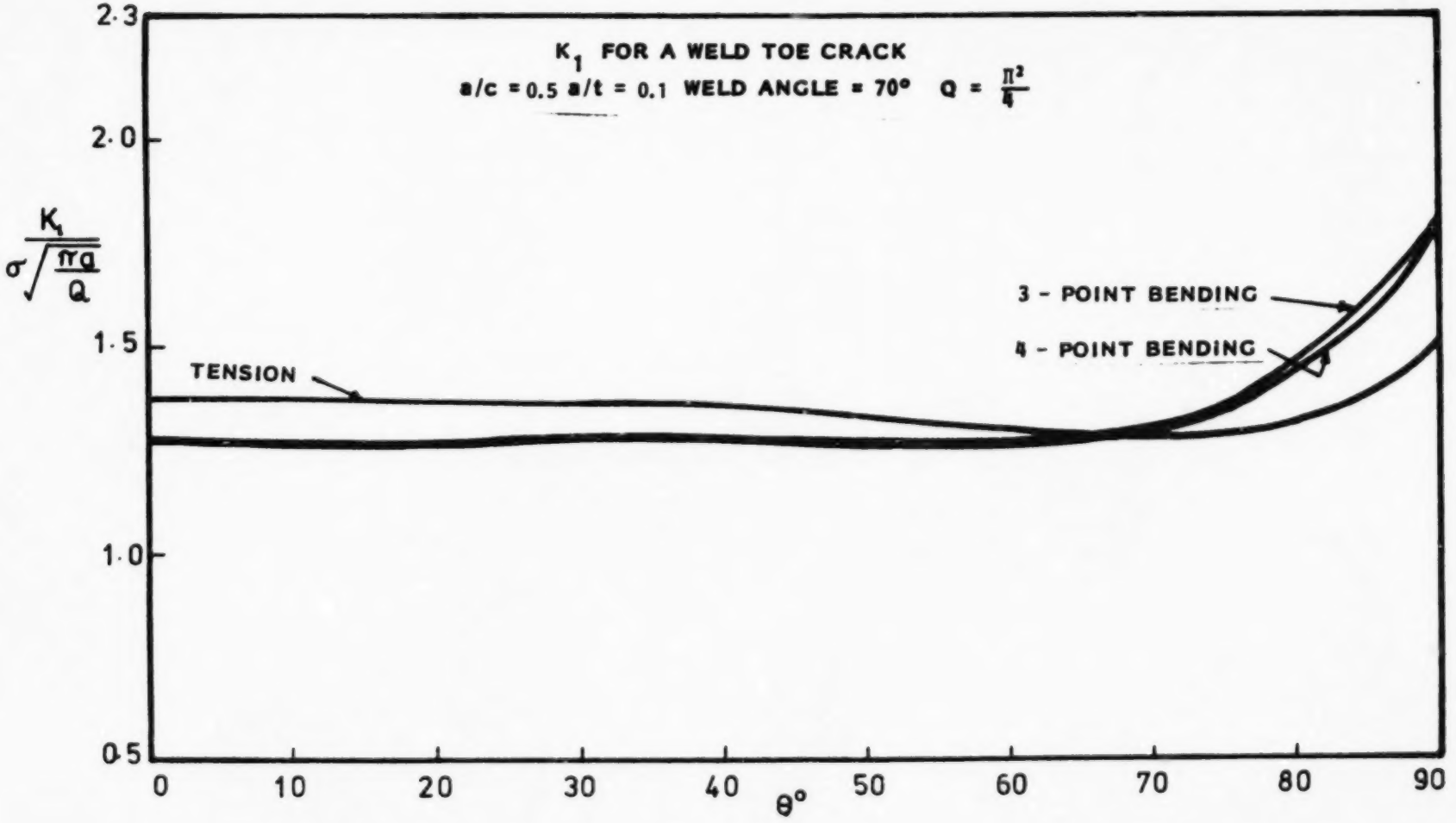
K_1 FOR A WELD TOE CRACK
a/c = 0.5 a/t = 0.1 WELD ANGLE = 70° Q = $\frac{\pi^2}{4}$
$\frac{K_1}{\sigma\sqrt{\frac{\pi a}{Q}}}$
2·3
2·0
1·5
1·0
0·5
TENSION
3 - POINT BENDING
4 - POINT BENDING
0
10
20
30
40
θ°
50
60
70
80
90

FIG. 5.34

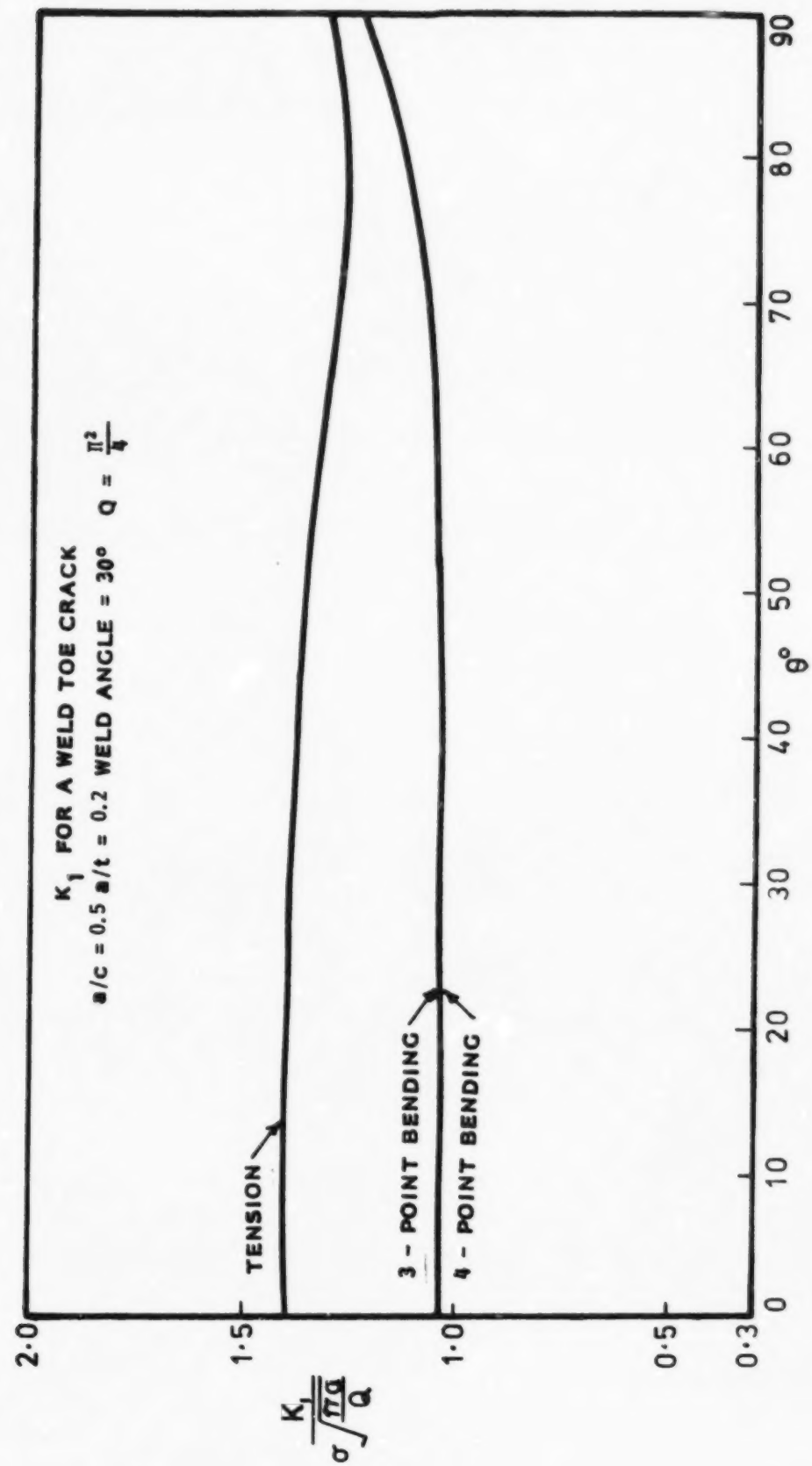
K_I FOR A WELD TOE CRACK
a/c = 0.5 a/t = 0.2 WELD ANGLE = 30° Q = $\frac{\Pi^2}{4}$
TENSION
3 - POINT BENDING
4 - POINT BENDING
$\frac{K_I}{\sigma\sqrt{\frac{\pi a}{Q}}}$
2·0
1·5
1·0
0·5
0·3
0
10
20
30
40
θ°
50
60
70
80
90

FIG. 5.35

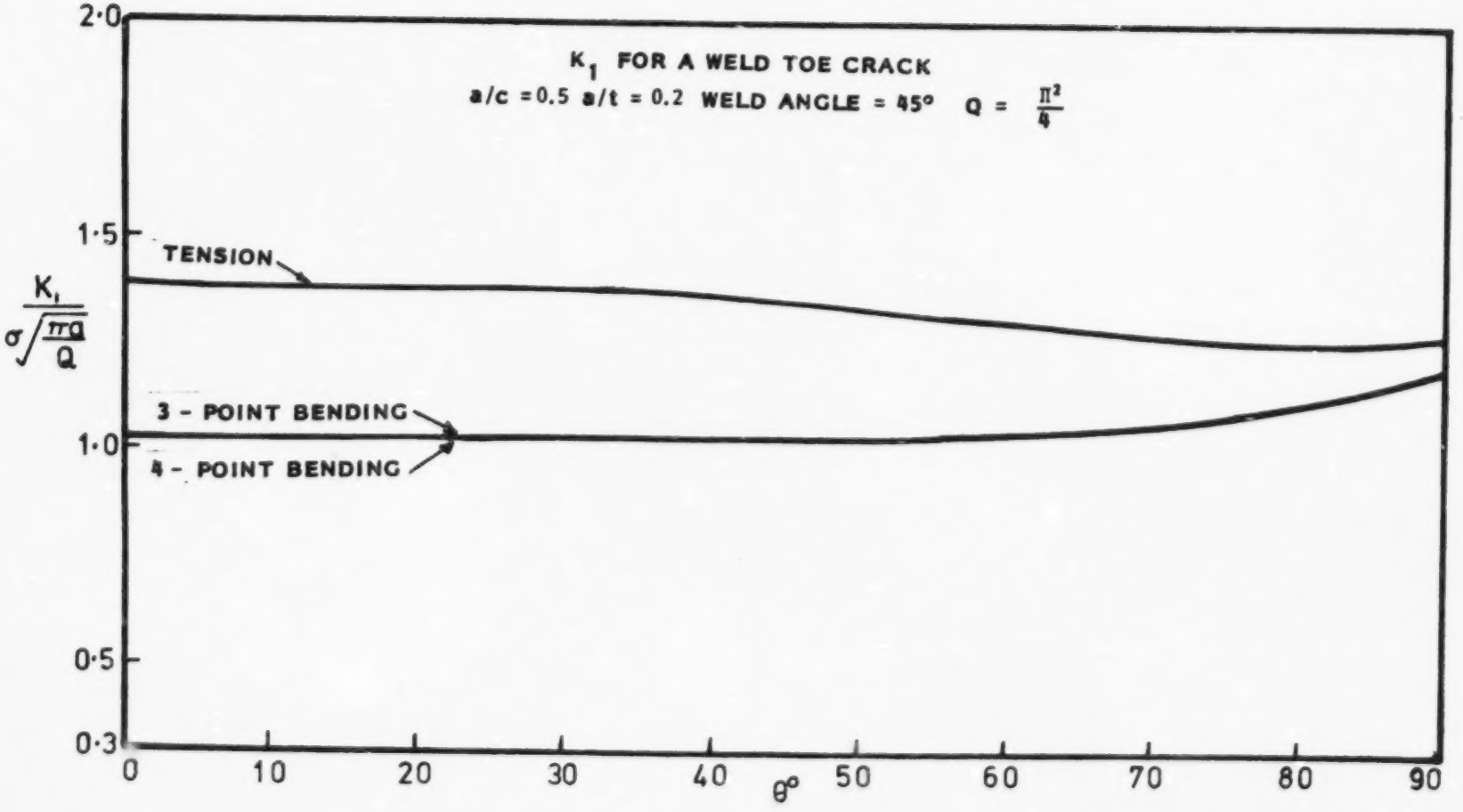
K_1 FOR A WELD TOE CRACK
a/c = 0.5 a/t = 0.2 WELD ANGLE = 45° Q = $\frac{\Pi^2}{4}$
TENSION
3 - POINT BENDING
4 - POINT BENDING
$\frac{K_1}{\sigma\sqrt{\frac{\pi a}{Q}}}$
2·0
1·5
1·0
0·5
0·3
0
10
20
30
40
θ°
50
60
70
80
90

FIG. 5.36

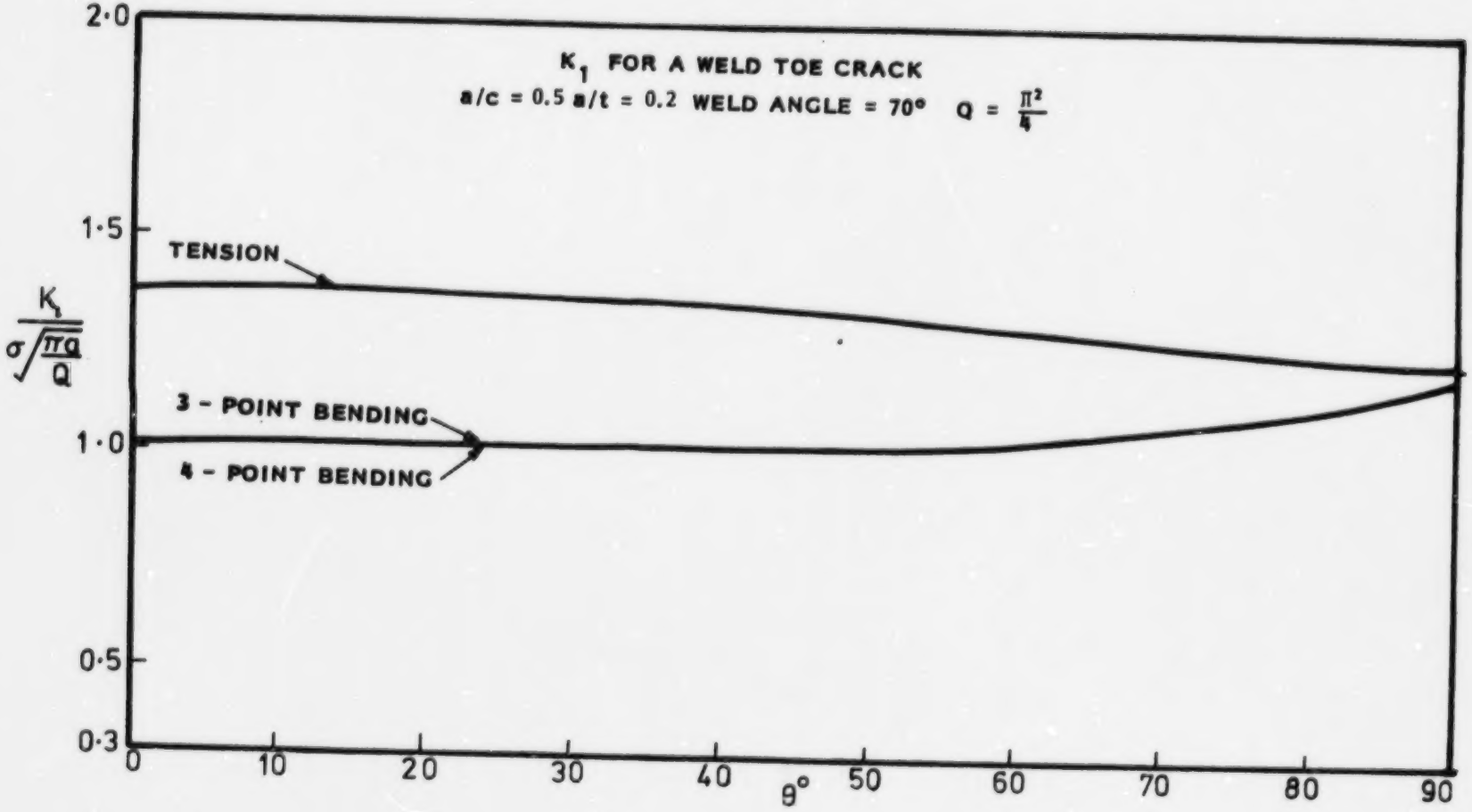
K_1 FOR A WELD TOE CRACK
a/c = 0.5 a/t = 0.2 WELD ANGLE = 70° Q = $\frac{\pi^2}{4}$
TENSION
3 - POINT BENDING
4 - POINT BENDING
$\frac{K_1}{\sigma\sqrt{\frac{\pi a}{Q}}}$
2·0
1·5
1·0
0·5
0·3
0
10
20
30
40
$\vartheta°$
50
60
70
80
90

FIG. 5.37

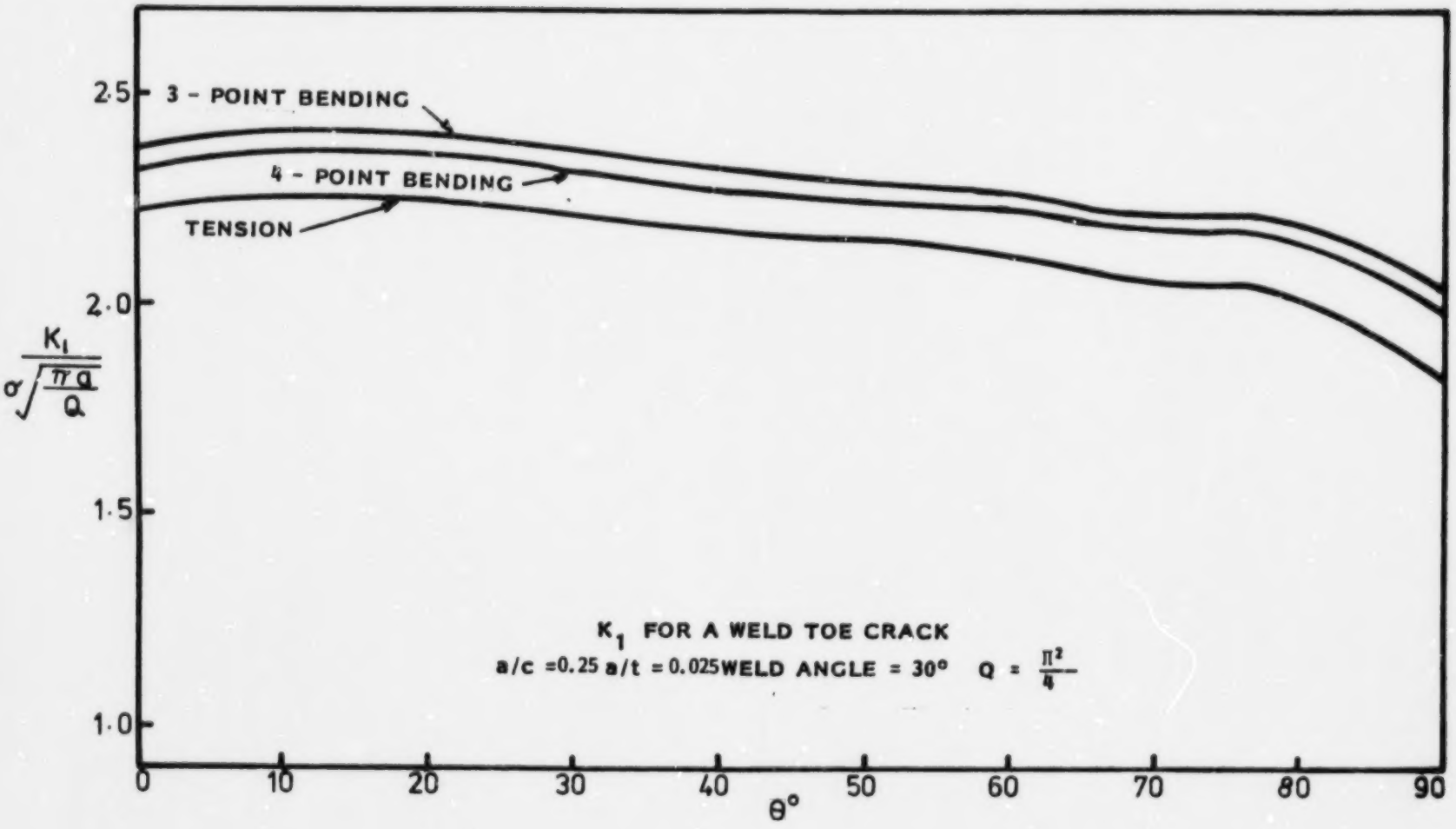
3 - POINT BENDING
4 - POINT BENDING
TENSION
2·5
2·0
1·5
1·0
$\frac{K_1}{\sigma\sqrt{\frac{\pi a}{Q}}}$
0
10
20
30
40
50
60
70
80
90
θ°
K_1 FOR A WELD TOE CRACK
a/c =0.25 a/t = 0.025 WELD ANGLE = 30° Q = $\frac{\pi^2}{4}$

FIG. 5.38

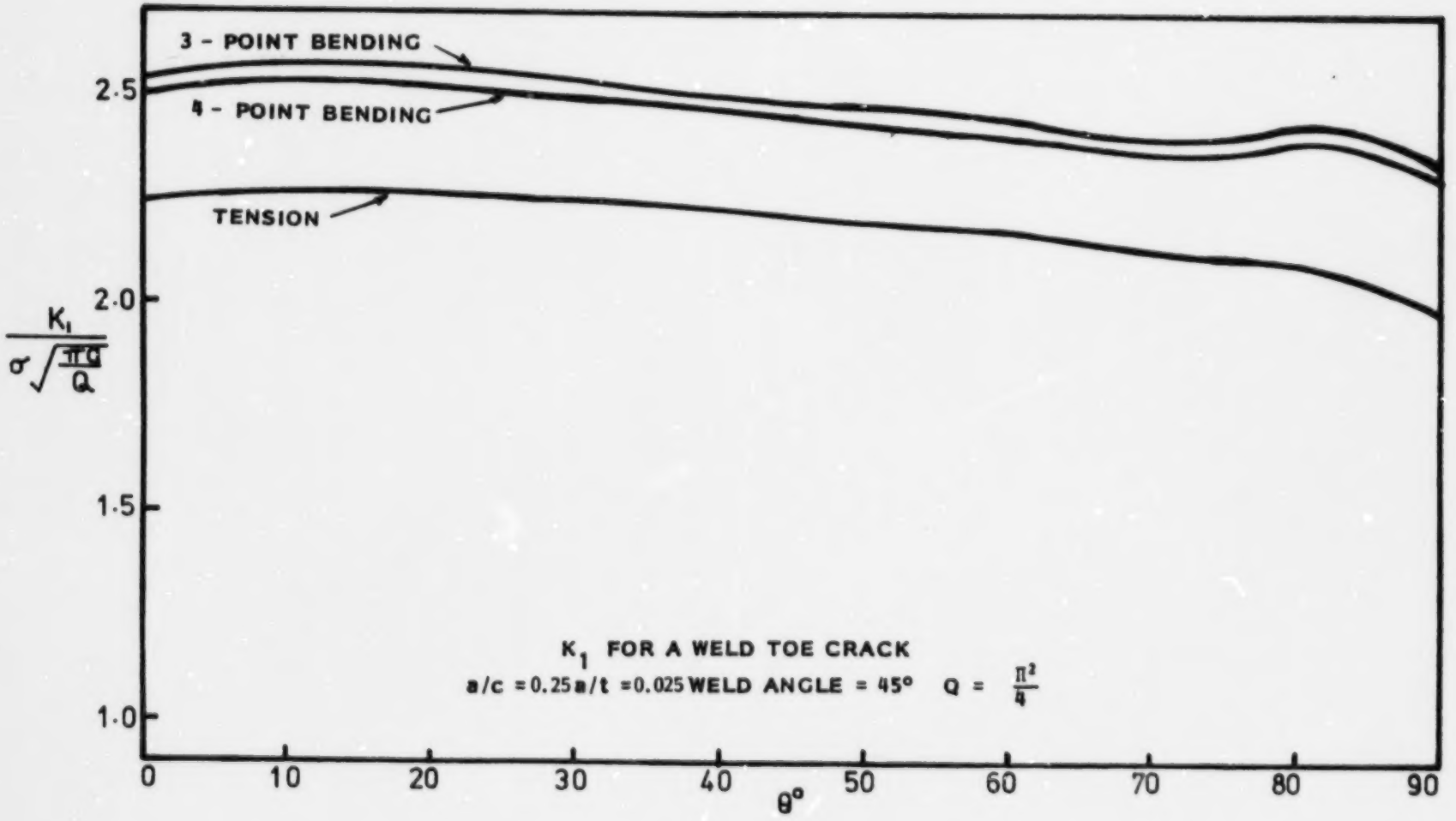
3 - POINT BENDING
4 - POINT BENDING
TENSION
2.5
2.0
1.5
1.0
$\frac{K_1}{\sigma\sqrt{\frac{\pi a}{Q}}}$
0
10
20
30
40
50
60
70
80
90
θ°
K_1 FOR A WELD TOE CRACK
a/c = 0.25 a/t = 0.025 WELD ANGLE = 45° Q = $\frac{\Pi^2}{4}$

FIG. 5.39

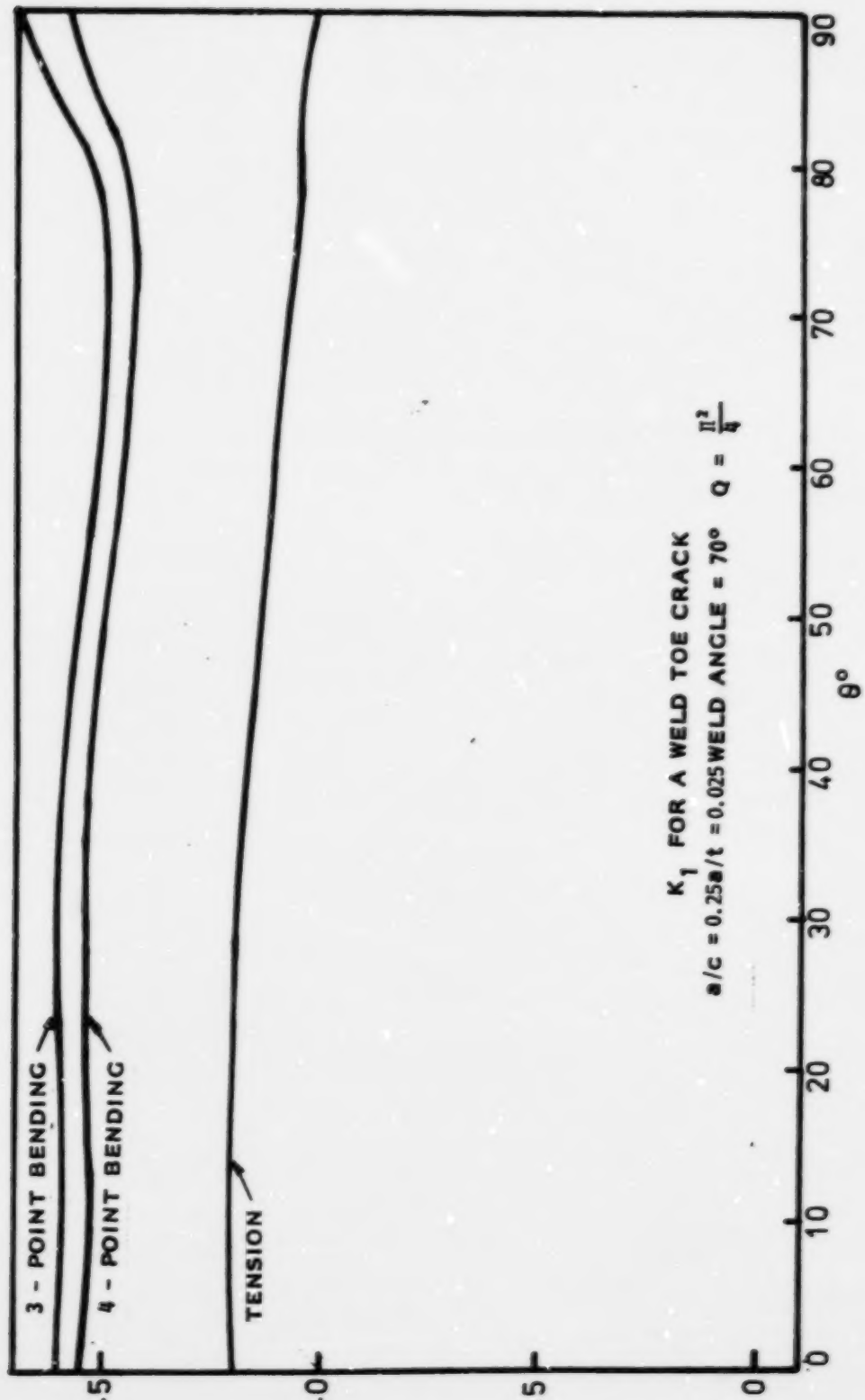
3 - POINT BENDING
4 - POINT BENDING
TENSION
K_1 FOR A WELD TOE CRACK
a/c = 0.25 a/t = 0.025 WELD ANGLE = 70° $Q = \frac{\Pi^2}{4}$
$\frac{K_1}{\sigma\sqrt{\frac{\Pi a}{Q}}}$
2.5
2.0
1.5
1.0
0
10
20
30
40
50
60
70
80
90
θ°

FIG. 5.40

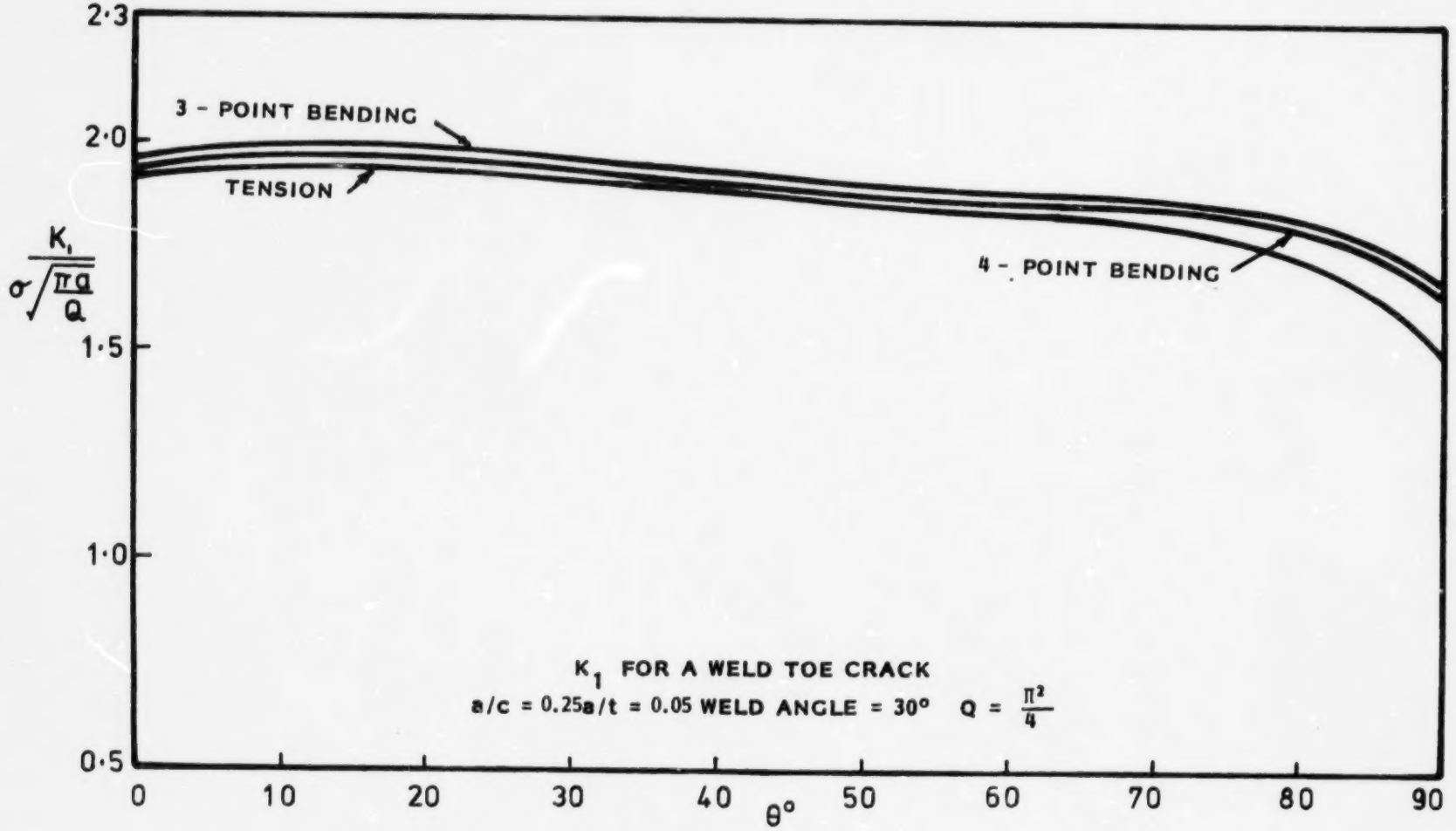
2·3
2·0
1·5
1·0
0·5
3 - POINT BENDING
TENSION
4 - POINT BENDING
$\frac{K_1}{\sigma\sqrt{\frac{\pi a}{Q}}}$
K_1 FOR A WELD TOE CRACK
a/c = 0.25 a/t = 0.05 WELD ANGLE = 30° Q = $\frac{\pi^2}{4}$
0
10
20
30
40
θ°
50
60
70
80
90

FIG. 5.41

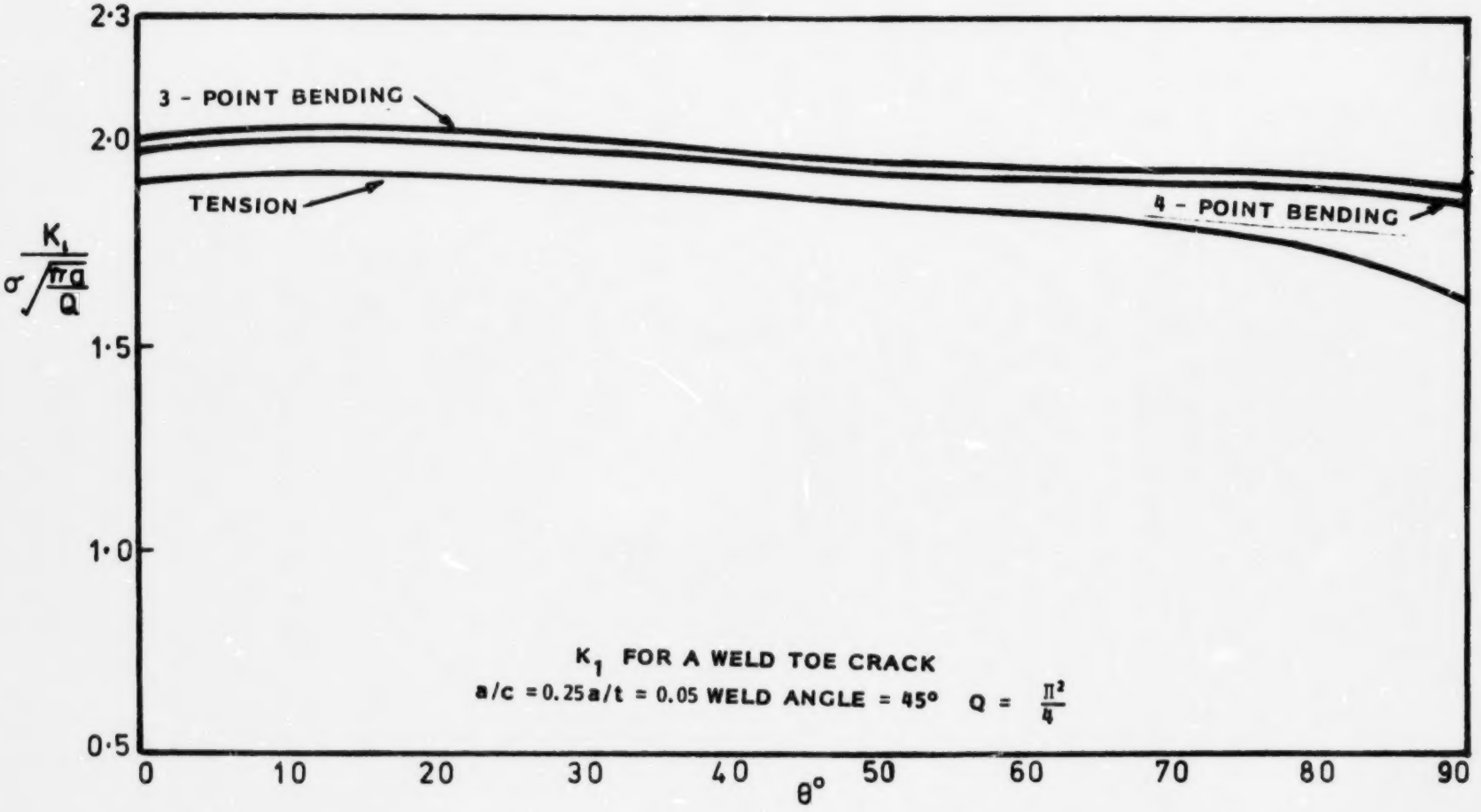
2·3
2·0
1·5
1·0
0·5
3 - POINT BENDING
TENSION
4 - POINT BENDING
$\frac{K_1}{\sigma\sqrt{\frac{\pi a}{Q}}}$
K_1 FOR A WELD TOE CRACK
a/c = 0.25 a/t = 0.05 WELD ANGLE = 45° Q = $\frac{\Pi^2}{4}$
0
10
20
30
40
θ°
50
60
70
80
90

FIG. 5.42

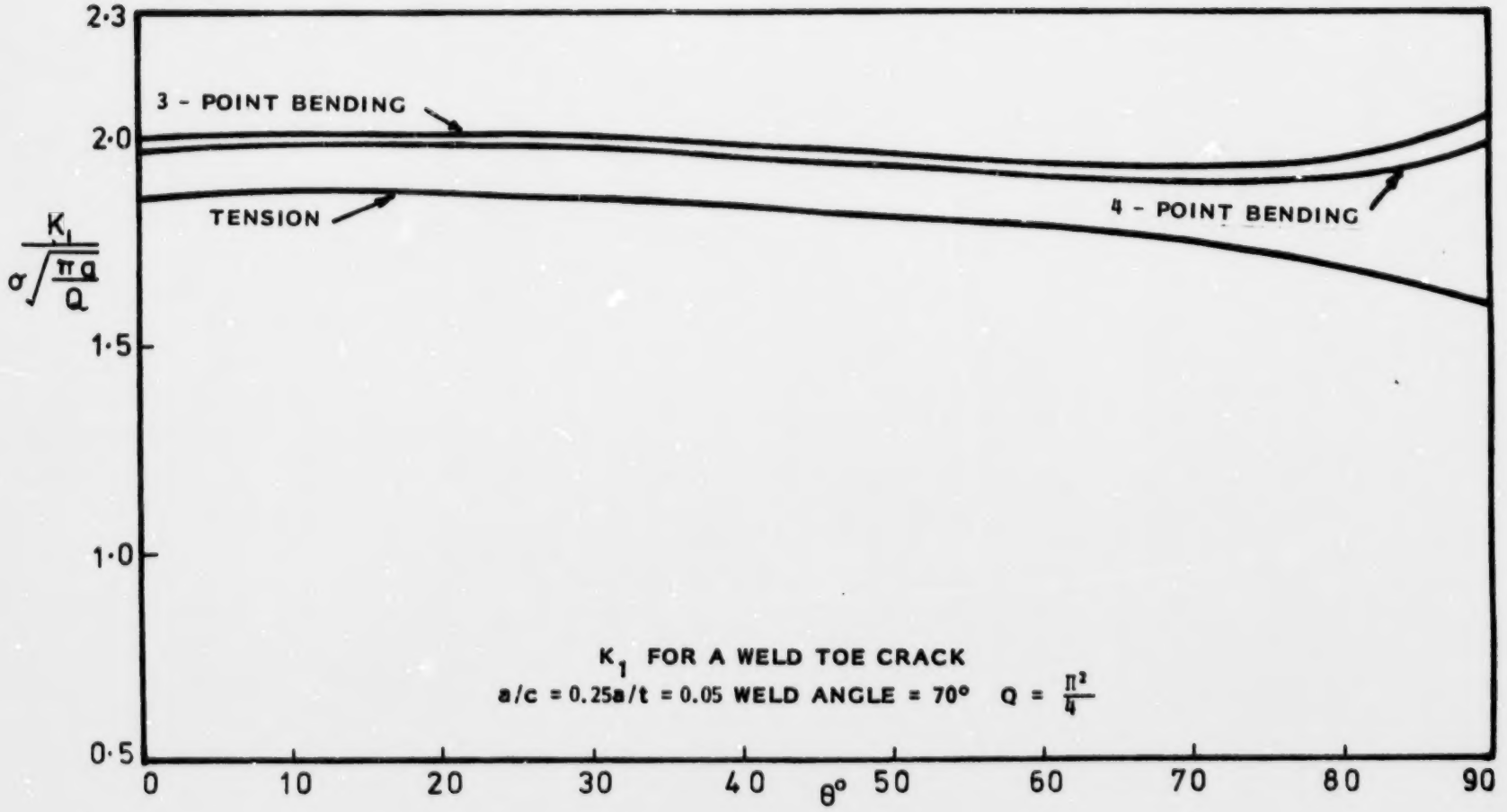
2·3
2·0
1·5
1·0
0·5
3 - POINT BENDING
TENSION
4 - POINT BENDING
$\frac{K_1}{\sigma\sqrt{\frac{\pi a}{Q}}}$
0
10
20
30
40
θ°
50
60
70
80
90
K_1 FOR A WELD TOE CRACK
a/c = 0.25 a/t = 0.05 WELD ANGLE = 70° Q = $\frac{\Pi^2}{4}$

FIG. 5.43

CHAPTER VI

CONCLUSIONS

1. The work described in this report utilizes the finite element program ASAS together with a specially developed mesh generator to efficiently analyse the welded 'T' specimens using linear elastic fracture mechanics.

2. The requirements of the original and the amended work statements have been met giving FE results for 2-dimensional and 3-dimensional determination of the SIF at weld toe cracks.

3. Results using 2-dimensional finite element analyses are presented for a range of weld toe cracks with crack depths between $a/t = 0.005$ and 0.7 and weld profiles of 30^{o}, 45^{o} and 70^{o}.

4. Empirical equations are fitted to the above 2-dimensional SIF results. These equations agree with the FE results for the weld angles considered to within 2 - 3%, depending on the crack depth.

5. A stress analysis was performed on a series of uncracked 'T' joints to obtain the stress distribution and the stress concentration factor SCF at the weld toe region. It was found from these analyses for the loading case of 3-point bending that the distance of the support points from the weld toe has an effect on the SCF. For the cases considered

this effect is quite small (5 - 13%); however further analyses should be performed to obtain the variation of SCF for a series of geometrically similar joints as the support distance is reduced.

6. Accuracy studies were performed on a semi-elliptical surface crack and an embedded crack in a cube subjected to tension. These analyses indicated that, for the best compromise between computing cost and accuracy, the mesh in the region of the crack should be constructed with a minimum of four crack tip elements around the crack, and the dimensions of these elements should be approximately $m/L = 2$ and $a/L = 5$.

7. The SIF for a series of crack shapes and crack depths for three different weld profiles are presented. In the main these results are for crack depths less than $a/t = 0.1$, which is the region indicated by the 2-dimensional studies where the weld profile has the greatest effect on the SIF obtained.

8. The variation of SIF around semi-circular and semi-elliptical crack shapes of $a/c = 1.0$, 0.5 and 0.25 and crack depths, a/t varying between 0.025 and 0.4 are presented. The effect of crack shape,crack depth and weld angle on the SIF is demonstrated.

9. The versatility of the ASAS substructuring capability has been demonstrated in these studies. This program facility together with the aforementioned mesh generator for elliptical crack FE meshes permitted the 3-dimensional studies to be carried out at reasonable cost.

References

1. Department of Energy U.K., "Offshore Installations: Guidance on Design and Construction", (HMSO: London, 1977).

2. N. W. Sneeden et al, "Offshore Installations: Guidance on Design and Construction. Proposed New Fatigue Design Rules for Steel Welded Joints in Offshore Structures". (Department of Energy: U.K. 1981)

3. Det Norske Veritas. "Rules for the Construction and Classification of Mobile Offshore Units", 1975.

4. American Petroleum Institute. "Recommended Practice for Planning, Designing and Constructing Fixed Offshore Platforms"; (API RP2A, Twelfth Edition; 1981).

5. P. Bristoll, "A review of the Fracture Mechanic Approach to the Problems of Design, Quality Assurance, Maintenance and Repair of Offshore Structures", (European Offshore Steels Research Seminar; Paper 24; Cambridge, U.K. 1978).

6. P. C. Paris, "The Growth of Cracks Due to Variations in Load", (Ph.D Thesis; Lehigh University; 1960).

7. "European Offshore Steels Research Seminar"; Cambridge 1978. (Published on behalf of the U.K. Dept. of Energy by the Welding Institute, Cambridge U.K. 1980).

8. "Steel in Marine Structures", (Commission of the European Communities, Paris, France 1981).

9. "Fatigue in Offshore Structural Steels" (Proc. of a Conference organized by Inst. of Civil Engineers, London 1981).

10. J. G. Kuang, A. B. Potvin, R. D. Leick and J. L. Kahlich, "Stress Concentration in Tubular Joints", (SPE Journal, p. 287 - 299, 1977).

11. A. C. Wordsworth and G. P. Smedley, "Stress Concentrations at Unstiffened Tubular Joints", (European Offshore Steels Research Seminar; Paper 31; Cambridge, U.K. 1978).

12. M. B. Gibstein, "Parametric Stress Analysis of 'T' Joints", (European Offshore Steels Research Seminar; Paper 26; Cambridge 1978).

13. P. J. Fisher, "Revised Fatigue Guidance and the Certifying Authority", (2nd Int. Conf. on Welding in Offshore Structures, London, Nov. 1982, Paper 57).

14. A. M. Clayton, "Prediction of Crack Growth in Tubular Joints - An Alternative Approach"; (Fatigue in Offshore Structural Steels, London 1981, Paper 11).

15. N. M. Irvine, "Comparison of Tubular Joint Stress Analysis Methods in the Near Weld Region", (Steel in Marine Structures, Paris, 1981, Paper 1.2).

16. K. M. Engesvik,"Analysis of Uncertainties in Fatigue Capacity of Welded Joints", (Report UR-82-17, Department of Marine Technology, University of Trondheim, Norway).

17. S. Berge, "Effect of Plate Thickness in Fatigue of Cruciform Welded Joints", (Report MK/R 67, Department of Marine Technology - Norwegian Institute of Technology, University of Trondheim 1983).

18. G. O. Johnston, "Influence of Plate Thickness on Fatigue Strength", (Welding Institute Report 3549/3/78).

19. G. S. Booth, "Constant Amplitude Fatigue Tests on Welded Steel Joints Performed in Air", (European Offshore Steels Research Seminar Cambridge 1978).

20. E. Haibach, R. Olivier and W. Ritter, "Fatigue Strength of Angular Fillet Welds Fabricated from 50 mm Plate", ibid.

21. H. Wildshut, J. de Back, W. Dortland and J. L. van Leeuwen, "Fatigue Behaviour of Welds in Air and Sea Water", ibid.

22. R. Olivier, M. Greif, W. Oberparleiter, W. Schutz, "Corrosion Fatigue Behaviour of Offshore Steel Structures Under Constant Amplitude Loading", ECSC Conference on Steel in Marine Structures, (Paris, Oct. 1981).

23. T. R. Gurney, "The Influence of Thickness on the Fatigue Strength of Welded Joints", (2nd Int. Conf. on Behaviour of Offshore Structures BOSS'79, London 1979).

24. C. L. Mullen and J. E. Merwin, "Fatigue Life Improvement Factors Obtained by Weld Reinforcement and Toe Grinding", (Offshore Technology Conference Paper OTC 4240, 1982).

25. G. S. Booth, "Constant Amplitude Fatigue Tests on Welded Steel Joints Performed in Sea Water", (Paper 9, European Offshore Steels Research Seminar, The Welding Institute, Nov. 1978).

26. T. R. Gurney, "Fatigue of Welded Structures", (Cambridge University Press, 2nd Edition 1979).

27. S. J. Maddox, "An Analysis of Fatigue Cracks in Fillet Welded Joints", (Int. J. of Fracture, Vol. 11, No. 2, 1975, pp. 221 - 243).

28. D. J. Hayes and S. J. Maddox, "The Stress Intensity Factor of a Crack at the Toe of a Fillet Weld", (The Welding Institute Research Bulletin 13(1) 1972).

29. T. R. Gurney and G. O. Johnston, "A Revised Analysis of the Influence of Toe Defects on the Fatigue Strength of Transverse Non-Load-Carrying Fillet Welds", (Welding Research International 9-3 pp. 43 - 79, 1979).

30. I. R. Smith, "Higher Order Elements and Fatigue Crack Growth", (Numerical Methods in Fracture Mechanics, A. R. Luxmoore and D. R. J. Owen, University College of Wales, Swansea, pp. 583-598, 1980).

31. P. Albrecht and K. Yamada, "Rapid Calculation of Stress Intensity Factors", (Journal of Struct. Div. Proc. ASCE 103(ST2) 1977, pp. 377 - 389).

32. A. F. Emery, "Stress Intensity Factors for Thermal Stresses in Thick Hollow Cylinders", (J. Basic Engineering, Trans. ASME (D) 88(1), 1966, pp. 45 - 52).

33. R. H. Gallagher, "A Review of Finite Element Techniques in Fracture Mechanics", (Numerical Methods in Fracture Mechanics, A. R. Luxmoore and D. R. J. Owen (Eds), University College of Wales, Swansea, pp. 1 - 25, 1978).

34. J. Mackerle et al. "Fracture Mechanics", (Structural Mechanics Software Series, III 1979, University of Virginia Press).

35. O. C. Zienkiewicz, "The Finite Element Method in Engineering and Science", (McGraw Hill, London 1971).

36. R. H. Gallagher, "Finite Element Fundamentals", (Prentice Hall, 1975).

37. S. K. Chan et al. "On the Finite Element Method in Linear Fracture Mechanics", (Engng. Fracture Mechanics, 2,1 pp. 1-17, 1970).

38. R. D. Henshell and K. G. Shaw, "Crack Tip Elements are Unnecessary", (Int. J. Numer Methods Eng, 9, pp. 495 - 509, 1975).

39. R. S. Barsoum, "On the Use of Isoparametric Finite Elements in Linear Fracture Mechanics", (Int. J. Numer Methods Eng. 10-1, p. 25 - 37, 1976).

40. D. M. Tracey, "Discussion of 'On the Use of Isoparametric Finite Elements in Linear Fracture Mechanics'", (Int. J. Num. Meth. in Engineering, 11-2, pp. 401 - 402, 1977).

41. A. R. Ingraffea et al, "Stress Intensity Factor Computation in Three Dimensions with Quarter Point Elements", (Int. J. Num. Meth. in Eng, 15 pp. 1427-1445, 1980).

42. D. M. Parks, "A Stiffness Derivative Finite Element Technique for Determination of Elastic Crack Tip Stress Intensity Factors", (Int. J. Fracture 10-4, pp. 487 - 502, 1974).

43. T. K. Hellen, "On the Method of Virtual Crack Extensions", (Int. J. for Num. Meth. in Eng. 9-1, pp. 187 - 208, 1973).

44. ASAS User Manual (Atkin Research and Development, Epsom, England, 1981).

45. J. Robinson, "Integrated Theory of Finite Element Methods", (John Wiley and Sons 1973).

46. D. P. Rooke and D. J. Cartwright, "Compendium of Stress Intensity Factors", (HMSO London, England, 1976).

47. R. Bell and J. Kirkhope, "The Evaluation of 3 Dimensional Stress Intensity Factors Using Finite Element Methods", (DSS Contract 8SV80-00010 Phase I. Faculty of Engineering, Carleton University 1981).

48. R. Bell, "Preliminary Investigation of the Stress Intensity Factor at Shallow Weld Toe Cracks", (Dept. of Energy, Mines and Resources Report ERP/PMRL 82-34 (Int.) , unpublished manuscript).

49. T. A. Cruse and G. T. Meyers, "Three Dimensional Fracture Mechanics Analysis", (Proc. ASCE J. Struct. Div., 13 (ST2) pp. 309-320, 1977.

50. J. C. Newman and I. S. Raju, "An Empirical Stress Intensity Factor Equation for a Surface Crack", (Engineering Fracture Mechanics, Vol. 15, No. 1-2, pp. 185-192, 1981).